

**On The Dynamic Stability
of
Functionally Graded Material Beams
Under Parametric Excitation**

**A THESIS SUBMITTED IN FULFILLMENT OF
THE REQUIREMENT FOR THE AWARD OF THE DEGREE**

OF

DOCTOR OF PHILOSOPHY

IN

MECHANICAL ENGINEERING

BY

TRILOCHAN ROUT

(ROLL NO. 508ME810)



**NATIONAL INSTITUTE OF TECHNOLOGY
ROURKELA - 769008, INDIA
May - 2012**



CERTIFICATE

This to certify that the thesis entitled “**On The Dynamic Stability of Functionally Graded Material Beams Under Parametric Excitation**” being submitted by Mr. **Trilochan Rout** for the award of the degree of Doctor of Philosophy (Mechanical Engineering) of NIT Rourkela, Odisha, India, is a record of bonafide research work carried out by him under our supervision and guidance. Mr. Trilochan Rout has worked for more than three and half years on the above problem and this has reached the standard, fulfilling the requirements and the regulation relating to the degree. The contents of this thesis, in full or part, have not been submitted to any other university or institution for the award of any degree or diploma.

(Dr. Sukesh Chandra Mohanty)
Associate Professor
Department of Mechanical Engineering
NIT, Rourkela
Supervisor

(Dr. Rati Ranjan Dash)
Professor
Department of Mechanical
Engineering
CET, Bhubaneswar
Co-Supervisor

Place: Rourkela

Date:

ACKNOWLEDGEMENT

This thesis is a result of research that has been carried out at **National Institute of Technology, Rourkela and Indira Gandhi Institute of Technology, Sarang**. During this period, I came across with a great number of people whose contributions in various ways helped my field of research and they deserve special thanks. It is a pleasure to convey my gratitude to all of them.

In the first place, I would like to express my deep sense of gratitude and indebtedness to my supervisors **Prof. S.C. Mohanty, Prof. R.R. Dash** and D.S.C. members **Prof. P.K. Ray, Prof. S.C. Mishra, and Prof. M. R. Barik** for their advice, and guidance from early stage of this research and providing me extraordinary experiences throughout the work. Above all, they provided me unflinching encouragement and support in various ways which exceptionally inspire and enrich my growth as a student, a researcher and a technologist.

I specially acknowledge **Prof. S.C. Mohanty** for his advice, supervision, and crucial contribution, as and when required during this research. His involvement with originality has triggered and nourished my intellectual maturity that will help me for a long time to come. I am proud to record that I had the opportunity to work with an exceptionally experienced technologist like him.

I am grateful to **Prof. S.K. Sarangi**, Director, **Prof. K.P. Maity**, Head of Mechanical Engineering Department, and **Prof. R.K. Sahoo**, former Head of Mechanical Engineering Department, National Institute of Technology, Rourkela, for their kind support and concern regarding my academic requirements.

I express my thankfulness to the faculty and staff members of the Mechanical Engineering Department for their continuous encouragement and suggestions. Among them, **Mr. J.R. Naik, Mr. P.K. Mohanty** and **Mr. P. K. Patra** deserve special thanks for their kind cooperation in non-academic matters during the research work.

I am indebted to **Mr. B. B. Sahoo, Dr. A. Rout, Dr. B. N. Padhi** and **Mr. S. Chainy** for their support and co-operation which is difficult to express in words. The time spent with them will remain in my memory for years to come.

Thanks are also due to my colleagues at **Indira Gandhi Institute of Technology, Sarang**, for their whole hearted support and cooperation during the course of this work.

My parents deserve special mention for their inseparable support and prayers. They were the persons who had shown me the joy of intellectual pursuit ever since I was a child. I thank them for sincerely bringing up me with care and love.

The completion of this work came at the expense of my long days of frequent absence from home. Words fail me to express my appreciation to my wife **Sayahnika**, my elder brothers **Kamala** and **Bimal**, elder sister **Mounabati** and my sister-in-laws **Rasmirekha** and **Ramani**, my father-in-law **Mr. S. K. Samal** and mother-in-law **Mrs. M. Samal** for their understanding, patience and active cooperation throughout the course of my doctoral dissertation. Thanks are also due to children **Pinki, Rinki, Lucky, Chiku, Niki** and **Pagulu** of our family for being supportive.

Last, but not the least, I thank the one above all of us, the omnipresent **God**, for giving me the strength during the course of this research work.

Trilochan Rout

ABSTRACT

The dynamic stability of functionally graded material (FGM) beams subjected to parametric excitation is studied using finite element method. First order shear deformation theory (Timoshenko beam theory) is used for the analysis of the beams. The shape functions for the beam element are established from the differential equation of static equilibrium. Floquet's theory is used to establish the stability boundaries. A steel-alumina functionally graded ordinary (FGO) beam with steel-rich bottom is considered for the analysis. For the analysis of functionally graded sandwich (FGSW) beam, alumina and steel are chosen as top and bottom skin respectively and the core is FGM with steel and alumina as constituent phases. The material properties in the direction of thickness of FGM are assumed to vary as per power law and exponential law.

The effect of property distribution laws on critical buckling load, natural frequencies and parametric instability of the beams is investigated. Also, the effect of variation of power law index on the critical buckling load, natural frequencies and dynamic stability of beams is determined. It is found that the property variation as per exponential law ensures better dynamic stability than property variation as per power law. Increase in the value of power law index is found to have detrimental effect on the dynamic stability of the beams.

Influence of the elastic foundations on the dynamic stability of the beams is studied. Pasternak elastic foundation is found to have more enhancing effect on the dynamic stability of the beam than Winkler elastic foundation.

The dynamic stability of FGO and FGSW beams used in high temperature environment is investigated. It is observed that increase in environmental temperature has an enhancing effect on the instability of the beams.

The effect of beam geometry, rotary inertia, hub radius and rotational speed on natural frequencies as well as on the parametric instability of

rotating FGO and FGSW cantilever beams is studied. It is observed that increase in rotational speed enhances the dynamic stability of the beams.

Parametric instability of a pre-twisted FGO cantilever beam is investigated. The effect of property distribution laws and pre-twist angle on critical buckling load, natural frequencies and parametric instability of the beam is studied. The increase in the value of power law index is found to have enhancing effect on the parametric instability of the beam. The increase in pre-twisting of the beam reduces the chance of parametric instability of the beam with respect to the first principal instability region. But the increase in pre-twist angle has a detrimental effect on the stability of the beam for second principal instability region.

Keywords: FGM; FGO; FGSW; Exponential law; Power law; Dynamic Stability; Dynamic load factor; Static load factor; Pre-twist angle; Rotary inertia; Foundation shear modulus; Winkler's constant.

CONTENTS

Chapter No.	Title	Page No.
	Acknowledgement	i
	Abstract	iii
	Contents	v
	List of Tables	viii
	List of Figures	ix
	Glossary of Terms	xvii
	Nomenclature	xviii
1	Background and Motivation	
	1.1 Introduction	1
	1.2 Need for the research	3
	1.3 Research objective	4
	1.4 Thesis outline	5
	1.5 Closure	6
2	Literature Review	
	2.1 Introduction	7
	2.2 Review of literature	7
	2.3 Classification of parametric resonance	8
	2.4 Methods of stability analysis of parametrically excited systems	8
	2.5 Effect of system parameters	10
	2.5.1 Effect of property distribution along coordinates	10
	2.5.2 Effect of foundation	11
	2.5.3 Effect of thermal environment	12
	2.5.4 Effect of rotation	13
	2.5.5 Effect of pre-twist angle	15
	2.6 Closure	16
3	Dynamic Stability of Functionally Graded Timoshenko Beam Under Parametric Excitation	
	3.1 Introduction	18
	3.2 Formulation	20
	3.2.1 Shape functions	21
	3.2.2 Element elastic stiffness matrix	25
	3.2.3 Element mass matrix	26
	3.2.4 Element geometric stiffness matrix	26
	3.3 Governing equations of motion	27
	3.3.1 Free vibration	29
	3.3.2 Static stability	30
	3.3.3 Regions of instability	30
	3.4 Results and discussion	30
	3.4.1 Validation of the formulation	31
	3.4.2 Functionally graded ordinary beam	32

	3.4.3 Functionally graded sandwich beam	35
	3.5 Closure	39
	3.5.1 Functionally graded ordinary beam	39
	3.5.2 Functionally graded sandwich beam	39
4	Dynamic Stability of Functionally Graded Timoshenko Beam on Elastic Foundations Under Parametric Excitation	
	4.1 Introduction	40
	4.2 Formulation	42
	4.2.1 Element elastic foundation stiffness matrix	42
	4.3 Governing equations of motion	43
	4.4 Results and discussion	44
	4.4.1 Validation of the formulation	44
	4.4.2 Functionally graded ordinary beam	47
	4.4.3 Functionally graded sandwich beam	50
	4.5 Closure	54
5	Dynamic Stability of Functionally Graded Timoshenko Beams in High Temperature Environment Under Parametric Excitation	
	5.1 Introduction	55
	5.2 Formulation	57
	5.2.1 Element thermal stiffness matrix	58
	5.3 Governing equations of motion	58
	5.4 Results and discussion	59
	5.4.1 Functionally graded ordinary beam	59
	5.4.2 Functionally graded sandwich beam	62
	5.5 Closure	64
6	Dynamic Stability of Rotating Functionally Graded Timoshenko Beam Under Parametric Excitation	
	6.1 Introduction	66
	6.2 Formulation	67
	6.2.1 Element centrifugal stiffness matrix	68
	6.2.2 Element effective stiffness matrix	69
	6.3 Governing equations of motion	69
	6.4 Results and discussion	70
	6.4.1 Validation of the formulation	70
	6.4.2 Functionally graded ordinary beam	71
	6.4.3 Functionally graded sandwich beam	76
	6.5 Closure	82
7	Dynamic Stability of Pre-twisted Functionally Graded Timoshenko Beam Under Parametric Excitation	
	7.1 Introduction	83
	7.2 Formulation	84
	7.2.1 Shape function	85

	7.2.2 Element elastic stiffness matrix	88
	7.2.3 Element mass matrix	89
	7.2.4 Element geometric stiffness matrix	90
	7.3 Governing equations of motion	90
	7.4 Results and discussions	91
	7.4.1 Validation of the formulation	91
	7.4.2 Functionally graded ordinary beam	91
	7.5 Closure	96
8	Conclusion and Scope for Future Work	
	8.1 Introduction	97
	8.2 Summary of findings	97
	8.2.1 FGO and FGSW beams	98
	8.2.2 FGO and FGSW beams resting on elastic foundations	98
	8.2.3 FGO and FGSW beams in high temperature thermal environment	99
	8.2.4 Rotating FGO and FGSW beams	99
	8.2.5 Pre-twisted FGO cantilever beam	99
	8.2.6 Important conclusions with respect to dynamic stability of FGM beams	100
	8.2.7 Some guide lines related to design of FGM beams	101
	8.3 Scope for future work	102
	Bibliography	104
	Appendix	119

LIST OF TABLES

Table No.	Caption	Page No.
3.1	Comparison of first five natural frequencies	31
3.2	Comparison of buckling load parameter	31
3.3	Variation of natural frequencies with power law index for Steel-alumina FGO beam (steel-rich bottom)	33
3.4	Critical buckling loads for FGO beam (steel-rich bottom)	33
4.1	Comparison of fundamental non-dimensional frequency	45
4.2	Comparison of first five natural frequencies	45
4.3	Fundamental natural frequency of a steel-alumina ss-ss FGO beam (steel-rich bottom) of length L=0.5 m	46
4.4	Fundamental natural frequency of a steel-alumina ss-ss FGO beam (steel-rich bottom) on Winkler and Pasternak elastic foundations (length L=0.5 m)	46
6.1	Variation of fundamental natural frequency of Timoshenko cantilever beam for different rotational speed parameters ($\delta = 0$, $r = 1/30$, $E/kG = 3.059$)	70
7.1	Comparison of first four mode frequencies (L=15.24 cm, b=2.54 cm, h=0.17272 cm, k=0.847458, E=206.86GPa, G=82.74GPa, $\rho=7857.6\text{kg/m}^3$)	91

LIST OF FIGURES

Figure No.	Caption	Page No.
1.1(a)	The increase of response with time of an unstable system	2
1.1(b)	Stability diagram of a parametrically excited system	2
3.1(a)	Functionally graded sandwich beam subjected to dynamic axial load	20
3.1(b)	The coordinate system with generalized forces and displacements for the FGSW beam element	21
3.1(c)	Beam element showing generalized degrees of freedom for i^{th} element	21
3.1(d)	Variation of Young's modulus along thickness of steel-alumina FGM with steel-rich bottom according to different laws	22
3.2(a)	Variation of the first mode frequency with power law index for steel-rich bottom FGO beam	32
3.2(b)	Variation of the second mode frequency with power law index for steel-rich bottom FGO beam	32
3.3(a)	The first mode instability regions of FGO (steel-rich bottom) beam, +exp. law, $*n=1.5$, $^{\circ}n=2.5$	34
3.3(b)	The second mode instability regions of FGO (steel-rich bottom) beam, +exp. law, $*n=1.5$, $^{\circ}n=2.5$	34
3.4(a)	The effect of static load factor on first mode instability regions for FGO-2.5 beam, $*\alpha=0.1$, $^{\circ}\alpha=0.5$	35
3.4(b)	The effect of static load factor on second mode instability regions for FGO-2.5 beam, $*\alpha=0.1$, $^{\circ}\alpha=0.5$	35
3.4(c)	The effect of static load factor on first mode instability regions of e-FGO beam, $^{\circ}\alpha=0.1$, $^{\circ}\alpha=0.5$	35
3.4(d)	The effect of static load factor on second mode instability regions of e-FGO beam, $*\alpha=0.1$, $^{\circ}\alpha=0.5$	35
3.5(a)	The effect of FGM content on the first mode frequency of FGSW beam	36
3.5(b)	The effect of FGM content on the second mode frequency of FGSW beams	36
3.6	The effect of FGM content on the critical buckling load of FGSW beams	36
3.7(a)	The first mode instability regions for FGSW beam, $n=1.5$ (*), $n=2.5$ ($^{\circ}$), exp. Law (†)	37
3.7(b)	The second mode instability regions for FGSW beam, $n=1.5$ (*), $n=2.5$ ($^{\circ}$), exp.law (†)	37
3.8(a)	The effect of static load factor on the first mode instability region of FGSW-2.5 beam, $\alpha=0.1$ (*), $\alpha=0.5$ ($^{\circ}$)	37
3.8(b)	The effect of static load factor on the second mode instability region of FGSW-2.5 beam, $\alpha=0.1$ (*), $\alpha=0.5$ ($^{\circ}$)	37
3.8(c)	The effect of static load factor on the first mode instability region of e-FGSW beam, $\alpha=0.1$ (*), $\alpha=0.5$ ($^{\circ}$)	37
3.8(d)	The effect of static load factor on the second mode instability region of e-FGSW beam, $\alpha=0.1$ (*), $\alpha=0.5$ ($^{\circ}$)	37
3.9(a)	The effect of FGM content on the first mode instability	37

	regions of FGSW-2.5 beam, $*d/h=0.3$, $^{\circ}d/h=0.8$	
3.9(b)	The effect of FGM content on the second mode instability regions of FGSW-2.5 beam, $*d/h=0.3$, $^{\circ}d/h=0.8$	37
3.9(c)	The effect of FGM content on the first mode instability regions of e-FGSW beam, $*d/h=0.3$, $^{\circ}d/h=0.8$	38
3.9(d)	The effect of FGM content on the second mode instability regions of e-FGSW beam, $*d/h=0.3$, $^{\circ}d/h=0.8$	38
4.1	Functionally graded sandwich beam resting on Pasternak elastic foundation and subjected to dynamic axial load	42
4.2(a)	Effect of Pasternak foundation on first mode frequency of FGO beam with Steel-rich bottom having properties according to exponential as well as power law ($K_2=1$)	48
4.2(b)	Effect of Pasternak foundation on second mode frequency of FGO beam with Steel-rich bottom having properties according to exponential as well as power law ($K_2=1$)	48
4.2(c)	Effect of Winkler foundation on first mode frequency of FGO beam with steel-rich bottom having properties according to exponential as well as power law	48
4.2(d)	Effect of Winkler foundation on second mode frequency of FGO beam with steel-rich bottom having properties according to exponential as well as power law	48
4.3(a)	Region of instability for first mode of FGO beam with steel-rich bottom resting on Pasternak foundation ($K_1=5, K_2=1$): $*n=1.5$, $^{\circ}n=2.5$, +exp. law	49
4.3(b)	Region of instability for second mode of FGO beam with steel-rich bottom resting on Pasternak foundation ($K_1=5, K_2=1$): $*n=1.5$, $^{\circ}n=2.5$, +exp. law	49
4.4(a)	Effect of foundation on first mode instability regions of FGO-2.5 beam: *No foundation ($K_1=0, K_2=0$), $^{\circ}$ Winkler foundation ($K_1=15, K_2=0$), +Pasternak foundation ($K_1=5, K_2=1$)	49
4.4(b)	Effect of foundation on second mode instability regions of FGO-2.5 beam: *No foundation ($K_1=0, K_2=0$), $^{\circ}$ Winkler foundation ($K_1=15, K_2=0$), +Pasternak foundation ($K_1=5, K_2=1$)	49
4.4(c)	Effect of foundation on first mode instability regions of e-FGO beam: *No foundation ($K_1=0, K_2=0$), $^{\circ}$ Winkler foundation ($K_1=15, K_2=0$), +Pasternak foundation ($K_1=5, K_2=1$)	50
4.4(d)	Effect of foundation on second mode instability regions of e-FGO beam: *No foundation ($K_1=0, K_2=0$), $^{\circ}$ Winkler foundation ($K_1=15, K_2=0$), +Pasternak foundation ($K_1=5, K_2=1$)	50
4.5(a)	Effect of Pasternak foundation on first mode frequency of steel-alumina FGSW beam having properties according to exponential as well as power law ($K_2=1$): $*n=1.5$, $^{\circ}n=2.5$, +exp law	51
4.5(b)	Effect of Pasternak foundation on second mode frequency of steel-alumina FGSW beam having properties according to exponential as well as power law (foundation shear modulus $K_2=1$): $*n=1.5$, $^{\circ}n=2.5$, +exp law	51

4.6(a)	Effect of FGM content (d/h) on the first mode frequency of a steel-alumina FGSW beam resting on Pasternak foundation ($K_1=5, K_2=1$) and having properties as per exponential as well as power law	51
4.6(b)	Effect of FGM content (d/h) on the second mode frequency of a steel-alumina FGSW beam resting on Pasternak foundation ($K_1=5, K_2=1$) and having properties as per exponential as well as power law	51
4.7(a)	Regions of instability of steel-alumina FGSW beam on Pasternak foundation ($K_1=5, K_2=1$) for first mode: $^*n=1.5, ^\circ n=2.5, +exp. law$	51
4.7(b)	Regions of instability of steel-alumina FGSW beam on Pasternak foundation ($K_1=5, K_2=1$) for second mode: $^*n=1.5, ^\circ n=2.5, +exp. law$	51
4.8(a)	Effect of foundation on first mode instability regions of FGSW-2.5 beam: $^*No foundation (K_1=0, K_2=0), ^\circ Winkler foundation (K_1=15, K_2=0), +Pasternak foundation(K_1=5, K_2=1)$	53
4.8(b)	Effect of foundation on second mode instability regions of FGSW-2.5 beam: $^*No foundation(K_1=0, K_2=0), ^\circ Winkler foundation (K_1=15, K_2=0), +Pasternak foundation(K_1=5, K_2=1)$	53
4.8(c)	Effect of foundation on first mode instability regions of e-FGSW beam: $^*No foundation (K_1=0, K_2=0), ^\circ Winkler foundation(K_1=15, K_2=0), +Pasternak foundation (K_1=5, K_2=1)$	53
4.8(d)	Effect of foundation on second mode instability regions of e-FGSW beam: $^*No foundation (K_1=0, K_2=0), ^\circ Winkler foundation (K_1=15, K_2=0), +Pasternak foundation(K_1=5, K_2=1)$	53
4.9(a)	Effect of FGM content (d/h) on the stability for first mode of steel-alumina FGSW-1.5 beam resting on Pasternak foundation($K_1=5, K_2=1$): $^\circ d/h=0.3, +d/h=0.8$	53
4.9(b)	Effect of FGM content (d/h) on the stability for second mode of steel-alumina FGSW-1.5 beam resting on Pasternak foundation($K_1=5, K_2=1$): $^\circ d/h=0.3, +d/h=0.8$	53
4.9(c)	Effect of FGM content (d/h) on the stability for first mode of steel-alumina e-FGSW beam resting on Pasternak foundation($K_1=5, K_2=1$): $^\circ d/h=0.3, +d/h=0.8$	54
4.9(d)	Effect of FGM content (d/h) on the stability for second mode of steel-alumina e-FGSW beam resting on Pasternak foundation($K_1=5, K_2=1$): $^\circ d/h=0.3, +d/h=0.8$	54
5.1(a)	Variation of first mode non-dimensional frequency with temperature of steel-alumina FGO beam with steel-rich bottom	60
5.1(b)	Variation of second mode non-dimensional frequency with temperature of steel-alumina FGO beam with steel-rich bottom	60
5.2(a)	Effect of property distribution laws on first mode instability region of steel-alumina FGO beam: $^*n=1.5), ^\circ n=2.5, +exp. law$	60

5.2(b)	Effect of property distribution laws on second mode instability region of steel-alumina FGO beam: $*n=1.5$, $^{\circ}n=2.5$, +exp. Law	60
5.3(a)	Effect of temperature on first mode instability region of steel-alumina FGO-2.5 beam: $*0^{\circ}$, $^{\circ}500^{\circ}$, $+1000^{\circ}$	61
5.3(b)	Effect of temperature on second mode instability region of steel-alumina FGO-2.5 beam: $*0^{\circ}$, $^{\circ}500^{\circ}$, $+1000^{\circ}$	61
5.3(c)	Effect of temperature on first mode instability region of steel-alumina e-FGO beam: $*0^{\circ}$, $^{\circ}500^{\circ}$, $+1000^{\circ}$	61
5.3(d)	Effect of temperature on second mode instability region of steel-alumina e-FGO beam: $*0^{\circ}$, $^{\circ}500^{\circ}$, $+1000^{\circ}$	61
5.4(a)	Variation of first mode non-dimensional frequency of FGSW beam($d/h=0.3$) with temperature	62
5.4(b)	Variation of second mode non-dimensional frequency of FGSW beam($d/h=0.3$) with temperature	62
5.5(a)	Effect of property distribution laws on first mode instability region of steel-alumina FGSW beam: $*n=1.5$, $^{\circ}n=2.5$, +exp. law	62
5.5(b)	Effect of property distribution laws on second mode instability region of steel-alumina FGSW beam: $*n=1.5$, $^{\circ}n=2.5$, +exp. law	62
5.6(a)	Effect of temperature on first mode instability region of steel-alumina FGSW-2.5 beam: $*0^{\circ}$, $^{\circ}500^{\circ}$, $+1000^{\circ}$	63
5.6(b)	Effect of temperature on second mode instability region of steel-alumina FGSW-2.5 beam: $*0^{\circ}$, $^{\circ}500^{\circ}$, $+1000^{\circ}$	63
5.6(c)	Effect of temperature on first mode instability region of steel-alumina e-FGSW beam: $*0^{\circ}$, $^{\circ}500^{\circ}$, $+1000^{\circ}$	63
5.6(d)	Effect of temperature on second mode instability region of steel-alumina e-FGSW beam: $*0^{\circ}$, $^{\circ}500^{\circ}$, $+1000^{\circ}$	63
5.7(a)	Effect of ratio (d/h) on the first mode instability regions of FGSW-2.5 beam: $*d/h=0.3$, $^{\circ}d/h=0.5$, $+d/h=0.8$	63
5.7(b)	Effect of ratio (d/h) on the second mode instability regions of FGSW-2.5 beam: $*d/h=0.3$, $^{\circ}d/h=0.5$, $+d/h=0.8$	63
5.7(c)	Effect of ratio (d/h) on the first mode instability regions of e-FGSW beam: $*d/h=0.3$, $^{\circ}d/h=0.5$, $+d/h=0.8$	64
5.7(d)	Effect of ratio (d/h) on the second mode instability regions of e-FGSW beam: $*d/h=0.3$, $^{\circ}d/h=0.5$, $+d/h=0.8$	64
6.1	Rotating functionally graded sandwich beam fixed at one end free at the other	68
6.2(a)	Variation of non-dimensional first mode frequency with slenderness parameter of steel-alumina FGO beam with steel-rich bottom for property distribution along thickness according to power law as well as exponential law. ($\bar{\omega}=344\text{rad/s}$, $\delta=0.1$)	71
6.2(b)	Variation of non-dimensional second mode frequency with slenderness parameter of steel-alumina FGO beam with steel-rich bottom for property distribution along thickness as per power law as well as exponential law. ($\bar{\omega}=344\text{rad/s}$, $\delta=0.1$)	71
6.3(a)	Variation of non-dimensional first mode frequency with hub	72

	radius parameter of steel-alumina FGO beam with steel-rich bottom for property distribution along thickness as per power law as well as exponential law. ($\bar{\omega}=344\text{rad/s}$, $s=0.2$)	
6.3(b)	Variation of non-dimensional second mode frequency with hub radius parameter of steel-alumina FGO beam with steel-rich bottom for property distribution along thickness as per power law as well as exponential law. ($\bar{\omega}=344\text{rad/s}$, $s=0.2$)	72
6.4(a)	Variation of non-dimensional first mode frequency with rotational speed parameter of steel-alumina FGO beam with steel-rich bottom for property distribution along thickness as per power law as well as exponential law. ($\delta=0.1$, $s=0.2$)	72
6.4(b)	Variation of non-dimensional second mode frequency with rotational speed parameter of steel-alumina FGO beam with steel-rich bottom for property distribution along thickness as per power law as well as exponential law. ($\delta=0.1$, $s=0.2$)	72
6.5(a)	Effect of property distribution laws on first mode instability region of steel-alumina FGO beam for $\delta=0.1$, $\bar{\omega}=344\text{rad/s}$, $s=0.2$: $^*n=1.5$, $^{\circ}n=2.5$, +exp. Law	74
6.5(b)	Effect of property distribution laws on second mode instability region of steel-alumina FGO beam for $\delta=0.1$, $\bar{\omega}=344\text{rad/s}$, $s=0.2$: $^*n=1.5$, $^{\circ}n=2.5$, +exp. Law	74
6.6(a)	Effect of hub radius parameter on first mode instability region of steel-alumina FGO beam for $n=2.5$, $h/L=0.2$, $\bar{\omega}=344\text{ rad/s}$ ($^*\delta=0.1$, $^{\circ}\delta=0.5$)	74
6.6(b)	Effect of hub radius parameter on second mode instability region of steel-alumina FGO beam for $n=2.5$, $s=0.2$, $\bar{\omega}=344\text{ rad/s}$ ($^*\delta=0.1$, $^{\circ}\delta=0.5$)	74
6.6(c)	Effect of hub radius parameter on first mode instability region of steel-alumina FGO beam for exp. law $s=0.2$, $\bar{\omega}=344\text{ rad/s}$ ($^*\delta=0.1$, $^{\circ}\delta=0.5$)	74
6.6(d)	Effect of hub radius parameter on second mode instability region of steel-alumina FGO beam for exp. Law, $h/L=0.2$, $\bar{\omega}=344\text{ rad/s}$ ($^*\delta=0.1$, $^{\circ}\delta=0.5$)	74
6.7(a)	Effect of rotational speed parameter on first mode instability region of steel-alumina FGO beam for $n=2.5$, $s=0.2$, $\delta=0.1$, ($^*v=0.1$, $^{\circ}v=0.5$, $^+v=1.0$)	75
6.7(b)	Effect of rotational speed parameter on second mode instability region of steel-alumina FGO beam for $n=2.5$, $s=0.2$, $\delta=0.1$, ($^*v=0.1$, $^{\circ}v=0.5$, $^+v=1.0$)	75
6.7(c)	Effect of rotational speed parameter on first mode instability region of steel-alumina FGO beam for exp. law, $s=0.2$, $\delta=0.1$, ($^*v=0.1$, $^{\circ}v=0.5$, $^+v=1.0$)	75
6.7(d)	Effect of rotational speed parameter on second mode instability region of steel-alumina FGO beam for exp. law, $s=0.2$, $\delta=0.1$, ($^*v=0.1$, $^{\circ}v=0.5$, $^+v=1.0$)	75
6.8(a)	Effect of slenderness parameter on first mode instability region of steel-alumina FGO beam for $n=2.5$, $\delta=0.1$, $\bar{\omega}=344\text{ rad/s}$ ($^*s=0.1$, $^{\circ}s=0.3$)	76

6.8(b)	Effect of slenderness parameter on second mode instability region of steel-alumina FGO beam for $n=2.5$, $\bar{\delta}=0.1$, $\bar{\omega}=344$ rad/s ($^*s=0.1$, $^{\circ}s=0.3$)	76
6.8(c)	Effect of slenderness parameter on first mode instability region of steel-alumina FGO beam for exp. law, $\bar{\delta}=0.1$, $\bar{\omega}=344$ rad/s ($^*s=0.1$, $^{\circ}s=0.3$)	76
6.8(d)	Effect of slenderness parameter on second mode instability region of steel-alumina FGO beam for exp. law, $\bar{\delta}=0.1$, $\bar{\omega}=344$ rad/s ($^*s=0.1$, $^{\circ}s=0.3$)	76
6.9(a)	Variation of non-dimensional first mode frequency with slenderness parameter of steel-alumina FGSW beam for property distribution in core thickness as per power law as well as exponential law. ($\bar{\omega}=344$ rad/s, $\delta=0.1$, $d/h=0.3$)	77
6.9(b)	Variation of non-dimensional second mode frequency with slenderness parameter of steel-alumina FGSW beam for property distribution in core thickness as per power law as well as exponential law. ($\bar{\omega}=344$ rad/s, $\delta=0.1$, $d/h=0.3$)	77
6.10(a)	Variation of non-dimensional first mode frequency with hub radius parameter of steel-alumina FGSW beam for property distribution in core thickness as per power law as well as exponential law. ($\bar{\omega}=344$ rad/s, $s=0.2$, $d/h=0.3$)	77
6.10(b)	Variation of non-dimensional second mode frequency with hub radius parameter of steel-alumina FGSW beam for property distribution in core thickness as per power law as well as exponential law. ($\bar{\omega}=344$ rad/s, $s=0.2$, $d/h=0.3$)	77
6.11(a)	Variation of non-dimensional first mode frequency with rotational speed parameter of steel-alumina FGSW beam for property distribution in core thickness as per power law as well as exponential law. ($\delta=0.1$, $s=0.2$, $d/h=0.3$)	78
6.11(b)	Variation of non-dimensional second mode frequency with rotational speed parameter of steel-alumina FGSW beam for property distribution in core thickness as per power law as well as exponential law. ($\delta=0.1$, $s=0.2$, $d/h=0.3$)	78
6.12(a)	Variation of non-dimensional first mode frequency with FGM content (d/h) of steel-alumina FGSW beam for property distribution in core thickness as per power law as well as exponential law. ($\bar{\omega}=344$ rad/s, $\delta=0.1$, $s=0.2$)	78
6.12(b)	Variation of non-dimensional second mode frequency with FGM content (d/h) of steel-alumina FGSW beam for property distribution in core thickness as per power law as well as exponential law. ($\bar{\omega}=344$ rad/s, $\delta=0.1$, $s=0.2$)	78
6.13(a)	Effect of property distribution laws on first mode instability region of steel-alumina FGSW beam for $\bar{\delta}=0.1$, $s=0.2$, $d/h=0.3$, $\bar{\omega}=344$ rad/s ($^*n=1.5$, $^{\circ}n=2.5$, $^+exp.$ law)	79
6.13(b)	Effect of property distribution laws on second mode instability region of steel-alumina FGSW beam for $\bar{\delta}=0.1$, $s=0.2$, $d/h=0.3$, $\bar{\omega}=344$ rad/s ($^*n=1.5$, $^{\circ}n=2.5$, $^+exp.$ law)	79
6.14(a)	Effect of hub radius parameter on first mode instability region of steel-alumina FGSW-2.5 beam. $s=0.2$, $d/h=0.3$, $\bar{\omega}=344$ rad/s ($^*\bar{\delta}=0.1$, $^{\circ}\bar{\delta}=0.5$)	79
6.14(b)	Effect of hub radius parameter on second mode instability	79

	region of steel-alumina FGSW-2.5 beam. $s=0.2, d/h=0.3$ $\bar{\omega}=344 \text{ rad/s}$ ($^* \delta=0.1, {}^{\circ} \delta=0.5$)	
6.14(c)	Effect of hub radius parameter on first mode instability region of steel-alumina e-FGSW beam. $s=0.2, d/h=0.3, \bar{\omega}=344 \text{ rad/s}$ ($^* \delta=0.1, {}^{\circ} \delta=0.5$)	80
6.14(d)	Effect of hub radius parameter on second mode instability region of steel-alumina e-FGSW beam. $s=0.2, d/h=0.3, \bar{\omega}=344 \text{ rad/s}$ ($^* \delta=0.1, {}^{\circ} \delta=0.5$)	80
6.15(a)	Effect of rotational speed parameter on first mode instability region of steel-alumina FGSW-2.5 beam. $s=0.2, \bar{\delta}=0.1, d/h=0.3$ ($^* v=0.1, {}^{\circ} v=0.5, {}^{+} v=1.0$)	80
6.15(b)	Effect of rotational speed parameter on second mode instability region of steel-alumina FGSW-2.5 beam. $s=0.2, \bar{\delta}=0.1, d/h=0.3$ ($^* v=0.1, {}^{\circ} v=0.5, {}^{+} v=1.0$)	80
6.15(c)	Effect of rotational speed parameter on first mode instability region of steel-alumina e-FGSW beam. $s=0.2, \bar{\delta}=0.1, d/h=0.3$ ($^* v=0.1, {}^{\circ} v=0.5, {}^{+} v=1.0$)	80
6.15(d)	Effect of rotational speed parameter on second mode instability region of steel-alumina e-FGSW beam. $s=0.2, \bar{\delta}=0.1, d/h=0.3$ ($^* v=0.1, {}^{\circ} v=0.5, {}^{+} v=1.0$)	80
6.16(a)	Effect of slenderness parameter on first mode instability region of steel-alumina FGSW-2.5 beam. $\bar{\delta}=0.1, d/h=0.3, \bar{\omega}=344 \text{ rad/s}$ ($^* s=0.1, {}^{\circ} s=0.3$)	81
6.16(b)	Effect of slenderness parameter on second mode instability region of steel-alumina FGSW-2.5 beam. $\bar{\delta}=0.1, d/h=0.3, \bar{\omega}=344 \text{ rad/s}$ ($^* s=0.1, {}^{\circ} s=0.3$)	81
6.16(c)	Effect of slenderness parameter on first mode instability region of steel-alumina e-FGSW beam. $\bar{\delta}=0.1, d/h=0.3, \bar{\omega}=344 \text{ rad/s}$ ($^* s=0.1, {}^{\circ} s=0.3$)	81
6.16(d)	Effect of slenderness parameter on second mode instability region of steel-alumina e-FGSW beam. $\bar{\delta}=0.1, d/h=0.3, \bar{\omega}=344 \text{ rad/s}$ ($^* s=0.1, {}^{\circ} s=0.3$)	81
6.17(a)	Effect of FGM content on first mode instability regions of steel-alumina FGSW-2.5 beam. $s=0.2, (^* d/h=0.3, {}^{\circ} d/h=0.8)$	81
6.17(b)	Effect of FGM content on second mode instability regions of steel-alumina FGSW-2.5 beam. $s=0.2, (^* d/h=0.3, {}^{\circ} d/h=0.8)$	81
6.17(c)	Effect of FGM content on first mode instability regions of steel-alumina e-FGSW beam. $s=0.2, (^* d/h=0.3, {}^{\circ} d/h=0.8)$	82
6.17(d)	Effect of FGM content on second mode instability regions of steel-alumina e-FGSW beam. $s=0.2, (^* d/h=0.3, {}^{\circ} d/h=0.8)$	82
7.1(a)	Pre-twisted cantilever beam subjected to dynamic axial force	84
7.1(b)	The coordinate system with generalized forces and displacements for the beam element	85
7.1(c)	Beam element showing generalized degrees of freedom for i^{th} element	85
7.2(a)	Effect of property distribution laws on first mode frequency of steel-alumina pre-twisted FGO beam with steel-rich bottom ($^* n=2, {}^{\circ} \text{exp law}$)	92

7.2(b)	Effect of property distribution laws on second mode frequency of steel-alumina pre-twisted FGO beam with steel-rich bottom (*n=2, ^o exp law	92
7.3(a)	Effect of power law index on first mode frequency of steel-alumina pre-twisted FGO beam with steel-rich bottom. Twist angle $\alpha_0=45^0$	93
7.3(b)	Effect of power law index on second mode frequency of steel-alumina pre-twisted FGO beam with steel-rich bottom. Twist angle $\alpha_0=45^0$	93
7.4	Effect of property distribution laws on the critical buckling load of steel-alumina pre-twisted FGO beam with steel-rich bottom (*n=2, ^o exp law)	93
7.5	Effect of power law index on the critical buckling load of steel-alumina pre-twisted FGO beam with steel-rich bottom. $\alpha_0=45^0$	93
7.6(a)	Effect of property distribution laws on first mode instability zone of steel-alumina pre-twisted FGO beam with steel-rich bottom. (*n=2, ^o n=3, +exp. law)	94
7.6(b)	Effect of property distribution laws on second mode instability zone of steel-alumina pre-twisted FGO beam with steel-rich bottom. (*n=2, ^o n=3, +exp. law)	94
7.7(a)	Effect of pre-twist angle on first mode instability zone of steel-alumina pre-twisted FGO-2 beam with steel-rich bottom. (* $\alpha_0=30^0$, ^o $\alpha_0=45^0$)	95
7.7(b)	Effect of pre-twist angle on second mode instability zone of steel-alumina pre-twisted FGO-2 beam with steel-rich bottom. (* $\alpha_0=30^0$, ^o $\alpha_0=45^0$)	95
7.8(a)	Effect of pre-twist angle on first mode instability zone of steel-alumina pre-twisted e-FGO beam with steel-rich bottom. (* $\alpha_0=30^0$, ^o $\alpha_0=45^0$)	95
7.8(b)	Effect of pre-twist angle on second mode instability zone of steel-alumina pre-twisted e-FGO beam with steel-rich bottom. (* $\alpha_0=30^0$, ^o $\alpha_0=45^0$)	95
7.9(a)	Effect of static load factor on first mode instability zone of steel-alumina pre-twisted FGO-2 beam with steel-rich bottom. (* $\alpha=0.1$, ^o $\alpha=0.5$)	95
7.9(b)	Effect of static load factor on second mode instability zone of steel-alumina pre-twisted FGO-2 beam with steel-rich bottom. (* $\alpha=0.1$, ^o $\alpha=0.5$)	95
7.10(a)	Effect of static load factor on first mode instability zone of steel-alumina pre-twisted e-FGO beam with steel-rich bottom. (* $\alpha=0.1$, ^o $\alpha=0.5$)	96
7.10(b)	Effect of static load factor on second mode instability zone of steel-alumina pre-twisted e-FGO beam with steel-rich bottom. (* $\alpha=0.1$, ^o $\alpha=0.5$)	96

GLOSSARY OF TERMS

FEM	Finite element method
FGM	Functionally graded material
FGO	Functionally graded ordinary
FGSW	Functionally graded sandwich
FGO-1.5 beam	FGO beam having properties along thickness as per power law with index value equal to 1.5
FGO-2 beam	FGO beam having properties along thickness as per power law with index value equal to 2
FGO-2.5 beam	FGO beam having properties along thickness as per power law with index value equal to 1.5
e-FGO beam	FGO beam having properties along thickness as per exponential law
FGSW-1.5 beam	FGSW beam having properties along thickness of core as per power law with index value equal to 1.5
FGSW-2.5 beam	FGSW beam having properties along thickness of core as per power law with index value equal to 2.5
e-FGSW beam	FGSW beam having properties along thickness of core as per exponential law
TBT	Timoshenko beam theory
DQM	Differential quadrature method
SSM	State space method
SS-SS	Simply supported-simply supported

NOMENCLATURE

Although all the principal symbols used in this thesis are defined in the text as they occur, a list of them is presented below for easy reference.

English symbols

a_1, a_2, \dots	Coefficients of polynomials
b_1, b_2, \dots	Coefficients of polynomials
b	Beam width
c_1, d_1	Constants for Fourier expansion
d	Thickness of FGM core
e	Exponent
(e)	Element
h	Beam thickness
k	Shear correction factor
k_1	Winkler's foundation constant per unit length of beam.
k_2	Shear foundation constant per unit length of beam
l	Element length
n	Index of power law variation
r	Rotary inertia parameter/radius of gyration
s	Slenderness parameter
t	Time
u	Axial displacement of reference plane
v	Transverse displacement in y-direction
w	Transverse displacement in z-direction
A	Cross-sectional area of beam
$A_{11}, B_{11}, D_{11}, D_{22}$	Stiffness coefficients
$E(z)$	Young's modulus
E_a	Young's modulus of alumina
E_s	Young's modulus of steel
$G(z)$	Shear modulus
I	Moment of inertia of cross-section
I_0, I_1, I_2, I_{22}	Mass moments
L	Length of the beam
M_y, M_z	Bending moments about Y and Z axis
N	Axial force
$P(t)$	Dynamic axial load
P^\oplus	Critical buckling load
R	Hub radius
R_b	Material property at the bottommost layer
R_t	Material property at topmost layer
$R(z)$	A material property
S	Element strain energy
T	Element kinetic energy
V_y, V_z	Shear forces along Y and Z axis

W_c	Work done by centrifugal force
W_p	Work done by axial force

Matrices

$[k_c]$	Element centrifugal stiffness matrix
$[k_e]$	Element elastic stiffness matrix
$[k_{ef}]$	Element effective stiffness matrix
$[k_f]$	Element Pasternak foundation stiffness matrix
$[k_g]$	Element geometric stiffness matrix
$[k_p]$	Element foundation shear layer stiffness matrix
$[k_{th}]$	Element thermal stiffness matrix
$[k_w]$	Element Winkler foundation matrix
$[m]$	Element mass matrix
$\{p\}$	Independent coefficient vector
$\{q\}$	Dependent coefficient vector
$\{\bar{u}\}$	Element displacement vector
$\{\hat{u}\}$	Nodal displacement vector
$\{\bar{u}_d\}, \{\bar{u}_r\}$	Deflection and Rotation vectors
$\{F\}$	Element load vector
$[\tilde{G}]$	Material constant matrix
$[K_c]$	Global centrifugal stiffness matrix
$[K_e]$	Global elastic stiffness matrix
$[K_{ef}]$	Global effective stiffness matrix
$[K_f]$	Global Pasternak foundation stiffness matrix
$[K_g]$	Global geometric stiffness matrix
$[K_p]$	Global foundation shear layer stiffness matrix
$[K_{th}]$	Global thermal stiffness matrix
$[K_w]$	Global Winkler foundation stiffness matrix
$[M]$	Global mass matrix
$\{R_{th}\}$	Thermal load vector
$\{\hat{U}\}$	Global nodal displacement vector

Greek symbols

α	Static load factor
α_0	Maximum twist angle
$\alpha(x)$	Twist angle
$\alpha(z)$	Coefficient of thermal expansion

β	Axial bending coupling parameter
β_d	Dynamic load factor
γ_{xz}	Shear strain
δ	Hub radius parameter
ε_{xx}	Axial strain
η_1, η_2	First mode and second mode non-dimensional frequencies
θ	Rotation of cross-section plane about z- axis
λ	Shear-bending coupling parameters
ν	Rotational speed parameter
$\rho(z)$	Density of material
σ_{xx}	Axial stress
τ_{xz}	Shear stress
ϕ	Rotation of cross-section plane about y- axis
φ	Increase in twist angle per unit length
ω	Natural frequency
$\bar{\omega}$	Angular velocity of beam
ΔT	Steady temperature change
Ω	Frequency of axial load
$[N(x)]$	Shape function matrix

CHAPTER 1

BACKGROUND AND MOTIVATION

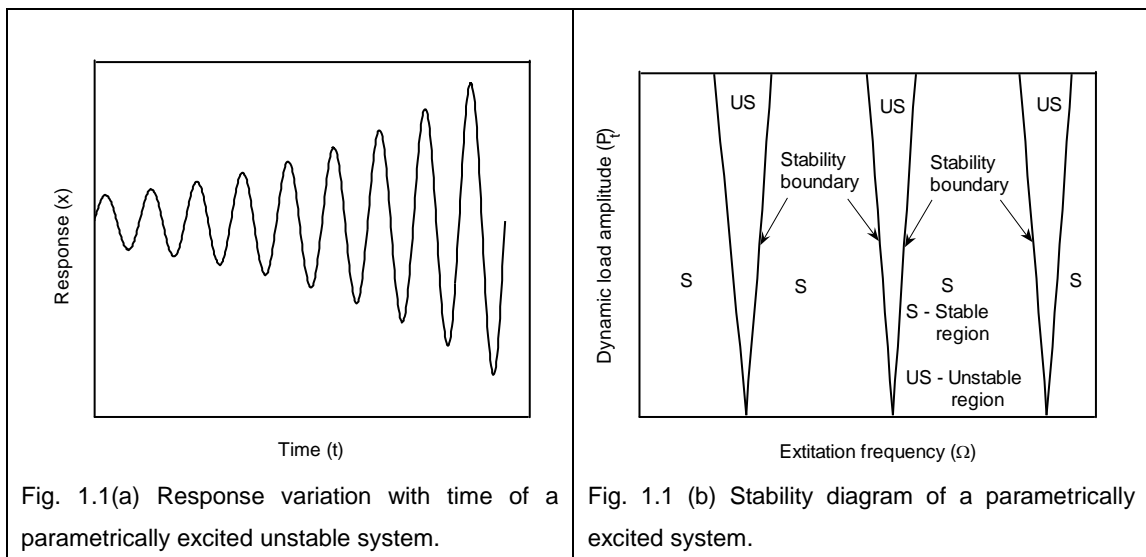
1.1 Introduction

Many failures of engineering structures have been attributed to structural instability, in which large deformations of the structures are observed. It is the nature of loading that characterizes the nature of the problem of structural stability to be solved. The loading may be either static or dynamic. The static loads are dead loads, which don't change their direction during the process of deformation caused by them. In contrary, the dynamic loads are dependent on time, and may change their direction. Moreover, the dynamic loadings on structures can either be deterministic or random. The deterministic loading may consist of either a harmonic function or a superposition of several harmonic functions, such as the excitation arising from unbalanced masses in rotating machinery. In engineering applications, loadings are quite often random forces, for example, those from earthquakes, wind, and ocean waves, in on-shore and off-shore structures. These forces can be described satisfactorily in probabilistic terms. There are also engineering systems which are subjected to loadings that contain both periodic components and stochastic fluctuations. An example of such a system is the uncoupled flapping motion of rotor blades in forward flight under the effect of atmospheric turbulence.

Very often elastic systems are loaded in such a way that the excitations appear as forcing terms on the right side of the equations of motion of the systems. The phenomenon of ordinary or main resonance occurs when the excitation frequency coincides with the natural frequency of the systems. The response

amplitudes that grow linearly with time can be reduced by damping. When the externally applied loads on an elastic system appear as coefficients or parameters in the equations of motion, the system is called a parametrically excited system and the instability is called as parametric instability or parametric resonance. The phenomenon of parametric resonance which is of practical importance occurs when the excitation frequency is equal to twice the natural frequency. Parametric resonance is characterized by an unbounded exponential build up of the response even in the presence of damping. Fig. 1.1 (a) shows the variation of the response with time of a dynamically unstable system under parametric excitation. Moreover the parametric instability occurs over area in parameter space rather than at discrete excitation frequencies as in the case of ordinary resonance.

One of the main objectives of the analysis of parametrically excited systems is to establish the regions in the parameter space in which the system becomes unstable. These regions are known as regions of dynamic instability. The boundary separating a stable region from an unstable one is called a stability boundary. Plot of these boundaries on the parameter space i.e. dynamic load amplitude, excitation frequency and static load component is called a stability diagram. Figure 1.1(b) shows a typical stability diagram. The dynamic load component is the time dependent component of the axial force. It can be seen from the figure that the



instability of the system doesn't occur at a single frequency rather occurs over a range of frequencies which makes the parametrically excited systems more dangerous than ordinary resonant systems. Moreover, as the amplitude of the time dependent component of the axial force increases the range of frequencies over which the system becomes unstable increases. The location of the unstable region

nearer to the dynamic load axis indicates that the system is more prone to dynamic instability, as the instability occurs at lower excitation frequencies. Similarly if the unstable region is located farther from the dynamic load axis, it indicates that the system is less prone to dynamic instability. If the area of the instability region is large, it indicates instability over a wider frequency range. Hence if the instability region shifts towards the dynamic load axis or there is an increase in its area, the instability of the system is said to be enhanced and when contrary to it happens, the stability is said to be improved.

Functionally graded materials (FGMs) consisting of two or more dissimilar materials possess properties which vary continuously with respect to spatial coordinates. The material properties of an FGM [162] can be designed by varying the volume fractions of its constituent phases along spatial coordinates so as to improve the strength, toughness and high temperature withstanding ability. FGMs are regarded as one of the most promising candidates for advanced composites in many engineering sectors such as aerospace, aircraft, automobile, defence, biomedical and electronic industries. Now a days FGMs are being preferred over traditional composites due to the fact that FGMs ensure smooth transition of stress distributions, minimization or elimination of stress concentration, and increased bonding strength along the interface of two dissimilar materials. Also, improved fracture toughness can be achieved by using an FGM at the interface. As the applications of FGMs are gaining increasing importance in the aforesaid sectors, wherein, these components are subjected to vibration and instability, a thorough investigation of the effect of FGM on vibration and instability characteristics of the structures may be worth of a research work.

1.2 Need for the research

Laminated composite materials attract the attention of designers due to their characteristics of high stiffness and strength to weight ratio. But they suffer an inherent problem of de-bonding and de-lamination resulting from large inter-laminar stress. FGMs having gradual variation of properties are out of the problems of laminated composite materials and can replace them successfully. The conventional armours are manufactured having compromised with toughness. FGMs can be used for manufacturing modern armours without compromising with hardness of ceramics and toughness of metals. These materials can also be used as ultrahigh temperature resistant materials for various engineering applications such as aircraft, space vehicles, engine combustion chamber and fusion reactors. FGMs with continuous

variation of thermo-mechanical properties possess various advantages over the conventional composite laminates, such as smaller thermal stresses, and stress concentrations. FGM can be used as a thermal barrier coating to improve the performance. FGMs as thermal barrier coating are attractive due to the potential for a reduction in thermal stresses, avoiding de-lamination and spallation tendencies and prevention of oxidation. FGM coating may result in a multifold increase in the resistance to thermal fatigue compared to a conventional counterpart. Many primary and secondary structural elements, such as helicopter rotor blades, turbine blades, robot arms and space erectable booms, can be idealised as beams. The vibration and stability analysis of FGM beams represents, therefore, an interesting and important research topic.

1.3 Research objective

Though FGMs have many potential applications in various engineering fields, it may pose difficulties in manufacturing and design. It is important to overcome them by developing proper understanding of mechanics of these materials. In this direction, Chapter 2 describes the efforts devoted by various researchers to reinforce the stand of FGMs as one of the fittest candidates for several applications. Exhaustive literature review reveals that vibration and dynamic stability of FGM is moderately explored. In this direction, present work emphasises on the study of dynamic behaviour of functionally graded ordinary (FGO) and functionally graded sandwich (FGSW) beams to understand the phenomenon of parametric resonance and make FGMs reliable and predictable in their applications.

Based on these guiding principles, the objectives of present research are as follows:

- Study on the effect of different property distribution laws on critical buckling load, natural frequencies and dynamic instability zones of FGO and FGSW beams.
- Investigation on the effect of property distribution laws, foundation stiffness and shear layer interaction on the critical buckling load, natural frequencies and dynamic instability zones of FGO and FGSW beams supported on foundation.
- Determination of effect of various property distribution laws and thermal environment on the critical buckling load, natural frequencies and dynamic instability of FGO and FGSW beams in high temperature environment.

- Study on the effect of different property distribution laws, rotational speed, and hub radius on critical buckling load, natural frequencies and dynamic instability of rotating FGO and FGSW beams.
- Study on the effect of different property distribution laws, static load component and pre-twist angle on critical buckling load, natural frequencies and dynamic instability of pre-twisted FGO beam.

1.4 Thesis outline

The remainder of this thesis is organized as follows:

- Chapter 2: Literature review.
It includes a literature review to provide a summary of the base of knowledge already available involving the issues of interest.
- Chapter 3: Dynamic stability of functionally graded Timoshenko beam under parametric excitation.
This part of the thesis includes an analysis involving critical buckling load, free vibration and dynamic stability of a functionally graded Timoshenko beam having properties along thickness of beam according to exponential and power law.
- Chapter 4: Dynamic stability of functionally graded Timoshenko beam on elastic foundations under parametric excitation.
This chapter presents the study of static buckling load, vibration and dynamic stability of functionally graded Timoshenko beam resting on Winkler's and Pasternak elastic foundations.
- Chapter 5: Dynamic stability of functionally graded Timoshenko beams in high temperature environment under parametric excitation.
It presents vibration and dynamic stability study of functionally graded Timoshenko beam in thermal environment.
- Chapter 6: Dynamic stability of rotating functionally graded Timoshenko beam under parametric excitation.
The chapter involves the study of effect of the hub radius, rotary inertia and angular speed of functionally graded rotating Timoshenko beams on their dynamic stability.
- Chapter 7: Dynamic stability of pre-twisted functionally graded Timoshenko beam under parametric excitation.
This chapter deals with the study of dynamic stability of pre-twisted functionally graded Timoshenko beam.
- Chapter 8: Conclusion and scope for future work.
The conclusion and scope for future work are given in this part of thesis.

1.5 Closure

Present chapter provides a food for thought of an advanced material suitable for numerous applications.

- A material advantageous over composite materials having distinct interface.
- A material, the properties of constituent phases of which can be utilized fully without any compromise.
- A material suitable in application of extreme operating conditions.
- A material having improved residual stress distribution.
- A material with higher fracture toughness and reduced stress intensity factor.

The above characteristics provide the scope for various potential applications. To have an understanding of the static and dynamic response of these materials, research objective along with the work outline is presented in this chapter.

In next chapter, the literature review is presented through exhaustive study.

CHAPTER 2

LITERATURE REVIEW

2.1 Introduction

The first scientist to observe the parametric resonance was Faraday [49] in 1831 who could notice the oscillation of wine at half the frequency of containing glass. Melde [103] in 1859 generated parametric oscillations in a string by employing a tuning fork to periodically vary the tension at twice the resonance frequency of the string. The work of Rayleigh [148-150] on parametric oscillations is worth reading for researchers. Beliaev [18] presented a theoretical analysis for parametric instability of prismatic rods. Alexanderson [5] was the first to use parametric amplifiers for radio telephony from Berlin to Vienna and Moscow.

The literature is classified into an assortment of sections dealing with development of theory of parametric resonance as presented in section 2.1. The section 2.2 presents some review works describing an exhaustive amount of literature on vibration and dynamic stability of structural components made of alloys, composites and FGMs. Section 2.3 describes briefly about the classifications of parametric resonances. The various methods which have been used to study about the parametric instability are explained in section 2.4. The next section gives the reported literatures describing the effects of various parameters on vibration and dynamic stability of structures especially beams. Finally in section 2.6, chapter is concluded by summarizing the advancement taken place in the chosen area and possible literature gap so that relevance of the present study can be emphasized.

2.2 Review of literature

Several researchers have contributed a lot towards the study of parametric resonance by presenting a good amount of literature already reported. Evan – Iwanowski [47] has presented a review of researches carried out on parametric resonance of structures. Ibrahim and co-workers [64-70] have provided an

exhaustive amount of work carried out by various eminent researchers on linear as well as non-linear parametric vibration of both deterministic and stochastic type. Ariaratnam [9] and Simitzes [139] have given an extensive account of literature on vibration and stability of parametrically excited systems. Nakra [109-111] has provided a good account of literature on vibration control by viscoelastic materials. An exhaustive review work on FGM encompassing its various aspects like stress, stability, manufacturing and design, applications, testing, and fracture is given by Victor [159] and his co-workers. Moreover, books by Bolotin [21], Schmidt [134] and Nayfeh and Mook [112] deals extensively on the basic theory of dynamic stability of systems under parametric excitations.

2.3 Classification of parametric resonance

A system with multi degree of freedom can exhibit simple resonance, sum type or difference type resonance depending on the type of loading, support conditions and system parameters.

Mettler [103] presented a classification for various types of resonances exhibited by linear periodic system. Iwatsubo and his co-workers [72-73] maintained that uniform columns with simple supported ends would not exhibit combination type resonances. Saito and Otomi [129] found that viscoelastic beams with viscoelastic support did not exhibit combination resonances of difference type for axial loading, but those did exhibit the aforesaid resonance for tangential type of loading. Celep [29] working on stability of simply supported pre-twisted column found that combination resonances of the sum type may exist or disappear depending on the pre-twist angle and rigidity ratio of the cross-section. "Elastic shaft with a disk can exhibit only difference type combination resonance" was revealed by Ishida et al. [71]. Chen and Ku [35] studied the effect of the gyroscopic moment on the principal region of instability of a cantilever shaft disk system.

2.4 Methods of stability analysis of parametrically excited systems

Parametrically excited systems are represented by second order differential equations with periodic coefficients. The exact solutions for these systems are not available. The researchers have always been interested to explore the existence of periodic solutions and their stability. Several methods have been applied for the solutions of the governing equations of parametrically excited systems. The most common among them are method proposed by Bolotin based on Floquet's theory, perturbation and iteration techniques, the Galerkin's method, the Lyapunov second method and the asymptotic technique by Krylov, Bogoliubov and Mitroploskii.

Bolotin's [21] method based on Floquet's theory is suitable for simple resonance only. Burney and Jaeger [24] used this method to determine the region of dynamic instability of a uniform column subjected to different end conditions. They assumed the column to be consisting of different segments, each segment being considered as a massless spring with lumped masses. Piovan and Machado [118] have used the method to determine dynamic instability regions of a functionally graded thin-walled beam subjected to heat conduction. Machado et al. [100] have also used the Bolotin's method for the parametric instability of a thin-walled composite beam. This method has been modified by Steven [147] for systems with complex differential equations of motion. Hsu [58-59] proposed an approximate method of stability analysis of systems having small parameter excitations. Hsu's method can be used to obtain instability zones of main, combination and difference types. Later Saito and Otomi [129] modified Hsu's method to suit systems with complex differential equations of motion. Ray and Kar [124] used the modified Hsu's method for the parametric instability analysis of a sandwich beam. Chung and Chen [39] also used this method to investigate the effect of core thickness, shear parameter, core loss factor and stiffness of constraining layer on the unstable region of a spinning pre-twisted sandwich beam with a constrained damping layer. Takahashi [153] has proposed a method free from the limitations of small parameter assumption. This method establishes both the simple and combination type instability zones. Lau et al. [84] proposed a variable parameter increment method, which is free from limitations of small excitation parameters. It has the advantage of treating non-linear systems.

Most of the recent works on parametric instability have been done by using finite element method (FEM). Brown et al. [23] studied the dynamic stability of uniform bars by applying this method. Abbas and Thomas [1] used finite element method to study the dynamic stability of beams for different end conditions. Shastry and Rao [135-136] plotted the stability boundaries for a cantilever column acted upon by an intermediate periodic concentrated load for various load positions. The parametric instability behaviour of a non-prismatic bar with localized zone of damage and supported on an elastic foundation was studied by Dutta and Nagraj [43] using finite element analysis. Svensson [153] applied this method to investigate the stability properties of a periodically loaded non-linear dynamic system, giving special attention to damping effects. Ozturk and Sabuncu [116] have used finite element method to study the dynamic stability of beams on elastic supports. Mohanty [105] used this method to study the effect of localised damage on the dynamic stability of a

pretwisted cantilever beam. Chen [37] employed the method of finite element to study the influence of spinning speed, twist angle and aspect ratio on the dynamic instability zone of a spinning twisted Timoshenko beam. Mohanty et al. [106, 107] have investigated the static and dynamic behaviour of functionally graded Timoshenko beams using this method also. Tylikowski [158] derived stochastic stability criteria for a first order shear deformable beam using the Liapunov direct method. The effect of shear deformation, rotary inertia and the gain factors on dynamic stability was predicted. The dynamic response of eccentrically pre-stressed viscoelastic Timoshenko beam under a moving harmonic load was studied by Kocaturk and Simsek [83] using Lagrange equation.

2.5 Effect of system parameters

2.5.1 Effect of property distribution along coordinates

Santare and Lambros [133] have developed integral finite elements to estimate the dynamic characteristics of elastic-viscoelastic composite (EVC) structures such as sandwich beam, plate and shell structures with viscoelastic material as core layer. Paulino and Jin [117] have made an attempt to show that the correspondence principle can be applied to the study of viscoelastic FGM under the assumption that the relaxation moduli for shear dilation are separable functions in space and time. Chakraborty et al [30] have developed a beam finite element to study the thermoelastic behaviour of functionally graded beam structures with exponential and power law variation of material properties along thickness. Zhu and Shankar [171] have developed a method to solve two-dimensional elasticity equations for an FGM beam. The Fourier series method along with Galerkin method is used for the analysis. It has been shown that the choice of polynomial for the variation of properties along the direction of thickness enables the method to be applied to the functionally graded structures with arbitrary variation of properties. Chaofeng et. al, [31] have investigated the stress distribution in thick FGM beam subjected to mechanical and thermal loads with arbitrary end conditions. Nirmala et al. [113] have derived an analytical expression to determine the thermoelastic stresses in a three layered composite beam system having an FGM as the middle layer. It has been shown that the method can be applicable where the gradation of the FGM is such that it may not be possible to express the volume fraction changes of the FGM constituents as a function of spatial coordinates. Moreover, the method can be useful where more than one layer of FGMs are used in a single composite beam structure as stated by the authors. Bhangale and Ganeshan [20] have studied

the static and dynamic behaviour of FGM sandwich beam in thermal environment having constrained viscoelastic layer using finite element method. It is found that materials with lower thermal coefficient of expansion possess high thermal buckling temperature. The critical buckling temperature for an FGM sandwich beam increases as the value of power law index increases. Li [92] has developed a unified approach to analyze static and dynamic behaviour of FGM beam of Timoshenko, Euler-Bernoulli and Rayleigh type. A single governing differential equation for an FGM Timoshenko beam has been derived from which the governing equation for Rayleigh as well as for Euler-Bernoulli beam can be deduced analytically. Salai et al, [131] have presented a theoretical analysis of FGM beams using sigmoid function. Aydogdu and Taskin [13] studied free vibration analysis of functionally graded beams with simply supported edges. Kapuria et al, [78] have used zigzag theory to investigate both the static and dynamic behaviour of beams made of FGM such as Al/SiC and Ni/Al₂O₃ for different end conditions. Free and forced vibration of a functionally graded beam subjected to a concentrated moving harmonic load was investigated by Simsek and Kocatürk [143]. The effects of material properties and inertia of the moving load on the dynamic behaviour of an FGM beam were studied by Khalili et al. [81] using a mixed Ritz-DQ method. Simsek [140-142] presented the dynamic analysis of FGM beams using different higher order theories. Akhtar and Kadoli [4] presented the static behaviour of various FGM beams. Emam [45] investigated the static and dynamic response of imperfect composite beams considering imperfection as control parameter. A detailed parametric study was conducted by Ke et al. [80] to study the influences of crack depth, crack location, material property gradient, and slenderness ratio on the postbuckling behaviour of cracked FGM beams. Arnaldo and Richard [11] have studied the effect of functionally graded materials on resonance of bending shafts under time dependent axial loading. It is observed that metal-ceramic FGM beams show substantial improvement in parametric resonance compared to metallic beams. Aminbaghai et al. [8] have carried out the modal analysis of second order shear deformable FGM-beams considering property variations in both transverse and longitudinal directions.

2.5.2 Effect of foundation

Ahuja and Duffield [3] studied the dynamic stability of beams having variable cross-sections and resting on elastic foundation. The effect of elastic foundation was found to have a decreasing effect on the width of the instability regions and the amplitude of parametric response. The authors had also conducted experiments to verify their results. Eisenberger and Clastronik [44] studied the dynamic stability of

beams on elastic foundation. Engel [46] investigated the dynamic stability of bars on elastic foundation with damping. It was found that the critical mode becomes a higher mode instead of fundamental mode when the foundation parameter had exceeded a certain value. Lee and Yang [88] and Matsunaga [102] investigated the dynamic behaviour of Timoshenko beams resting on elastic foundations. Morfidis [108] developed stiffness and transfer matrices and load vectors of Timoshenko beam resting on Kerr type 3-parameter elastic foundation. Pradhan and Murmu [121] investigated the effect of various parameters on the dynamic response of FGM beams resting on variable elastic foundation. The chosen parameters were temperature distribution, power law index, variable Winkler foundation modulus, elastic foundation modulus and the normalized core thickness. Aminbaghai et al. [7] have studied free vibration of multilayer FGM beams under longitudinal variable elastic foundation with effect of large axial force.

2.5.3 Effect of thermal environment

Sladek et al. [144] have developed an efficient numerical method to calculate the fracture parameters such as stress intensity factor and T-stresses of a functionally graded orthotropic beam subjected to thermal and impact mechanical load. The fact that getting fundamental solution for non-homogeneous anisotropic and linear elastic solid is very difficult can be circumvented by using the proposed local integration method. Huang et al. [61] investigated the bending problem of a functionally graded anisotropic beam subjected to thermal and uniformly distributed load using a polynomial stress function. Jian and Li [76] have investigated the static and the active vibration control of a piezothermoelastic composite beam using a finite element model. The dynamic behaviour of a rotating thin-walled blade made of functionally graded material under high temperature supersonic flow has been investigated by Fazelzadeh et al. [50] using differential quadrature method (DQM). Accurate results have been obtained using only a few grid points with consequent low computational expense. It has been seen from the equation of motion that DQM can be applied to the analysis of damped vibration. Jurij and Maks [77] have investigated the effect of thermal load on the natural frequencies of simply supported beam and clamped beam. They have applied the theory of vibration and statistical thermodynamics simultaneously for the purpose. A study of thermal buckling and vibration of sandwich beam with composite facings and viscoelastic core is carried out by Pradeep et al. [120]. Evandro and Joao [48] have used finite element method to evaluate nonlinear response of structures subjected to thermo-mechanical loading. A beam made up of functionally graded material simply supported at both the ends

and subjected to lateral thermal shock loads is investigated by Babai et al. [14]. It is found that there is an optimum value of power law index for which the beam's lateral deflection is the minimum. In addition the amplitude of lateral vibration increases considerably as the aspect ratio of the beam decrease. The effect of coupling is to decrease the amplitude of vibration and increase the frequency of the vibration. Guo et al. [56] have investigated the coupled thermoelastic vibration characteristics of axially moving beams using differential quadrature (DQ) method. The effects of the dimensionless coupled thermoelastic factor, the ratio of length to height, the dimensionless moving speed on the stability of the beam are analyzed. The bending response of sandwich plates subjected to thermomechanical loads is studied by Zenkour and Alghamdi [170]. Mahi et al. [101] have studied the free vibration of functionally graded beams with temperature dependent properties. The effects of material constants, transverse shear deformation, temperature-dependent material properties, in-plane loading and boundary conditions on the nonlinear behaviour of FGM beams are investigated by Ma and Lee [99] using a shooting method. Chen and Levy [34] studied the effect of temperature on frequency, loss factor and control of a flexible beam with a constrained viscoelastic layer and shape memory alloy layer. Piovan and Machado [109] have explored the influence of longitudinal vibration on the dynamic stability of functionally graded thin-walled beams allowing for shear deformability. The effects of material composition, temperature dependent properties, slenderness ratio on thermal buckling and vibration of functionally graded beams are investigated by Wattanasakulpong et al. [163]. The third order shear deformation theory is considered by the authors.

2.5.4 Effect of rotation

Stafford and Giurdiutiu [146] have developed a simplified model of helicopter blade considering shear deformation and rotary inertia corrections and investigated the natural frequencies using transfer matrix method. Yoo and Shin [167] have used Rayleigh-Ritz method to determine the effect of gyroscopic couple on the natural frequencies of rotating cantilever beam. They have also computed the tuned angular velocity of the beam. Chung and Yoo [38] investigated the effect of angular speed on the natural frequency of a rotating cantilever beam. They have used finite element method considering stretch deformation of the beam. Different models for investigation of rotating cantilever beams are compared by the authors. Telli and Kopmaz [157], Sabuncu and Evran [125] have studied static and dynamic stability of a blade having asymmetric aerofoil cross-section subjected to an axial periodic force using the finite element method. The effects of shear deformation and rotary inertia

are included in the analysis. It is found that as the length of the beam decreases, the effect of rotation on the static buckling load parameters decreases and the effects of coupling and the shear coefficient on the stability become significant. Yoo et al. [166] have investigated the flap-wise bending vibration analysis of a rotating multi-layered composite beam considering the shear deformation and the rotary inertia effects. Kaya [79] has studied the flapwise bending vibration analysis of a rotating cantilever Timoshenko beam using Differential transform method. Vinod et al. [161] have formulated an approximate spectral element for uniform as well as tapered rotating Euler-Bernouli beam in order to carry out both free vibration and wave propagation analysis. A super element having shape functions as a combination of polynomials and trigonometric functions is used by Gunda et al. [55] to study the dynamic analysis of rotating tapered beams. Comparable results are obtained using one super element with only 14 degrees of freedom compared to 50 conventional finite elements with cubic shape functions with a total of 100 degrees of freedom for a rotating cantilever beam. Bazoune [17] has investigated the problem of free vibration of a rotating tapered beam by developing explicit expressions for the mass, elastic and centrifugal stiffness matrices in terms of the taper ratios. Lesaffre et al. [90] have done the stability analysis of rotating beams using the Routh-Hurwitz criterion. Lee and Sheu [87] have developed an exact power-series solution for free vibration of a rotating inclined Timoshenko beam. It is shown that both the extensional deformation and the Coriolis force have significant influence on the natural frequencies of the rotating beam when the dimensionless rotating extension parameter is large. The effects of Mach number, rotating speed, geometric parameters and material properties on the natural frequencies are examined. Das et al. [41] have studied the large displacement free vibration analysis of linearly tapered rotating beam. Ouyang and Wang [115] have presented a dynamic model for the vibration of a rotating Timoshenko beam subjected to a three-directional load moving in the axial direction. Attarnejad and Shahba [12] have studied free vibration of non-prismatic rotating Euler-Bernoulli beams using differential transform method. The effects of rotational speed parameter and taper ratio on natural frequencies have been investigated. Lin et al. [96] have modelled the blade of a horizontal-axis wind power turbine as a rotating Bernoulli-Euler beam with pre-cone angles and setting angles. The influences of the pre-cone angle, the angular speed and the setting angle on the natural frequencies of the beam are explored. The phenomenon of divergence instability is also discussed. A rotating beam finite element is developed by Gunda and Ganguli [54] in which the basis functions are obtained by the exact solution of the governing static homogenous differential equation of a stiff string. Piovan and

Sampaio [119] have developed a rotating non-linear beam model accounting for arbitrary axial deformation to study the dynamics of rotating beams made of FGM. Yuksel and Aksoy [169] have studied bending vibrations of a radially rotating beam with end mass subjected to different base excitations using the Lagrangian's approach. Ahmad and Naeem [2] have investigated the vibration characteristics of rotating FGM cylindrical shells using Budiansky and Sanders, thin shell theory. Hosseini and Khadem [57] have used multi-scale method to investigate free vibration analysis of simply supported rotating shaft with nonlinear curvature. Huang et al. [61] have provided a power series solution to free vibration of rotating inclined Euler beam. Divergence instability and vibration of a rotating Timoshenko beam with pre-cone and pitch angles are investigated by Lee et al. [86]. Yardimoglu [164] has used a finite element model based on the coupled displacement field for vibration analysis of rotating Timoshenko beam of equal strength. Chattopadhyay et al. [32] developed a composite box beam model to investigate the behaviour of helicopter rotor blades built around the active box beam. Piezoelectric actuators and sensors which were surface bonded at the walls of the composite beam were found to have significantly reduced the deflection along the span of box beam.

2.5.5 Effect of pre-twist angle

Jensen [74] used perturbation technique to analyse free vibration of thin rectangular plate with small pre-twist. The author used shell theory for the purpose and observed that the effect of pre-twist angle depended on the geometry of the plate. Subrahmanyam and Rao [152] applied Reisner method to study the vibration of tapered pre-twisted cantilever beam. Liao and Huang [93] investigated the effect of pre-twist angle, spinning speed and steady-state part of end axial force on the instability zone of a cantilever beam. Onipede and Dong [114] studied vibration of pre-twisted inhomogeneous beam of arbitrary cross-section by using variational method. Dynamic instability of a pre-twisted beam due to both the summed and difference type resonances is studied by Tan et. al. [155]. It is observed that the narrower regions flutter instability separate the stable critical speed zones into smaller stable sub-regions. The authors [156] also investigated the dynamic instability zones of a spinning pre-twisted beam. The multiple scale method was used to determine the regions of instability due to the resulting parametric excitations. As the spin speed varied within the stable sub-regions, consistent shifts and widening of unstable regions due to axial load perturbation were observed. Widths of the unstable regions were found to decrease with decreasing pre-twist angle and compressive axial force as well as increasing aspect ratio towards unity. Vibration

and stability of a spinning pre-twisted thin walled composite beam were studied by Song et al. [145] considering a number of non-classical features such as transverse shear, anisotropy and pre-twist. Vielsack [160] has shown that the influence of small pre-twist on lateral vibration of beams depends on the ratio of bending stiffness about principal axes. It is observed that the deep-webbed beams are mostly affected. Lin et. al. [97] have studied the coupled bending–bending vibration of a rotating pre-twisted beam with an elastically restrained root and a tip mass, subjected to the external transverse forces and rotating at a constant angular velocity. Young and Gau [168] have investigated the dynamic stability of a spinning pre-twisted beam subjected to random axial force by using stochastic averaging method along with mean square stability criterion. The effect of pre-twist angle of an aerofoil blade simplified as a rotating Euler as well as Timoshenko beam has been investigated by Subuncu and Ervan [127-128] using finite element method. Jhung and Jo [75] have studied the vibration characteristics of a rectangular twisted beam with pins surrounded with liquid and the safety assessment of the potential for fretting-wear damages caused by foreign particles. Mohanty [105] has studied parametric instability of pre-twisted cantilever beam with localized damage. The effects of various parameters such as shroud dimensions, pre-twist angle, stagger angle, rotational speed and distance of shear centre from the centroid on the stability of the rotating pre-twisted blade packets of aerofoil cross-section are investigated by Sakar and Sabunku [130] using finite element method. Hsu [60] has investigated dynamic behaviour of pre-twisted beams using spline collocation method. Liu et al. [98] have carried out an investigation on the coupled axial-torsional vibration of pre-twisted beams. Leung and Fan [91] have studied the influence of multiple kinds of initial stresses due to compression, shears, moments and torque on the natural vibration of pre-twisted straight beam based on the Timoshenko theory. Chen [36, 37] has found the influence of thickness-to-width ratio, twist angle, spinning speed and axial load on the natural frequency, buckling load and instability zone of a pre-twisted Timoshenko beam by using finite element method.

2.6 Closure

This chapter provides the insight into various past developments in the area of structural mechanics. For the sake of simplicity, it is divided into six main sections. In section 2.2, a review of literature on parametric resonance is presented. Section 2.3 depicts a brief classification of parametric resonance. Various methods used by several researchers for the analysis of dynamic stability are described in section 2.4. The section 2.5 is devoted to the findings regarding the effect of various system

parameters on vibration and stability of structural elements. The effect of spatial variation of properties on the static and dynamic behaviour is explained in section 2.5.1. The effect of foundation stiffness on natural frequencies and instability zones is presented in section 2.5.2. The interaction of the shear layer is also described. The section 2.5.3 presents an exhaustive review of literature on vibration and stability of structures in thermal environment. Turbine blades, helicopter blades are idealised as rotating cantilever beams. The influence of rotating speed and hub radius on dynamic response is given in section 2.5.4. The blades are twisted as a functional requirement. The vibration and stability of pre-twisted beams are presented in section 2.5.5. The effect of pre-twist on natural frequencies and instability zones are revealed. It is observed from the reported literature that a great deal of work is done on dynamic stability of structural components made of metals, alloys and composites. Also a good account of research on vibration of structural elements made of FGMs has been carried out. But the amount of work done on dynamic stability of FGM beams is found to be very less as realized from the reviewed literature. Therefore, it may be concluded in this section that dynamic stability study of FGM beams remains an open problem to be taken up.

CHAPTER 3

DYNAMIC STABILITY OF FUNCTIONALLY GRADED TIMOSHENKO BEAM UNDER PARAMETRIC EXCITATION

3.1 Introduction

The dynamic stability of structures is a subject of considerable engineering importance and many investigations have been carried out in this regard. The study of behaviour of functionally graded materials (FGMs) has been an interesting topic of considerable research interest during the past decade. The intensity and rapid growth of research on this class of materials is actually due to their continuously varying material properties, which give great advantages over the conventional homogeneous and layered materials. The weakness of conventional laminated composite materials, such as debonding, huge residual stress, locally large plastic deformations can be eliminated by using FGM. FGMs are regarded as one of the most promising candidates for advanced composites in many engineering sectors such as the aerospace, aircraft, automobile and defence industries and most recently the electronic and the biomedical sectors. Application of FGM is gaining increasing importance in the aforesaid sectors, wherein, these components are subjected to vibration and dynamic stability. The blades of turbine, helicopter and spacecraft, rail etc. can be modelled as beams to investigate their dynamic behaviour.

Iwatsubo et al. [73] have calculated the regions of instability for columns by solving Mathieu equations obtained by applying Galerkin method to governing

equations of motion. The effects of internal and external damping on stability of the column are also determined. Abbas and Thomas [1], Aristizabal-Ochoa[10], Briseghella et. al. [22] and Ozturk and Sabuncu [116] have used finite element method to study the dynamic stability of beams. Shastry and Rao [137] have compared the stability parameter of simply supported beam and clamped beam for different locations of two symmetrically placed intermediate supports. It is found that the stability parameter of simply supported beam approaches that of clamped beam when the intermediate supports are placed at a distance equal to one eighth of beam length from ends. Zhu and Shankar [171] have developed a method to solve two-dimensional elasticity equations for an FGM beam. Fourier series method along with Galerkin method is used for the analysis. It has been shown that the choice of polynomial for the variation of properties along the direction of thickness enables the method to be applied to the functionally graded structures with arbitrary variation of properties. Lim et al. [95] have studied the static failure modes and load capabilities of foam core composite sandwich beams both analytically and experimentally. Li [92] has developed a unified approach to analyze static and dynamic behaviour of FGM beam of Timoshenko, Euler-Bernoulli and Rayleigh type. A single governing differential equation for an FGM Timoshenko beam has been derived from which the governing equation for Rayleigh as well as for Euler-Bernoulli beam can be deduced analytically. Babai et al. [14], Gharib et al. [52], and Benatta et al. [19] have studied the static response of a functionally graded beam under external excitation. Salai et al. [131] have presented a theoretical analysis of FGM beams using sigmoid function. Kapuria et al. [78] have used zigzag theory to investigate both the static and dynamic behaviour of beams made of FGM such as Al/SiC and Ni/Al₂O₃ for different end conditions. Alshorbagy et al. [6] have studied the dynamic characteristics of a functionally graded Euler-Bernoulli beam applying principle of virtual work. Several models have been compared by Giunta et al [53] for the free vibration analysis of functionally graded beams. Multiple time scale solutions are presented by Shooshtari and Rafiee [138] to study the nonlinear forced vibration of a beam made of symmetric functionally graded (FG) materials based on Euler–Bernoulli beam theory and von Kármán geometric nonlinearity. Arnaldo and Richard [11] have studied the effect of functionally graded materials on resonance of bending shafts under time dependent axial loading. It is observed that metal-ceramic FGM beams show substantial improvement in parametric resonance compared to metallic beams. The effects of material composition, temperature dependent properties, slenderness ratio on thermal buckling and vibration of functionally graded beams are investigated by Wattanasakulpong et al. [163]. The third order shear deformation theory is

considered by the authors. Aminbaghai et al. [8] have carried out the modal analysis of second order shear deformable FGM-beams considering property variations in both transverse and longitudinal directions.

It is learnt from the reported literature that FGMs [159] have scope for numerous applications in diversified fields. These materials should be predictable as regards their behaviour under parametric resonance before use in related applications. The present chapter is devoted to the study of dynamic stability of FGO and FGSW beams under parametric excitation.

3.2 Formulation

A functionally graded sandwich beam with top skin as alumina, bottom skin as steel and core as FGM is shown in figure 3.1(a). The beam, hinged at both the ends is subjected to a pulsating axial force $P(t) = P_s + P_t \cos \Omega t$, acting along its undeformed axis. The static component of the axial force is P_s . The amplitude and frequency of the dynamic component of the force are P_t and Ω respectively, and t is time. The coordinate system of a typical two noded beam element used to derive the governing equations of motion is shown in figure 3.1(b). The mid-longitudinal(x-y) plane is chosen as the reference plane for expressing the displacements as shown in figure 3.1(b).

The thickness coordinate is measured as z from the reference plane. Figure 3.1(c) shows the beam element with three degrees of freedom per node. The axial displacement, the transverse displacement, and the rotation of the cross-section are u , w and ϕ respectively.

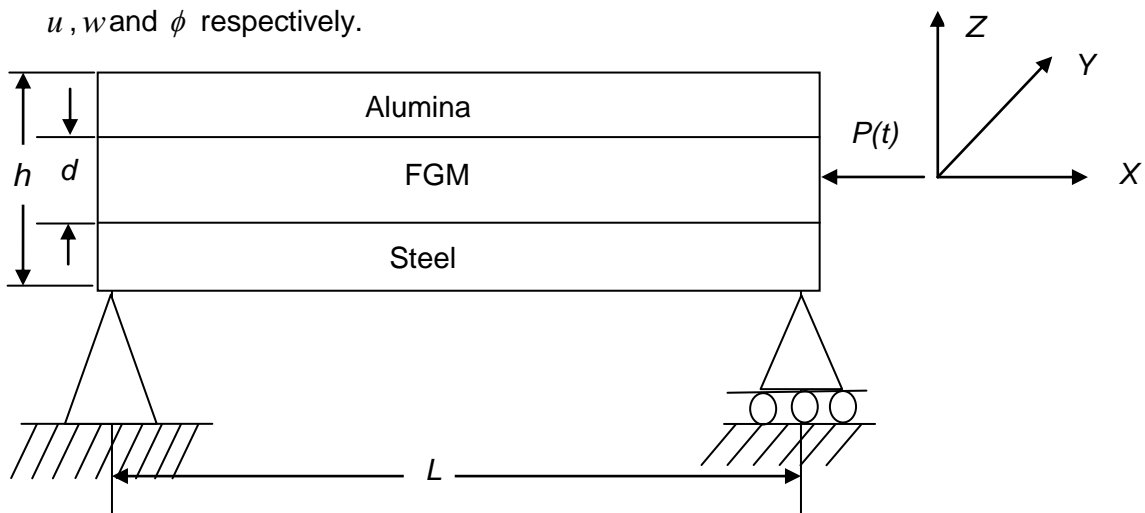


Figure 3.1(a) Functionally graded sandwich beam subjected to dynamic axial load.

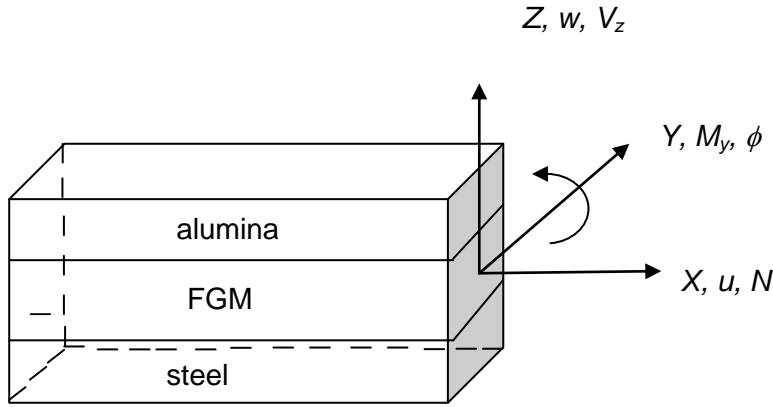


Figure 3.1(b) The coordinate system with generalized forces and displacements for the FGSW beam element.

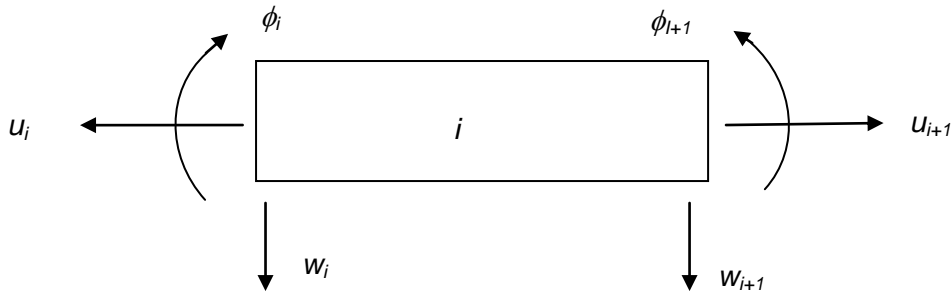


Figure 3.1(c) Beam element showing generalized degrees of freedom for i^{th} element.

The element matrices for the functionally graded sandwich (FGSW) beam element are derived following the method as proposed by Chakraborty et al. [30]. Moreover the same element can be used for the analysis of a functionally graded ordinary beam by making the thickness of the skins equal to zero.

3.2.1 Shape functions

The displacement fields considering first order shear deformation (Timoshenko beam theory) is expressed as

$$U(x, y, z, t) = u(x, t) - z\phi(x, t), \quad W(x, y, z, t) = w(x, t), \quad (3.1)$$

The corresponding linear strains are expressed as

$$\varepsilon_{xx} = \frac{\partial u}{\partial x} - z \frac{\partial \phi}{\partial x}, \quad \gamma_{xz} = -\phi + \frac{\partial w}{\partial x}. \quad (3.2)$$

The stress-strain relation in matrix form can be given by

$$\{\sigma\} = \begin{Bmatrix} \sigma_{xx} \\ \tau_{xz} \end{Bmatrix} = \begin{bmatrix} E(z) & 0 \\ 0 & kG(z) \end{bmatrix} \begin{Bmatrix} \varepsilon_{xx} \\ \gamma_{xz} \end{Bmatrix} \quad (3.3)$$

where σ_{xx} and ε_{xx} are normal stress and normal strains in x direction, τ_{xz} and γ_{xz} are shear stress and shear strain in x - z plane. $E(z)$, $G(z)$ and k are Young's modulus, shear modulus along thickness and shear correction factor respectively. The material properties of the FGM [82,162] that varies along the thickness of the beam are assumed to follow exponential law given by

$$R(z) = R_t \exp(-e(1-2z/h)), \quad e = \frac{1}{2} \log\left(\frac{R_t}{R_b}\right) \quad (3.4)$$

and power law given by

$$R(z) = (R_t - R_b) \left(\frac{z}{h} + \frac{1}{2}\right)^n + R_b, \quad (3.5)$$

where, $R(z)$ denotes a material property such as, E , G , ρ etc., R_t and R_b denote the values of the properties at topmost and bottommost layer of the beam respectively, and n is an index. The variation of Young's modulus along the thickness is shown in Figure 3.1(d) for different laws and other properties follow the same type of variation.

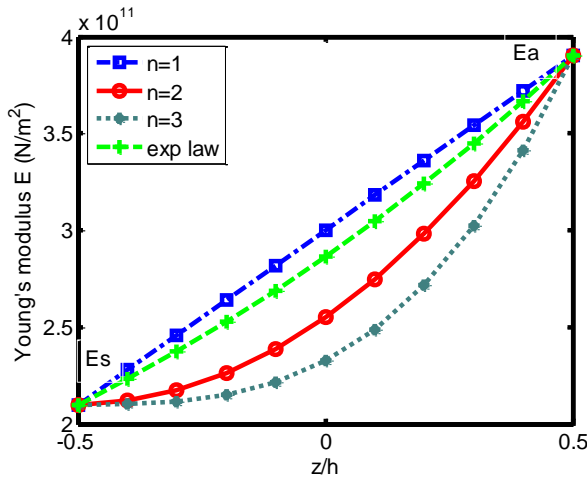


Figure 3.1(d) Variation of Young's modulus along the thickness of steel-alumina FGM with steel-rich bottom according to different laws.

The kinetic energy T and the strain energy S of the beam element can be expressed as

$$T = \frac{1}{2} \int_0^l \int_A \rho(z) \left[\left(\frac{\partial U}{\partial t} \right)^2 + \left(\frac{\partial W}{\partial t} \right)^2 \right] dA dx \quad (3.6)$$

$$S = \frac{1}{2} \int_0^l \int_A (\sigma_{xx} \varepsilon_{xx} + \tau_{xz} \gamma_{xz}) dA dx \quad (3.7)$$

Substituting eq. (3.1) into eq. (3.6) we get

$$T = \frac{1}{2} \int_0^l \int_A \rho(z) \left[\left(\frac{\partial u}{\partial t} \right)^2 + z^2 \left(\frac{\partial \phi}{\partial t} \right)^2 - 2z \left(\frac{\partial u}{\partial t} \right) \left(\frac{\partial \phi}{\partial t} \right) + \left(\frac{\partial w}{\partial t} \right)^2 \right] dA dx \quad (3.8)$$

Substituting eq. (3.3) and eq. (3.2) into eq. (3.7) subsequently we get

$$\begin{aligned} S &= \frac{1}{2} \int_0^l \int_A (E(z) \varepsilon_{xx}^2 + kG(z) \gamma_{xz}^2) dA dx \\ &= \frac{1}{2} \int_0^l \int_A E(z) \left[\left(\frac{\partial u}{\partial x} \right)^2 + z^2 \left(\frac{\partial \phi}{\partial x} \right)^2 - 2z \left(\frac{\partial u}{\partial x} \right) \left(\frac{\partial \phi}{\partial x} \right) \right] dA dx \\ &\quad + \frac{1}{2} \int_0^l \int_A kG(z) \left[\phi^2 + \left(\frac{\partial w}{\partial x} \right)^2 - 2\phi \frac{\partial w}{\partial x} \right] dA dx \end{aligned} \quad (3.9)$$

where, $\rho(z)$, l and A are density, length and area of cross-section of the element respectively. The governing differential equation can be derived by applying Hamilton's principle which states that

$$\delta \int_{t_1}^{t_2} (T - S) dt = 0 \quad (3.10)$$

The governing differential equations in terms of the degrees of freedom u , w and ϕ can be written as

$$\left. \begin{aligned} \frac{\partial(T-S)}{\partial u} &= I_0 \frac{\partial^2 u}{\partial t^2} - I_1 \frac{\partial^2 \phi}{\partial t^2} - A_{11} \frac{\partial^2 u}{\partial x^2} + B_{11} \frac{\partial^2 \phi}{\partial x^2} = 0, \\ \frac{\partial(T-S)}{\partial w} &= I_0 \frac{\partial^2 w}{\partial t^2} - A_{55} \left(\frac{\partial^2 w}{\partial x^2} - \frac{\partial \phi}{\partial x} \right) = 0, \text{ and} \\ \frac{\partial(T-S)}{\partial \phi} &= I_2 \frac{\partial^2 \phi}{\partial t^2} - I_1 \frac{\partial^2 u}{\partial t^2} + B_{11} \frac{\partial^2 u}{\partial x^2} - D_{11} \frac{\partial^2 \phi}{\partial x^2} - A_{55} \left(\frac{\partial w}{\partial x} - \phi \right) = 0 \end{aligned} \right\} \quad (3.11)$$

$$\left. \begin{aligned} \text{where, } [A_{11} \ B_{11} \ D_{11}] &= \int_A E(z) [1 \ z \ z^2] dA, \\ [I_0 \ I_1 \ I_2] &= \int_A \rho(z) [1 \ z \ z^2] dA, \text{ and} \\ A_{55} &= k \int_A G(z) dA \end{aligned} \right\} \quad (3.12)$$

The shape functions for the displacement field for finite element formulation are obtained by solving the static part of the eq. (3.11) with the following consideration.

$$\begin{aligned} u &= a_1 + a_2 x + a_3 x^2, \\ w &= a_4 + a_5 x + a_6 x^2 + a_7 x^3, \\ \phi &= a_8 + a_9 x + a_{10} x^2. \end{aligned} \quad (3.13)$$

Substituting eq. (3.13) into the static part of eq. (3.11) we get

$$\{\bar{u}\} = [u \ w \ \phi]^T = [N(x)]\{a\} \quad (3.14)$$

$$\{a\} = [a_1 \ a_2 \ a_4 \ a_5 \ a_8 \ a_9]^T \quad (3.15)$$

$$N(x) = \begin{bmatrix} 1 & x & 0 & -\frac{\lambda}{2}x^2 & \frac{\lambda}{2}x^2 & 0 \\ 0 & 0 & 1 & \left(x - \frac{\beta}{6}x^3\right) & \frac{\beta}{6}x^3 & \frac{x^2}{2} \\ 0 & 0 & 0 & -\frac{\beta}{2}x^2 & 1 + \frac{\beta}{2}x^2 & x \end{bmatrix} \quad (3.16)$$

$$\lambda = \frac{B_{11}A_{55}}{(A_{11}D_{11} - B_{11}^2)}, \quad \beta = \frac{A_{11}A_{55}}{(A_{11}D_{11} - B_{11}^2)} \quad (3.17)$$

The coefficients $\{a\}$ can be found in terms of nodal displacements by substituting $x=0$ and $x=l$ in eq. (3.14) and can be expressed as

$$\{a\} = [G]\{\hat{u}\} \quad (3.18)$$

$$\text{where } [G] = \begin{bmatrix} N(0) \\ N(l) \end{bmatrix}^{-1} \quad (3.19)$$

Now substituting eq. (3.18) into eq. (3.14) we get

$$\{\bar{u}\} = [S(x)]\{\hat{u}\} \quad (3.20)$$

where, $[S(x)] = [N(x)][G]$, a 3x6 matrix is the required shape function matrix.

$$\{\hat{u}\} = [u_i \ w_i \ \phi_i \ u_{i+1} \ w_{i+1} \ \phi_{i+1}] \quad (3.21)$$

Now $S(x)$ can be expressed in the following form

$$\mathfrak{N}(x) = [\mathfrak{N}_u(x) \quad \mathfrak{N}_w(x) \quad \mathfrak{N}_\phi(x)]^T \quad (3.22)$$

where, $\mathfrak{N}_u(x)$, $\mathfrak{N}_w(x)$, $\mathfrak{N}_\phi(x)$ are the shape functions for the axial, transverse and rotational degree of freedom respectively. The shape function matrix is given in appendix.

It is seen above that unlike the conventional elements the shape function not only depends on x and l but it also depends on cross-sectional area and material properties which ensures better accuracy. Moreover, better convergence can be achieved as the shape functions are obtained from the exact solution of static part of the governing differential equation.

3.2.2 Element elastic stiffness matrix

The general force boundary conditions for the element can be given as

$$\left. \begin{aligned} N &= \int_A \sigma_{xx} dA = A_{11} \frac{\partial u}{\partial x} - B_{11} \frac{\partial \phi}{\partial x} \\ V_z &= \int_A \tau_{xz} dA = A_{55} \left(\frac{\partial w}{\partial x} - \phi \right) \\ M_y &= - \int_A z \sigma_{xx} dA = -B_{11} \frac{\partial u}{\partial x} + D_{11} \frac{\partial \phi}{\partial x} \end{aligned} \right\} \quad (3.23)$$

where, N , V_z , M_y are axial force, shear force and bending moment respectively acting at the boundary nodes.

Similarly substituting eq. (3.14) into eq. (3.23) we get

$$[\tilde{G}(x)]\{a\} = \{F(x)\} \quad (3.24)$$

$$\text{where, } [\tilde{G}(x)] = \begin{bmatrix} 0 & A_{11} & 0 & (B_{11}\beta - A_{11}\lambda)x & (A_{11}\lambda - B_{11}\beta)x & -B_{11} \\ 0 & 0 & 0 & A_{55} & -A_{55} & 0 \\ 0 & -B_{11} & 0 & (D_{11}\beta - B_{11}\lambda) & (B_{11}\lambda - D_{11}\beta) & D_{11} \end{bmatrix}, \quad (3.25)$$

$$\text{and } \{F(x)\} = [N \quad V_z \quad M_y]^T \text{ is the element load vector} \quad (3.26)$$

By substitution of $x=0$ and $x=l$ into eq. (3.24) we can have

$$[\tilde{G}]\{a\} = \{F\} \quad (3.27)$$

so that

$$\{F\} = [-N(0) \quad -V_z(0) \quad -M_y(0) \quad N(l) \quad V_z(l) \quad M_y(l)]^T \quad (3.28)$$

is the nodal load vector.

$$\text{and } [\tilde{G}] = \begin{bmatrix} 0 & -A_{11} & 0 & 0 & 0 & B_{11} \\ 0 & 0 & 0 & -A_{55} & A_{55} & 0 \\ 0 & B_{11} & 0 & 0 & 0 & -D_{11} \\ 0 & A_{11} & 0 & (B_{11}\beta - A_{11}\lambda)l & (A_{11}\lambda - B_{11}\beta)l & -B_{11} \\ 0 & 0 & 0 & A_{55} & -A_{55} & 0 \\ 0 & -B_{11} & 0 & (B_{11}\lambda - D_{11}\beta) & (D_{11}\beta - B_{11}\lambda) & D_{11} \end{bmatrix} \quad (3.29)$$

Now substituting eq. (3.18) into eq. (3.27) we get

$$[k_e]\{\hat{u}\} = \{F\} \quad (3.30)$$

$[k_e] = [\tilde{G}][G]$ is the required element elastic stiffness matrix.

The elastic strain energy of the element can also be expressed as

$$S = \frac{1}{2} \{\hat{u}\}^T [k_e] \{\hat{u}\} \quad (3.31)$$

3.2.3 Element mass matrix

The element mass matrix is derived by substituting eq. (3.20) into eq. (3.8).

$$T = \frac{1}{2} \{\dot{\hat{u}}\}^T [m] \{\dot{\hat{u}}\}, \text{ where} \quad (3.32)$$

$[m] = [m_u] + [m_w] + [m_\phi] + [m_{u\phi}]$, is the element mass matrix.

$$\begin{aligned} [m_u] &= \int_0^l I_0 ([S_u]^T [S_u]) dx, & [m_w] &= \int_0^l I_0 ([S_w]^T [S_w]) dx, \\ [m_\phi] &= \int_0^l I_2 ([S_\phi]^T [S_\phi]) dx, & [m_{u\phi}] &= -\int_0^l I_1 ([S_u]^T [S_\phi] + [S_\phi]^T [S_u]) dx \end{aligned} \quad (3.33)$$

m_u , m_w , m_ϕ , represent the contribution of u , w , ϕ degree of freedom to the mass matrix and $m_{u\phi}$ represents the mass matrix arising due to the coupling between u and ϕ .

3.2.4 Element geometric stiffness matrix

When the axial load $P(t)$ is applied on the beam element, the work done by the load can be expressed as

$$W_p = \frac{1}{2} \int_0^l P(t) \left(\frac{\partial w}{\partial x} \right)^2 dx \quad (3.34)$$

Substituting the value of w from eq. (3.20) into eq. (3.34) the work done can be expressed as

$$\begin{aligned} W_p &= \frac{P(t)}{2} \int_0^l \{\hat{u}\}^T [\mathbb{S}'_w]^T [\mathbb{S}'_w] \{\hat{u}\} dx \\ &= \frac{P(t)}{2} \{\hat{u}\} [k_g] \{\hat{u}\} \end{aligned} \quad (3.35)$$

where, $[k_g] = \int_0^l [\mathbb{S}'_w]^T [\mathbb{S}'_w] dx$ is called the element geometric stiffness matrix.

3.3 Governing equations of motion

The element equation of motion for a beam subjected to axial force is obtained by using Hamilton's principle.

$$\delta \int_{t_1}^{t_2} (T^{(e)} - S^{(e)} + W_p^{(e)}) dt = 0 \quad (3.36)$$

Substituting eqs.(3.32, 3.31 and 3.35) in to eq. (3.36) the equation of motion for the beam element is obtained as follows

$$[m] \{\ddot{\hat{u}}\} + [[k_e] - P(t)[k_g]] \{\hat{u}\} = 0 \quad (3.37)$$

$$\text{The axial load } P(t) \text{ is taken as } P(t) = \alpha P^\oplus + \beta_d P^\oplus \cos \Omega t, \quad (3.38)$$

P^\oplus is the critical buckling load of a isotropic steel beam with similar geometrical dimensions and end conditions, α , β_d are called static and dynamic load factors respectively and Ω is the frequency of the applied load $P(t)$. Substituting eq.(3.38) in eq (3.37) we get

$$[m] \{\ddot{\hat{u}}\} + [[k_e] - P^\oplus (\alpha + \beta_d \cos \Omega t) [k_g]] \{\hat{u}\} = 0 \quad (3.39)$$

Assembling the element matrices as used in eq. (3.39), the equation in global matrix form which is the equation of motion for the beam, can be expressed as

$$[M] \{\ddot{\hat{U}}\} + [[K_e] - P^\oplus (\alpha + \beta_d \cos \Omega t) [K_g]] \{\hat{U}\} = 0 \quad (3.40)$$

$[M]$, $[K_e]$, $[K_g]$ are global mass, elastic stiffness, and geometric stiffness matrices respectively and $[\hat{U}]$ is global displacement vector. Equation (3.40) represents a system of second order differential equations with periodic coefficients of the Mathieu-Hill type. The periodic solutions for the boundary between the dynamic stability and instability zones can be obtained from Floquet's theory [21] as follows. From the theory of Mathieu functions [21], it is evident that the nature of solution is

dependent on the choice of load frequency and load amplitude. The frequency amplitude domain is divided in to regions, which give rise to stable solutions and to regions, which cause unstable solutions.

The eq.(3.40) does not change its form on addition of the period, $T = \frac{2\pi}{\Omega}$ to t . This

follows from the fact that $\cos\Omega t = \cos\Omega(t+T)$. Therefore if $\hat{U}(t)$ is a solution of the eq.(3.26), then $\hat{U}(t+T)$ is also its solution.

According to the Floquet solutions the k^{th} solution of eq.(3.40) can be written as,

$$\hat{U}_k(t+T) = \mu_k \hat{U}_k(t) \quad (3.41)$$

where μ_k the characteristic constant.

These solutions which acquire a constant multiplier by the addition of the period T to t , can be represented in the form

$$\hat{U}_k(t) = \chi_k(t) e^{(t/T)\ln \mu_k} \quad (3.42)$$

where $\chi_k(t)$ is a periodic function of period T .

It follows from the eq.(3.42) that the behaviour of the solutions as $t \rightarrow \infty$, depends on the value of the characteristic roots, more precisely, on the value of its moduli.

Taking in to account that $\ln \mu_k = \ln |\mu_k| + i \arg \mu_k$

$$\hat{U}_k(t) = \Phi_k(t) e^{(t/T)\ln |\mu_k|} \quad (3.43)$$

$$\Phi_k(t) = \chi_k(t) e^{(it/T)\arg \mu_k} \quad (3.44)$$

If the characteristic number μ_k is greater than unity, then the corresponding solution, eq.(3.43) will have an unbounded exponential multiplier, hence the solution is unlimited. If the same characteristic number is less than unity, then the corresponding solution is damped as t increases. Finally, if the characteristic number is equal to unity, then the solution is periodic, i.e. it will be bounded in time. These are the conclusions of the Floquet's theory.

Thus the periodic solutions characterize the boundary conditions between the dynamic stability and instability zones. So the periodic solution can be expressed as Fourier series.

A solution with period $2T$ is represented by:

$$\hat{U}(t) = \sum_{K=1,3,\dots}^{\infty} \left[\{c_k\} \sin \frac{K\Omega t}{2} + \{d_k\} \cos \frac{K\Omega t}{2} \right] \quad (3.45)$$

A solution with period T is represented by:

$$\hat{U}(t) = \{c_0\} + \sum_{K=2,4,\dots}^{\infty} \left[\{c_k\} \sin \frac{K\Omega t}{2} + \{d_k\} \cos \frac{K\Omega t}{2} \right] \quad (3.46)$$

The boundaries of the principal instability regions with period $2T$ are of practical importance [21]. If the series expansions of eq.(3.45) are used in eq.(3.40), term wise comparison of the sine and cosine coefficients will give infinite systems of homogeneous algebraic equations for the vectors $\{c_k\}$ and $\{d_k\}$ for the solutions on the stability borders. Non-trivial solutions exist if the determinant of the coefficient matrices of these equation systems of infinite order vanishes. When looking for numerical solutions, systems of finite order are required and as it is shown in reference [21], a sufficiently close approximation of the infinite eigen value problem is obtained by taking $k=1$ in the expansion in eq.(3.45) and putting the determinant of the coefficient matrices of the first order equal to zero. This technique is adopted originally in reference [21]. The first order expansion of eq. (3.45) gives

$$\hat{U}(t) = c_1 \sin \frac{\Omega t}{2} + d_1 \cos \frac{\Omega t}{2} \quad (3.47)$$

Substituting eq. (3.47) into eq. (3.40) and comparing the coefficients of $\sin \frac{\Omega t}{2}$ and $\cos \frac{\Omega t}{2}$ terms the condition for existence of these boundary solutions with period $2T$ is given by

$$\left([K_e] - (\alpha \pm \beta_d / 2) P^\oplus [K_g] - \frac{\Omega^2}{4} [M] \right) \{\hat{U}\} = 0 \quad (3.48)$$

Equation (3.48) represents an eigen value problem for known values of α , β_d , and P^\oplus . This equation gives two sets of eigen values (Ω) binding the regions of instability due to the presence of plus and minus sign. The instability boundaries can be determined from the solution of the equation

$$\left| [K_e] - (\alpha \pm \beta_d / 2) P^\oplus [K_g] - \frac{\Omega^2}{4} [M] \right| = 0 \quad (3.49)$$

3.3.1 Free vibration

When $\alpha=0$, $\beta_d=0$, and $\Omega=2\omega$, eq. (3.49) is reduced to a problem of free vibration as

$$|[K_e] - \omega^2[M]| = 0 \quad (3.50)$$

The solution of eq. (3.50) gives the value of natural frequencies $\{\omega\}$.

3.3.2 Static stability

When $\alpha=1$, $\beta_d=0$, and $\Omega=0$, eq. (3.49) is reduced to the problem of static stability as

$$|[K_e] - P^\oplus[K_g]| = 0 \quad (3.51)$$

The solution of eq. (3.51) gives the values of buckling loads.

3.3.3 Regions of instability

The fundamental natural frequency ω_1 and the critical buckling load P^\oplus of an isotropic steel beam with similar geometrical dimensions and end conditions as that of FGO beam are calculated from eq. (3.50) and eq. (3.51) respectively.

Choosing $\Omega = \left(\frac{\Omega}{\omega_1}\right)\omega_1$, eq. (3.49) can be rewritten as

$$\left|[K_e] - (\alpha \pm \beta_d/2)P^\oplus[K_g] - \left(\frac{\Omega}{\omega_1}\right)^2 \frac{\omega_1^2}{4}[M]\right| = 0 \quad (3.52)$$

The solution of eq. (3.52) gives two sets of values of $\left(\frac{\Omega}{\omega_1}\right)$ for given values of α , β_d , P^\oplus , and ω_1 . The plot between β_d and $\left(\frac{\Omega}{\omega_1}\right)$ gives the regions of dynamic instability.

3.4 Results and discussion

The numerical study is carried out for a beam, simply supported at both the ends. The beam is discretized into 100 elements. A typical discretization of the beam is given in Appendix. The boundary conditions used for the numerical study are as given below.

At $x=0$, $w=0$ and $u=0$, at $x=L$, $w=0$.

A FGO beam with steel and alumina as its constituent phases is considered for the analysis followed by the investigation of an FGSW beam made up of steel and alumina.

3.4.1 Validation of the formulation

The FGSW beam becomes functionally graded ordinary (FGO) beam when the thickness of the skins are made equal to zero. In order to establish the correctness of calculation, the first five natural frequencies of a steel aluminum FGO beam are calculated and compared with Li [92]. The dimensions of the beam [92] are, Length, $L=0.5\text{m}$, breadth, $b=0.1\text{m}$ and thickness $h=0.125\text{m}$. The comparison is provided in table 3.1. It is found that the present results are in good agreement.

Table 3.1 Comparison of first five natural frequencies

Natural Frequencies (rad/s)	Present Method	X. F. Li [92]	difference (%)
ω_1	6431.54	6457.93	-0.41
ω_2	21699.29	21603.18	0.44
ω_3	40007.90	40145.42	-0.34
ω_4	59728.3	59779.01	-0.08
ω_5	80153.98	79686.16	0.58

Table 3.2 Comparison of buckling load parameter.

$\frac{L}{r}$	Critical buckling load parameter ($P^{\oplus}L^2 / EI$)		
	Present	Raju and Rao [122]	difference (%)
10	7.575	7.546	0.38
25	9.4206	9.406	0.15
50	9.753	9.750	0.03
100	9.839	9.839	0.0

The FGO beam reduces to a homogeneous beam when the value of power law index (n) is made equal to zero. The critical buckling load parameter for various

(L/r) ratios is computed and compared with the result of Raju and Rao [122] and are found to be in good agreement as shown in table 3.2. Here, 'r' corresponds to radius of gyration.

3.4.2 Functionally graded ordinary beam

A steel-alumina FGO beam with steel-rich bottom is considered for vibration and dynamic stability analysis. The properties of constituent phases are:

Steel: $E=2.1 \times 10^{11}$ Pa, $G=0.8 \times 10^{11}$ Pa $\rho=7.85 \times 10^3 \text{kg/m}^3$,

Alumina: $E=3.9 \times 10^{11}$ Pa, $G=1.37 \times 10^{11}$ Pa, $\rho=3.9 \times 10^3 \text{kg/m}^3$, $k=0.8667$.

The shear correction factor is chosen as $k=(5+\nu)/(6+\nu)=0.8667$ as mentioned by Hutchinson [63], where ν , the poisson's ratio and is assumed as 0.3 in the present case.

The effect of variation of power law index on first two natural frequencies of FGO beam are presented in figures 3.2(a) and 3.2(b). The corresponding data are presented in table 3.3. It is found for both the modes that the frequency decreases as the power law index (n) increases from one to fifteen. This may be attributed to the following fact. The composition of the constituent phases at a given point changes as the power law index varies. The material properties at the point such as E , ρ and G are dependent on composition of the phases. As the elements of stiffness and mass matrices are functions of these coordinate dependent properties, so variation in power law index alters the stiffness matrix $[K]$ and mass matrix $[M]$ and hence the natural frequencies.

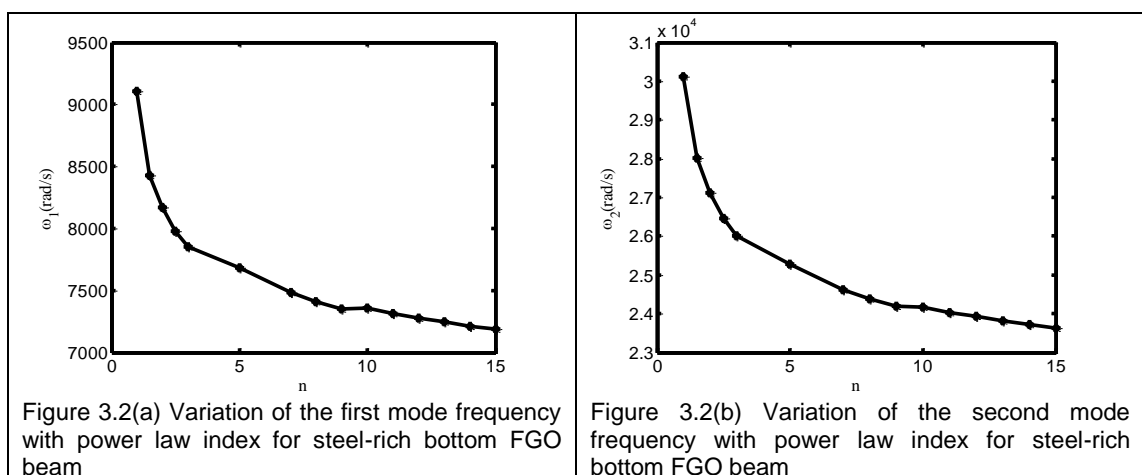


Table 3.3 Variation of natural frequencies with power law index for steel-alumina FGO beam (steel-rich bottom).

Power index (n)	Natural frequencies (rad/s)		
	ω_1	ω_2	ω_3
1	9106.78	30117.72	55123.50
1.5	8424.07	28007.59	51402.84
2	8168.70	27120.25	49694.54
2.5	7979.96	26468.72	48490.07
3	7850.75	26005.89	47659.08
5	7683.84	25270.87	46180.58
7	7481.00	24613.57	45015.09
8	7412.18	24388.93	44630.19
9	7352.96	24198.53	44306.63
10	7356.02	24169.83	44215.63
11	7314.84	24037.99	43992.39
12	7278.29	23922.06	43796.71
13	7245.71	23819.61	43624.67
14	7210.69	23715.94	43445.77
15	7185.05	23635.69	43311.06

Table 3.4 Critical buckling loads for FGO beam (steel-rich bottom).

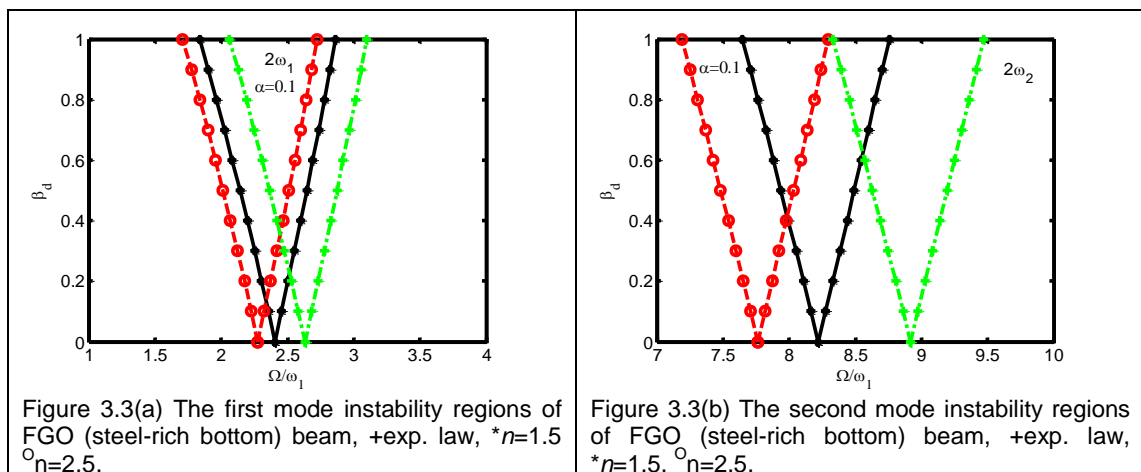
Power law index (n)	Critical buckling load P^{\oplus} ($\times 10^7$ N)
1	16.561
2	14,908
5	14.166
10	13.412
25	12.552
50	12.157

The effect of variation of power law index on critical buckling load is evaluated and is presented in Tables 3.4. It is found that, the critical buckling load decreases with increase in the value of power law index. This is due to the fact that the FGO beam with steel-rich bottom becomes richer in steel as the power law index becomes higher. FGO beam rich in steel implies beam with lower effective material properties as steel has got lower E and G as compared to alumina. The lower values of

effective material properties of the beam reduce its stiffness which in turn decreases the critical buckling load.

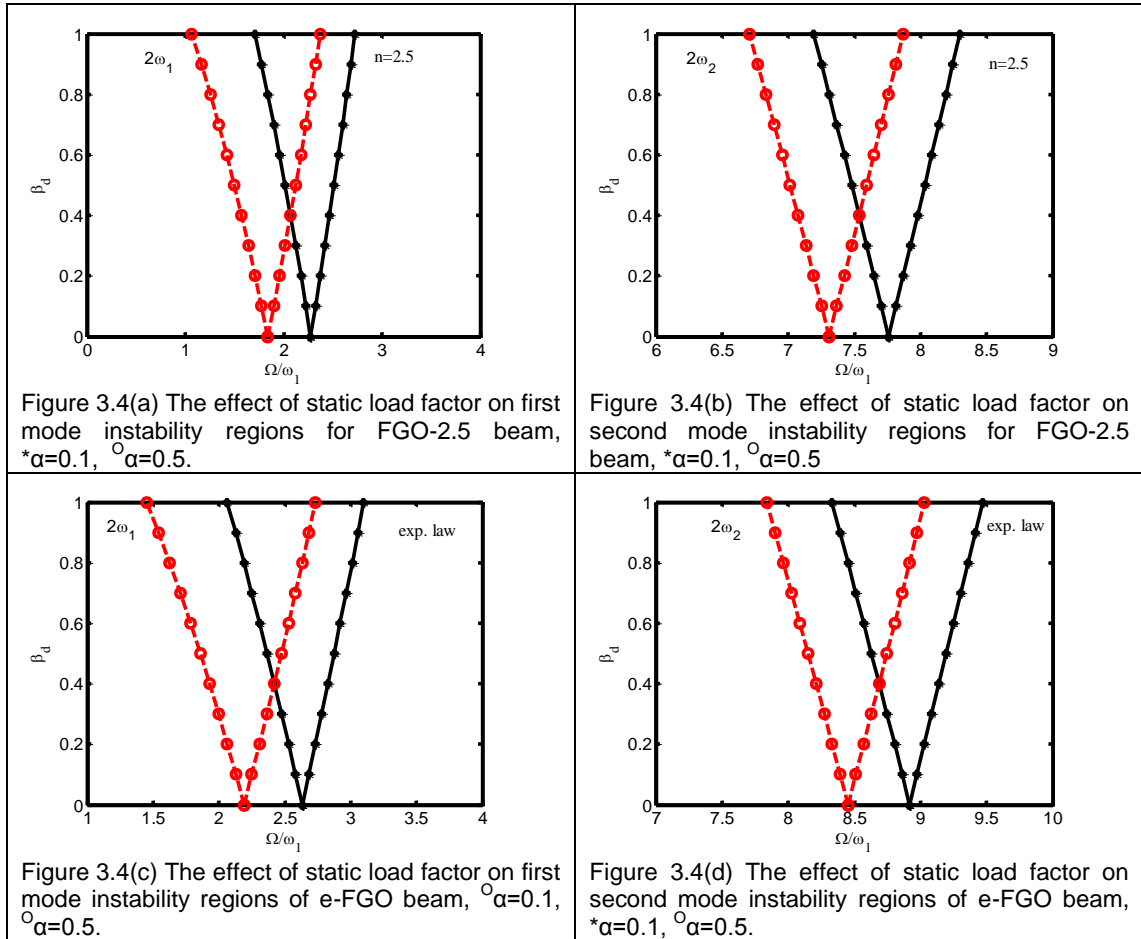
The additional data for dynamic stability analysis are taken as follows. $P^{\oplus}=11.37 \times 10^7$ N, $\omega_1=6724.9$ rad/s. P^{\oplus} and ω_1 corresponds to the critical buckling load and fundamental natural frequency of a homogenous steel beam of same dimensions and end conditions as of the FGO beam.

The effect of property distribution laws on the dynamic stability of FGO beam is studied. The first two principal regions of instability are shown in figure 3.3(a) and figure 3.3(b) respectively. The static load factor, $\alpha=0.1$ is used for the analysis. The instability regions of beam having properties along thickness according to power law with index $n=1.5$ (FGO-1.5) beam, with index $n=2.5$ (FGO-2.5) beam and properties according to exponential law (e-FGO) beam are superimposed for the purpose of comparison. It is clear from the figures 3.3(a) and 3.3(b) that the e-FGO beam is the most stable among the three as its instability region is located at farthest from the dynamic load factor axis. The first and second mode instability regions are shifted towards the dynamic load factor axis as the power law index increases from 1.5 to 2.5 thereby enhancing the chance of parametric instability. The relative amount of alumina is highest in e-FGO beam and this causes the beam's stiffness to be of highest magnitude. As the stiffness of the e-FGO beam happens to be the highest, the dynamic instability occurs at the highest excitation frequency thereby reducing the chance of instability. Similarly, as the value of power law index increases, the stiffness of the beam reduces and hence the excitation frequency to cause instability decreases making the beam more prone to instability.



Figures 3.4(a) and 3.4(b) depict the effect of static load factor α on the first and second principal regions of instability of the FGO-2.5 beam respectively. The values

of static load factor are taken as 0.1 and 0.5. Figures 3.4(c) and 3.4(d) show the corresponding plots for e-FGO beam. It is observed that more the static load factor, more prone to dynamic instability is the beam and it happens for both the laws of property distribution. This is expected as the increase of static load factor means the increase of the time independent component of the axial load.



3.4.3 Functionally graded sandwich beam

A functionally graded sandwich (FGSW) beam of length 0.5m, thickness 0.125m and width 0.1m with core as FGM is chosen for analysis. The top layer is alumina, bottom layer is steel and core is mixture of steel and alumina whose properties along the thickness are assumed to follow power law as well as exponential law.

The effect of FGM content (d/h) on the natural frequencies of the beam is shown in figures 3.5(a) and 3.5(b). FGSW beam having properties along core thickness according to power law with index $n=1.5$ (FGSW-1.5) beam, $n=2.5$ (FGSW-2.5) beam and according to exponential law (e-FGSW) is considered for the analysis.

It is found that the natural frequencies decrease with the increase of FGM content in FGSW beams having properties along thickness of core according to power law whereas the frequencies increase with increase of FGM content for e-FGSW beam. Moreover, the increase in power law index causes decrease in frequencies of the FGSW beam.

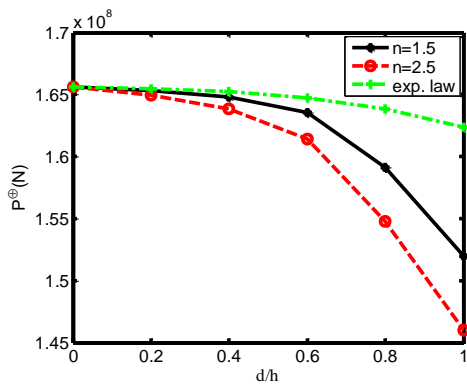
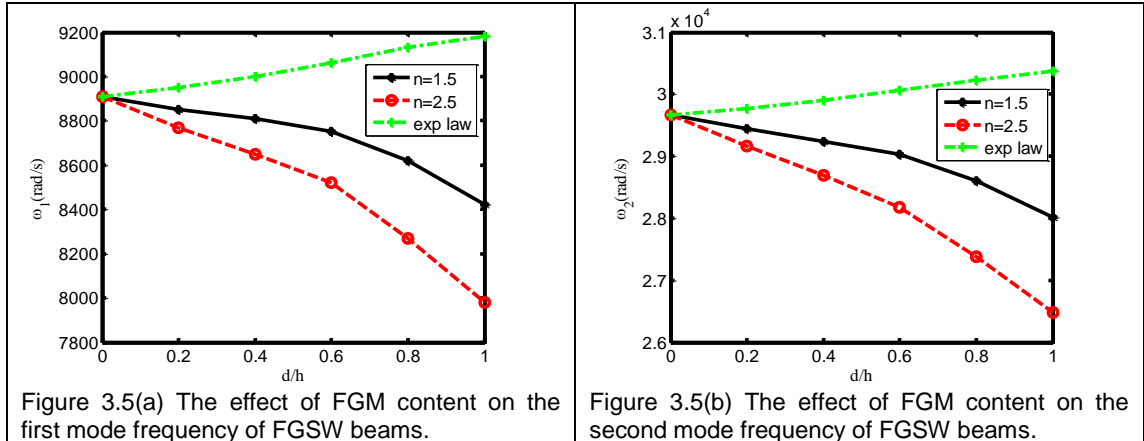


Figure 3.6 The effect of FGM content on the critical buckling load of FGSW beams.

Figure 3.6 shows the effect of FGM content on the static buckling load. It is seen that the critical buckling load decreases with increase in FGM content irrespective of the kind of property variation along the thickness of core of the beam.

Effect of different property distribution laws on the first two principal instability regions of the beam are depicted in figure 3.7(a) and 3.7(b) respectively. The static load factor(α) and FGM content(d/h) are taken as 0.1 and 0.3 respectively. The e-FGSW beam is the most stable and FGSW-2.5 beam is the least stable beam. This is due to the fact that the FGM core becomes richest in alumina in former case and least rich in alumina in later case. Enrichment of the core with alumina enhances the effective

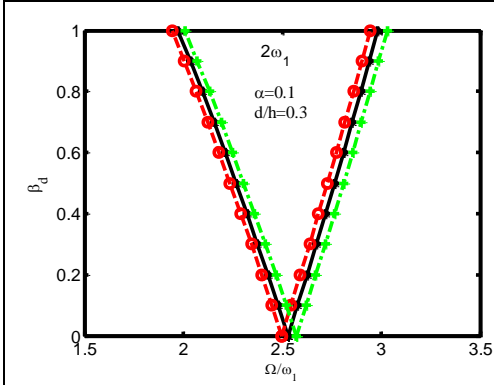


Figure 3.7 (a) The first mode instability regions for FGSW beam, $n=1.5$ (*), $n=2.5$ (○), exp. Law (△)

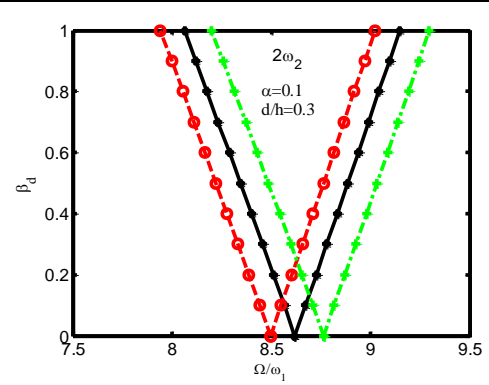


Figure 3.7 (b) The second mode instability regions for FGSW beam, $n=1.5$ (*), $n=2.5$ (○), exp.law (△).

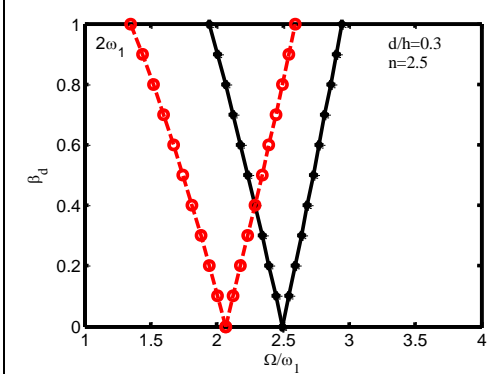


Figure 3.8(a) The effect of static load factor on the first mode instability region of FGSW-2.5 beam, $\alpha=0.1$ (*), $\alpha=0.5$ (○).

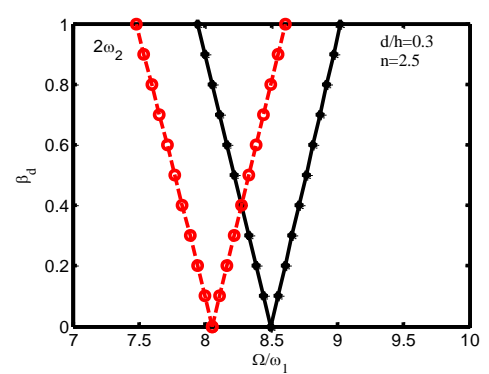


Figure 3.8(b) The effect of static load factor on the second mode instability region of FGSW-2.5 beam, $\alpha=0.1$ (*), $\alpha=0.5$ (○).

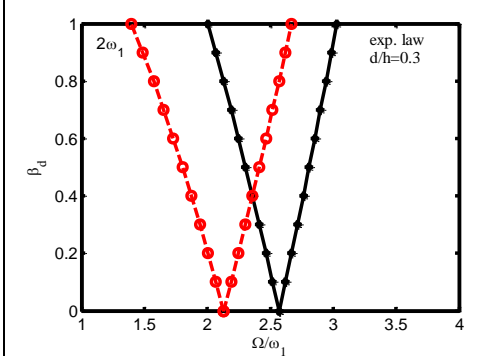


Figure 3.8(c) The effect of static load factor on the first mode instability region of e-FGSW beam, $\alpha=0.1$ (*), $\alpha=0.5$ (○).

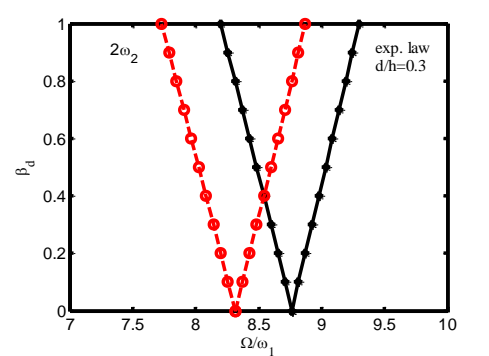


Figure 3.8(d) The effect of static load factor on the second mode instability region of e-FGSW beam, $\alpha=0.1$ (*), $\alpha=0.5$ (○).

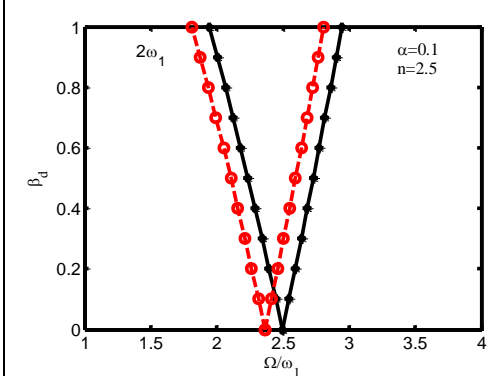


Figure 3.9 (a) The effect of FGM content on the first mode instability regions of FGSW-2.5 beam, * $d/h=0.3$, $^{\circ}d/h=0.8$.

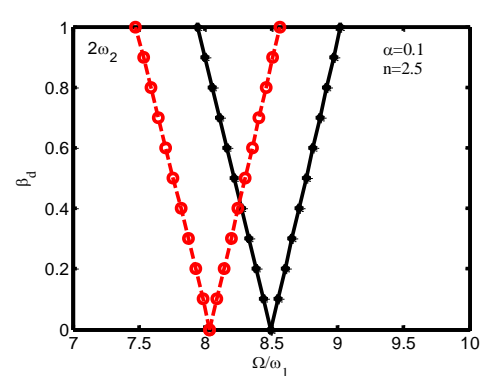
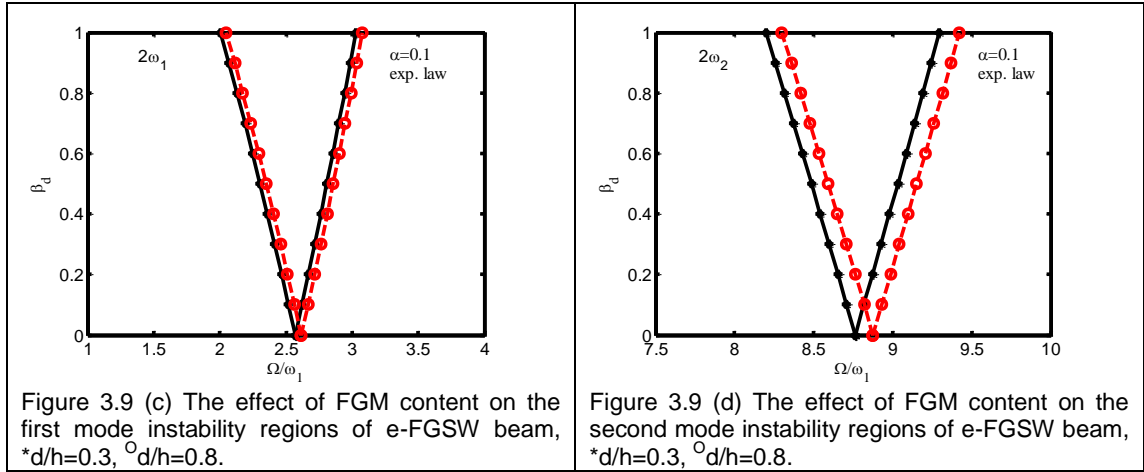


Figure 3.9 (b) The effect of FGM content on the second mode instability regions of FGSW-2.5 beam, * $d/h=0.3$, $^{\circ}d/h=0.8$.



value of E and leads to increase in natural frequencies. The trend of results obtained in this case is similar to that obtained in case of FGO beam.

Figure 3.8(a) and figure 3.8(b) show the effect of static load component on the dynamic instability of FGSW-2.5 beam for first and second principal modes respectively. The static load factor of values 0.1 and 0.5 are taken for the comparison. The case with $\alpha = 0.5$ is found to be more prone to dynamic instability compared to the case with $\alpha = 0.1$ as obtained earlier for the FGO beams. Similar trend of the results are observed for e-FGSW beam as shown in figures 3.8(c) and 3.8(d) for first and second main mode respectively.

The effect of FGM content (d/h) on dynamic instability of FGSW beams is investigated. Figure 3.9(a) and figure 3.9(b) show the plots of first two main regions of instabilities of FGSW-2.5 beam with different FGM contents respectively. FGM content of 30% ($d/h=0.3$) and 80% ($d/h=0.8$) are considered for the purpose. Figure 3.9(a) shows the plot of FGSW-2.5 beam for first mode and Figure 3.9(b) shows the corresponding plot for second mode. For both the cases, $\alpha = 0.1$ is taken for the calculation. It is obvious from the plots that the beam with higher value of (d/h) is less stable. The effect of FGM content on stability of e-FGSW beam is opposite to that of FGSW-2.5 beam. In this case, the stability of the beam is enhanced with the increase of FGM content as shown in figures 3.9(c) and 3.9(d) for first and second mode respectively. Moreover, it is learnt, that the effect of FGM content on the principal instability regions of FGSW-2.5 beam is more prominent as compared to that of e-FGSW beam. This is due to the fact that increase in FGM content increases relative amount of steel in FGSW-2.5 beam compared to e-FGSW beam. As steel has lower value of Young's modulus compared to alumina, so increase in steel phase causes more prominent effect on instability regions of FGSW-2.5 beam compared to e-FGSW beam.

3.5 Closure

The effect of various system parameters on dynamic stability behaviour of both FGO and FGSW beams have been studied using finite element method. The important conclusions are outlined below.

3.5.1 Functionally graded ordinary beam

- (i) Critical buckling load decreases with increase of power law index for FGO beam with steel-rich bottom.
- (ii) The natural frequencies of first two modes decrease with increase in the value of power law index.
- (iii) The FGO beam with properties along thickness according to exponential law is found to be the most stable beam.
- (iv) The stability of FGO beam decreases as the value of power law index increases from 1.5 to 2.5.
- (v) Increase in static load factor enhances the instability.

3.5.2 Functionally graded sandwich beam

- (i) Critical buckling load decreases with increase of FGM content for the FGSW beams with exponential and power law distribution of properties.
- (ii) The first two mode natural frequencies increase with increase of FGM content for beam with exponential distribution of properties.
- (iii) The first two natural frequencies decrease with increase of FGM content for beam with power law distribution of properties.
- (iv) Increase in core thickness enhances the stability of beam with exponential distribution of properties, whereas it reduces the stability of beam with power law distribution of properties.
- (v) The FGSW beam with properties along thickness of the core according to exponential law is found to be the most stable. The stability of the beam decreases as the value of power law index increases.
- (vi) Increase in static load component enhances the instability.

The property distribution laws are found to have a prominent role on the dynamic stability behaviour of the beam.

CHAPTER 4

DYNAMIC STABILITY OF FUNCTIONALLY GRADED TIMOSHENKO BEAM ON ELASTIC FOUNDATIONS UNDER PARAMETRIC EXCITATION

4.1 Introduction

The theory of beams on elastic foundation was conceived to face the practical problem of railway track. A long rail that has to sustain the large wheel loads is a beam of moderate bending stiffness. The rail is supported almost along its entire length by closely spaced cross-ties in order to sustain the large loads. The investigation of the problem of interaction between a beam of moderate bending stiffness and the supporting foundation was done by Winkler. Winkler has developed a mathematical model wherein it is assumed that the foundation imposes reaction forces on the beam that are proportional to the deflection of the foundation. The model is named as Winkler's elastic foundation model. The railway tracks can be made of functionally graded materials with its constituent phases as metal and ceramic. The ceramic-rich surface can be used for frictional contact ensuring minimum wear and tear. Large scale cost effective commercial manufacturing of such rails can be possible in future with advancement of FGM manufacturing

technology. An extensive literature survey is carried out on work on beams on elastic foundations and presented below.

Ahuja and Duffield [3] investigated both theoretically and experimentally the dynamic stability of beams having variable cross-sections and resting on elastic foundation. The effect of elastic foundation was found to have a decreasing effect on the width of the instability regions and the amplitude of parametric response. Abbas and Thomas [1], Briseghella et al. [22] and Ozturk and Sabuncu [116] used finite element method to study the dynamic stability of beams. Eisenberger and Clastronik [44], Dutta and Nagraj [43] and Engel [46] studied the dynamic stability of beams on elastic foundation. The parametric instability behaviour of a non-prismatic bar with localized zone of damage and supported on an elastic foundation was studied by Dutta and Nagraj [43] using finite element analysis. It is found that a flaw in the beam near the narrow end affects the static and dynamic behaviour more than a flaw does near the wider end. Engel [46] investigated the dynamic stability of bars on elastic foundation with damping. It was found that the critical mode became a higher mode instead of fundamental mode when the foundation parameter exceeded a certain value. Lee and Yang [88] and Matsunaga [102] investigated the dynamic behaviour of Timoshenko beams resting on elastic foundations. Morfidis [108] developed stiffness and transfer matrices and load vectors of Timoshenko beam resting on Kerr type 3-parameter elastic foundation. Pradhan and Murmu [121] investigated the effect of various parameters on the dynamic response of FGM beams and functionally graded sand witch (FGSW) beam resting on variable elastic foundation. The parameters chosen were temperature distribution, power law index, variable Winkler foundation modulus, elastic foundation modulus and the normalized core thickness of the FGSW beam. Baghani et al. [15] have used variational iteration method to study the free vibration and post-buckling analysis of a laminated composite beam considering both geometric and foundation nonlinearity. Calim and Akurt [25] have investigated the static and free vibration of circular straight beam on elastic foundation. The authors have used complementary function method for the solution of governing differential equations in Laplace domain.

There are many engineering applications of beam structures resting on foundations, such as highway pavement, building structures, offshore structures, transmission towers and transversely supported pipe lines. In the present chapter the dynamic stability of FGO and FGSW beams supported on Winkler and Pasternak foundation is studied. Effect of foundation parameters on dynamic stability is investigated.

4.2 Formulation

The FGSW beam is supported on elastic foundation as shown in figure 4.1. The beam, hinged at both the ends is subjected to a pulsating axial force $P(t)$. The coordinate system of a typical two noded beam element used to derive the governing equations of motion is shown in figure 3.1(b) in chapter 3. The mid-longitudinal(x-y) plane is chosen as the reference plane for expressing the displacements.

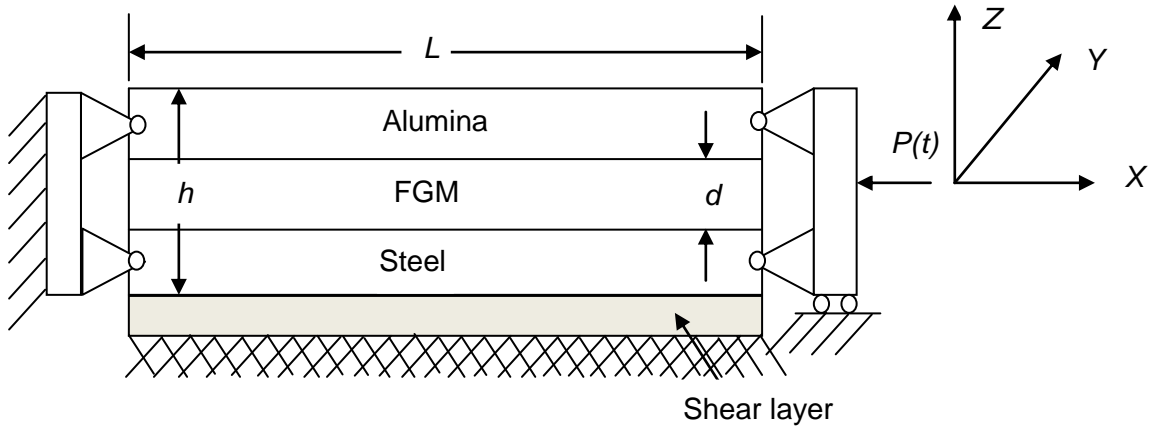


Figure 4.1 Functionally graded sandwich beam resting on Pasternak elastic foundation and subjected to dynamic axial load.

The thickness coordinate is measured as z from the reference plane. The beam with three degrees of freedom adopted in this case is same as that shown in Figure 3.1(c) and described in chapter 3. The axial displacement, the transverse displacement, and the rotation of the cross-section are u , w and ϕ respectively.

The elastic stiffness matrix and mass matrix for the FGSW beam element derived in section 3.2 are also applicable in this case and hence have not been repeated.

The effect of foundation is introduced as foundation stiffness matrix which is derived from the work done by the foundation and is presented in the next section.

4.2.1 Element elastic foundation stiffness matrix

The work done by the foundation against transverse deflection is given by the expression

$$W_1 = \frac{1}{2} k_1 \int_0^l w^2 dx \quad (4.1)$$

Substituting the value of w from eq. (3.20) in eq. (4.1) we get

$$\begin{aligned}
W_1 &= \frac{1}{2} k_1 \int_0^l \{\hat{u}\}^T [\mathbb{S}_w]^T [\mathbb{S}_w] \{\hat{u}\} dx \\
&= \frac{1}{2} \{\hat{u}\}^T [k_w] \{\hat{u}\}
\end{aligned} \tag{4.2}$$

$$[k_w] = k_1 \int_0^l [\mathbb{S}_w]^T [\mathbb{S}_w] dx \tag{4.3}$$

is element foundation stiffness matrix without considering the interaction of the shear layer. This is also called as Winkler's foundation stiffness matrix and k_1 is the Winkler's foundation constant per unit length of the beam.

The work done due to the interaction of shear layer can be given as

$$W_2 = k_2 \int_0^l \left(\frac{\partial w}{\partial x} \right)^2 dx, \tag{4.4}$$

Similarly substituting w from eq. (3.20) in eq. (4.4) we get

$$W_2 = \frac{1}{2} \{\hat{u}\}^T [k_p] \{\hat{u}\} \tag{4.5}$$

$$[k_p] = k_2 \int_0^l [\mathbb{S}'_w]^T [\mathbb{S}'_w] dx \tag{4.6}$$

where k_2 is foundation shear layer constant per unit length of the beam. The element elastic foundation matrix is given as

$$[k_f] = [k_w] + [k_p] \tag{4.7}$$

where $[k_f]$ is the Pasternak foundation stiffness matrix.

4.3 Governing equations of motion

The total work done on the beam is the sum of work done by axial force as given in eq. (3.35), work done by foundation as given in eq. (4.2) and work done by the shear layer as given in eq. (4.4). The equation of motion for the beam element referring section 3.3 can be modified for the present case and given as

$$[m] \{\ddot{\hat{u}}\} + [[k_{ef}] - P^\oplus (\alpha + \beta_d \cos \Omega t) [k_g]] \{\hat{u}\} = 0 \tag{4.8}$$

$$\text{Where } [k_{ef}] = [k_e] + [k_f] \tag{4.9}$$

$[k_{ef}]$ is the element effective stiffness matrix and $[k_e]$, $[k_f]$, $[m]$ and $[k_g]$ are element elastic stiffness matrix, Pasternak foundation stiffness matrix, mass matrix and geometric stiffness matrix respectively.

Assembling the element matrices as used in eq. (4.8), the equation in global matrix form which is the equation of motion for the beam on elastic foundation, can be expressed as

$$[M]\{\ddot{\hat{U}}\} + \left([K_{ef}] - P^{\oplus}(\alpha + \beta_d \cos \Omega t)[K_g] \right) \{\hat{U}\} = 0 \quad (4.10)$$

$$[K_{ef}] = [K_e] + [K_f] \text{ and } [K_g] = [K_w] + [K_p] \quad (4.11)$$

$[M]$, $[K_e]$, $[K_f]$, $[K_g]$ are global mass, elastic stiffness, foundation stiffness and geometric stiffness matrices respectively and $\{\hat{U}\}$ is global displacement vector.

The condition for existence of the boundary solutions with period $2T$ is given by

$$\left([K_{ef}] - (\alpha \pm \beta_d / 2)P^{\oplus}[K_g] - \frac{\Omega^2}{4}[M] \right) \{\hat{U}\} = 0 \quad (4.12)$$

The instability boundaries can be determined from the solution of the equation

$$\left| [K_{ef}] - (\alpha \pm \beta_d / 2)P^{\oplus}[K_g] - \frac{\Omega^2}{4}[M] \right| = 0 \quad (4.13)$$

Following the procedure described in section 3.3.1-3.3.3, the natural frequencies, critical buckling load and instability regions of the beam on elastic foundation are determined.

4.4 Results and discussion

The numerical calculation has been carried out for the beam, simply supported at both the ends. The beam is discretized into 100 elements. The boundary conditions used for the numerical study are as given below.

$$\text{At } x=0, w=0 \text{ and } u=0, \text{ at } x=L, w=0.$$

FGO and FGSW beams with steel and alumina as their constituent phases have been considered for the analysis.

4.4.1 Validation of the formulation

In the present formulation the FGSW beam becomes FGO beam when the thickness of the skins are made equal to zero and the FGO beam reduces to a homogeneous beam when the power law index (n) for the property distribution is made equal to zero. In order to establish the correctness of calculation, the first mode

Table 4.1 Comparison of fundamental non-dimensional frequency

L/h	Winkler Modulus $K_1 = \frac{k_1 L^4}{EI}$	Foundation shear modulus $K_2 = \frac{k_2 L^2}{\pi^2 EI}$	Non-dimensional frequency $\eta_1 = \omega_1 \sqrt{\frac{\rho A L^4}{EI}}$ (present)	η_1 Matsunaga [102]	η_1 TBT [102]
2	0	0	7.4493	7.4664	7.4127
	10	0	8.0435	8.0102	8.0106
	100	0	12.1243	11.2820	12.1084
	0	1	12.0268	11.2136	12.0106
	10	1	12.3987	11.4721	12.3836
	100	1	15.3231	13.2672	15.3153
5	0	0	9.2861	9.2903	9.2740
	10	0	9.7962	9.7912	9.7848
	100	0	13.5485	13.4726	13.5408
	0	1	13.4551	13.3812	13.4473
	10	1	13.8120	13.7307	13.8045
	100	1	16.6839	16.5354	16.6781
10	0	0	9.7109	9.7121	9.7071
	10	0	10.2091	10.2078	10.2057
	100	0	13.9113	13.8941	13.9086
	0	1	13.8186	13.8018	13.8162
	10	1	14.1731	14.1548	14.1709
	100	1	17.0346	17.0046	17.0326

Table 4.2 Comparison of first five natural frequencies

Natural Frequencies (rad/s)	Present Method	X. F. Li [92]	Simsek M [141]
ω_1	6431.54	6457.93	6443.08
ω_2	21699.29	21603.18	21470.95
ω_3	40007.90	40145.42	39775.55
ω_4	59728.3	59779.01	59092.37
ω_5	80153.98	79686.16	8638.36

Table 4.3 Fundamental natural frequency of a steel-alumina simply supported-simply supported FGO beam (steel-rich bottom) of length L=0.5 m.

L/h	Fundamental Natural frequencies ω_1 ($\times 10^4$ rad/s)							Exp. law
	Variation of properties along thickness as per power law with different indices							
	$n=0$	$n=0.5$	$n=1$	$n=2$	$n=3$	$n=5$	$n=10$	
2	2.121	1.601	1.519	1.371	1.310	1.247	1.204	1.514
5	1.068	0.7899	0.7623	0.6855	0.6564	0.6396	0.6098	0.7699
10	0.5601	0.4314	0.3992	0.3668	0.3523	0.3369	0.3202	0.4033

Table 4.4 Fundamental natural frequency of a steel-alumina simply supported-simply supported FGO beam (steel-rich bottom) on Winkler and Pasternak elastic foundations (length L=0.5 m)

L/h	Foundation		Fundamental natural frequency ω_1 ($\times 10^4$ rad/s)					Exponential law
	Winkler Modulus	shear modulus	Power law indices					
	$K_1 = \frac{k_1 L^4}{EI}$	$K_2 = \frac{k_2 L^2}{\pi^2 EI}$	$n=1$	$n=2$	$n=3$	$n=5$		
2	0	0	1.519	1.371	1.310	1.247	1.514	
	5	0	1.564	1.415	1.355	1.291	1.561	
	10	0	1.607	1.458	1.397	1.334	1.606	
	5	1	2.260	2.098	2.031	1.963	2.279	
	10	1	2.290	2.127	2.059	1.991	2.309	
	0	0	0.7623	0.6855	0.6564	0.6396	0.7699	
5	5	0	0.7774	0.7006	0.6714	0.6543	0.7854	
	10	0	0.7921	0.7153	0.6860	0.6686	0.8006	
	5	1	1.028	0.9473	0.9155	0.8933	1.042	
	10	1	1.039	0.9583	0.9263	0.9038	1.054	
	0	0	0.3992	0.3668	0.3523	0.3369	0.4033	
	5	0	0.4066	0.3739	0.3594	0.3441	0.4108	
10	10	0	0.4138	0.3809	0.3664	0.3510	0.4183	
	5	1	0.5296	0.4934	0.4773	0.4610	0.5372	
	0	0	0.3992	0.3668	0.3523	0.3369	0.4033	
	5	0	0.4066	0.3739	0.3594	0.3441	0.4108	
	10	0	0.4138	0.3809	0.3664	0.3510	0.4183	
	5	1	0.5296	0.4934	0.4773	0.4610	0.5372	

fundamental non-dimensional natural frequencies of a homogenous steel beam simply supported at both the ends are calculated for different (L/h) ratio of the beam and compared with the results of Matsunaga [102]. The comparison has been provided in table 4.1. It is found that the present results are in good agreement with that of Timoshenko Beam Theory (TBT) and Matsunaga for all the chosen values of (L/h). In order to further establish the correctness of the calculations, the first five natural frequencies of a steel-aluminum FGO beam are calculated and compared with [92, 141]. The present results are in good agreement as shown in table 4.1.

Table 4.3 shows the fundamental frequency of a steel-alumina FGO beam simply supported at both ends, with various L/h ratios considering different property distribution laws along the thickness of beam and table 4.4 shows the fundamental frequency of the beam resting on Winkler and Pasternak elastic foundations.

4.4.2 Functionally graded ordinary beam

A steel-alumina functionally graded ordinary beams with steel-rich bottom resting on Pasternak foundation is considered for the dynamic analysis. The length, breadth and thickness of the beam are 0.5m, 0.1m and 0.25m respectively. The frequencies of the FGO and FGSW beams are normalized with respect to the frequency of first mode of a steel beam of similar geometrical dimensions and end conditions. The properties of constituent phases are:

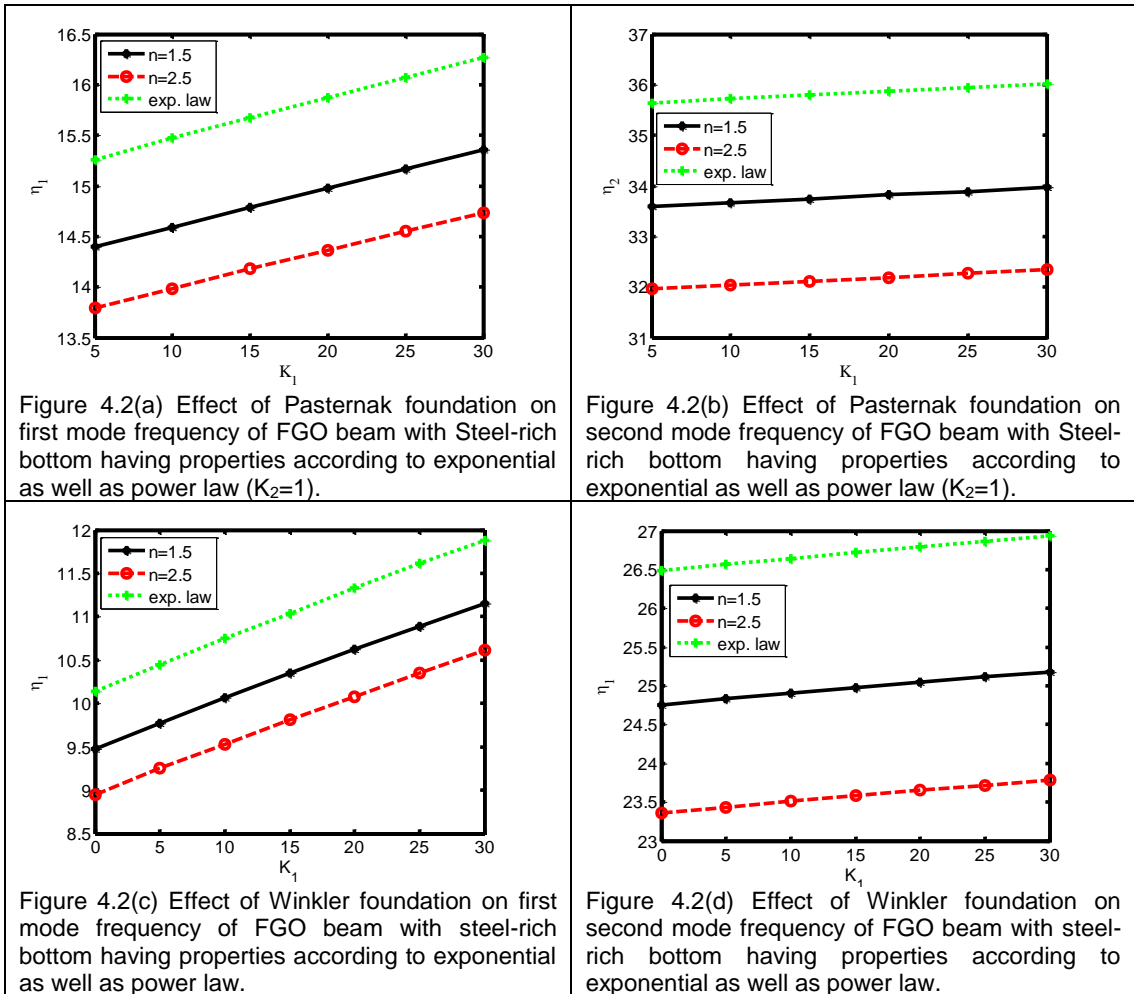
Steel: $E=2.1 \times 10^{11}$ Pa, $G=0.8 \times 10^{11}$ Pa $\rho = 7.85 \times 10^3 \text{kg/m}^3$,

Alumina: $E=3.9 \times 10^{11}$ Pa, $G=1.37 \times 10^{11}$ Pa, $\rho = 3.9 \times 10^3 \text{kg/m}^3$, $k=0.8667$.

The effects of Pasternak foundation on non-dimensional natural frequencies of beam for different laws of property distribution are shown in figures 4.2(a) and 4.2(b). Figure 4.2(a) shows the variation of first mode non-dimensional frequency with Winkler modulus (K_1), the foundation shear modulus (K_2) being one. It is observed that the frequency increases with increase in Winkler modulus for all the cases of property distribution. The frequency corresponding to any foundation stiffness is the highest for e-FGO beam and it is the lowest for FGO-2.5 beam. Figure 4.2(b) represents the effect of foundation on second mode frequency of the beams. A similar trend of results is obtained as obtained for first mode.

The effect of Winkler foundation on first two mode natural frequencies of the beam is shown in figures 4(c) and 4(d) for first and second mode respectively. A similar trend of variation of frequencies with foundation stiffness is observed as found

in case of Pasternak foundation. However the frequency of the beam on Pasternak foundation is found to be higher than that on Winkler foundation which is observed for all the kinds of beams considered.



This may be due to the fact that the Pasternak foundation has an additional contribution to increase of the effective stiffness of beam in the form of interaction of the shear layer that causes a higher frequency of the beam than the frequency of the beam resting on Winkler’s elastic foundation.

For dynamic stability study of beam, the following parameters are considered. The fundamental natural frequency $\omega_1 = 6724.9$ rad/s and the critical buckling load $P^\oplus = 11.37 \times 10^8$ N of an isotropic steel beam ($L=0.5$ m, $b=0.1$ m, $h=0.125$ m) of similar end conditions are calculated from eq. (4.19) and eq. (4.20) respectively without considering the effect of foundation.

Figures 4.3(a) and 4.3(b) show the effect of property distribution laws on the main instability regions of FGO beam with steel-rich bottom and resting on Pasternak

foundation ($K_1=5, K_2=1$) for first and second mode respectively. Figure 4.3(a) shows that the first mode instability region of e-FGO beam is situated farthest from the dynamic load factor axis. Hence it is the most stable beam. Similarly, the FGO-2.5 beam is the least stable and FGO-1.5 beam is the intermediate stable beam. The effect of foundation on second mode instability regions is found to be similar as found in case of first mode which can be noticed from figure 4.3(b).

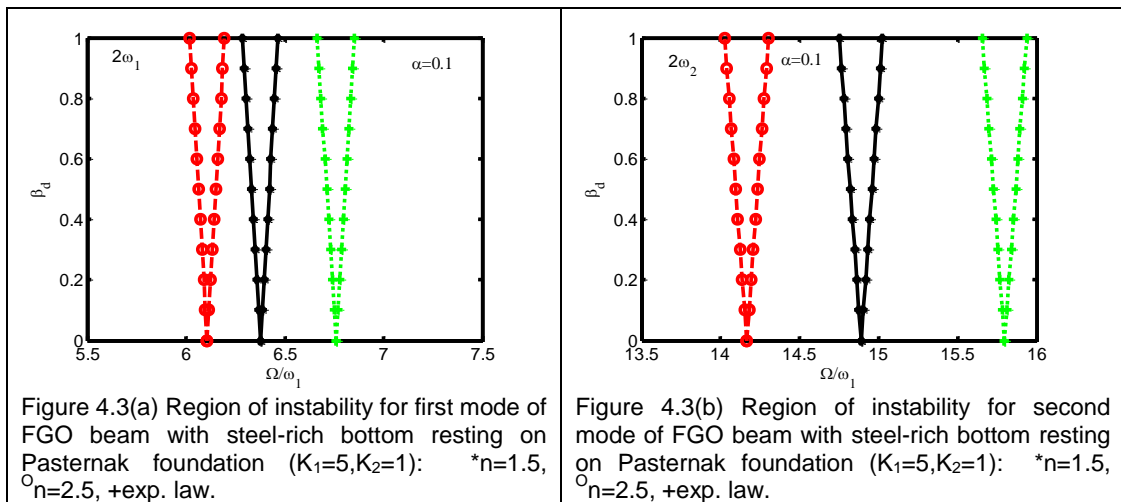
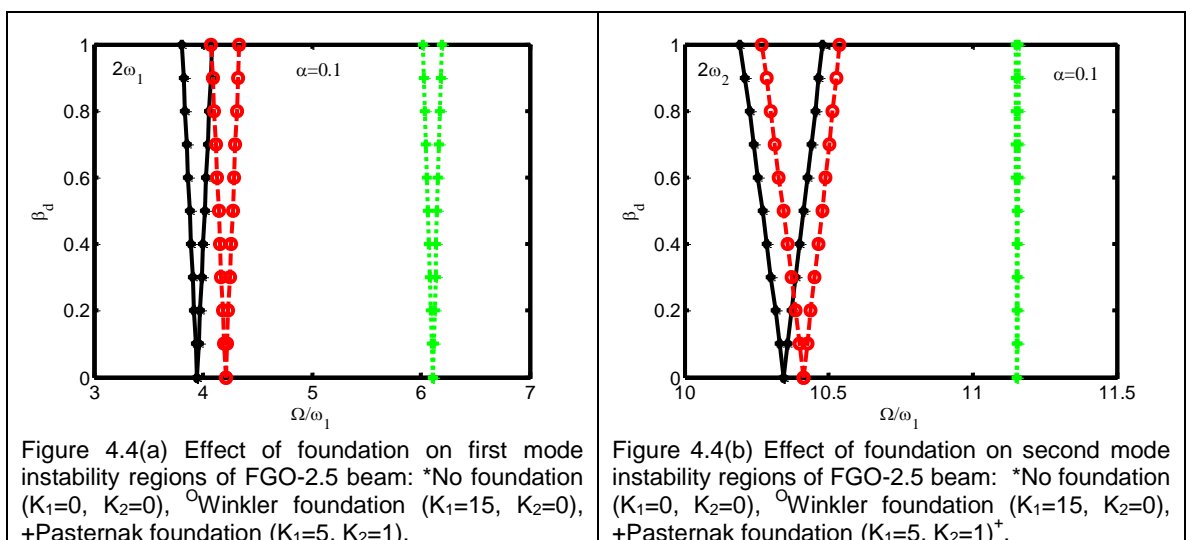
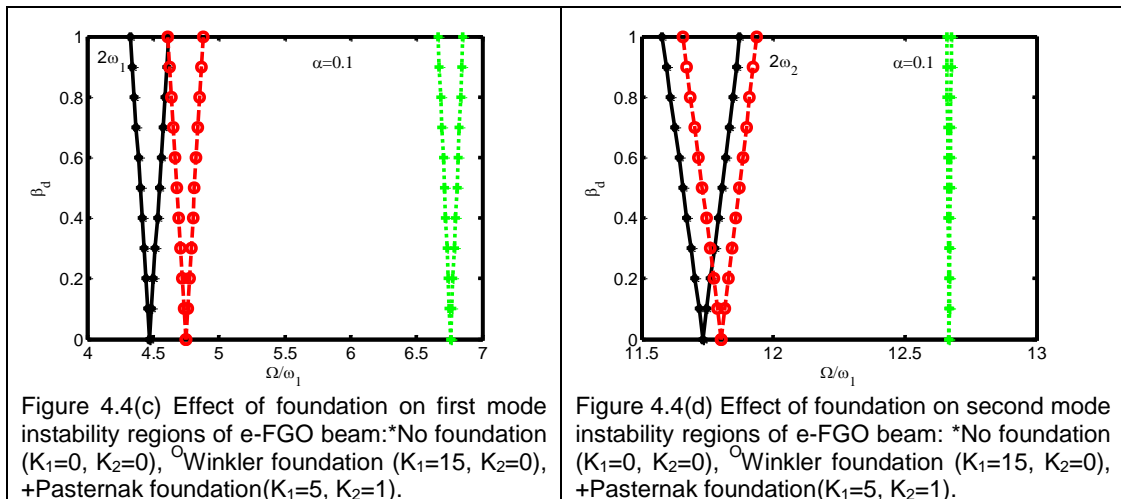


Figure 4.4 represents the comparison of effect of Winkler's foundation and Pasternak foundation on the stability of FGO beam for first two principal modes. Figures 4.4(a) and 4.4(b) show the instability regions of FGO-2.5 beam supported by Winkler foundation ($K_1=15, K_2=0$), Pasternak foundation ($K_1=5, K_2=1$) and no foundation ($K_1=0, K_2=0$) for first mode and second mode respectively. It is found that the beam on Pasternak foundation is more stable as compared to beam on Winkler's



foundation. This may be due to the fact that higher frequency of beam on Pasternak foundation as compared to Winkler's foundation causes the instability to occur at higher excitation frequencies.

The first and second principal instability regions of e-FGO beam resting on Winkler foundation ($K_1=10, K_2=0$), Pasternak foundation ($K_1=5, K_2=1$) and no foundation ($K_1=0, K_2=0$) are shown in figures 4.4(c) and 4.4(d) respectively. In this case also the Pasternak foundation has got more enhancing effect on the stability of beam as compared to Winkler foundation. Because, the instability regions of the FGO beam on Pasternak foundation are of less width and are located farther from the dynamic load factor axis as compared with the corresponding instability regions of the beam on Winkler's foundation.



4.4.3 Functionally graded sandwich beam

A functionally graded sandwich (FGSW) beam with steel as bottom skin, alumina as top skin and an FGM consisting of steel and alumina as core is chosen for dynamic analysis. The length width and thickness of the beam are taken as 0.5m, 0.1m and 0.25m respectively.

The effect of Pasternak foundation on non-dimensional frequency of steel-alumina FGSW beam for different distribution of properties is presented in figures 4.5(a) and 4.5(b) for first and second mode respectively. The foundation shear modulus (K_2) in this case is chosen as one and Winkler modulus (K_1) is varied from 5 to 30. From figures 4.5(a) and 4.5(b) it is found that the frequencies increase with the increase of foundation modulus appreciably for first mode. But the increase of frequency of second mode with the increase of foundation modulus is very small

irrespective of the type of property distribution laws. Moreover, the frequency of the e-FGSW beam is the highest corresponding to any foundation modulus (K_1). Similarly the frequency of FGSW-2.5 beam is the lowest of all. The above effects are observed for first two modes.

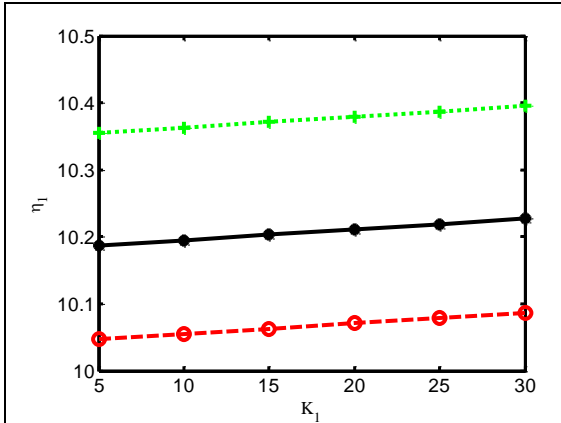


Figure 4.5(a) Effect of Pasternak foundation on first mode frequency of steel-alumina FGSW beam having properties according to exponential as well as power law ($K_2=1$): * $n=1.5$, $^{\circ}n=2.5$, +exp law.

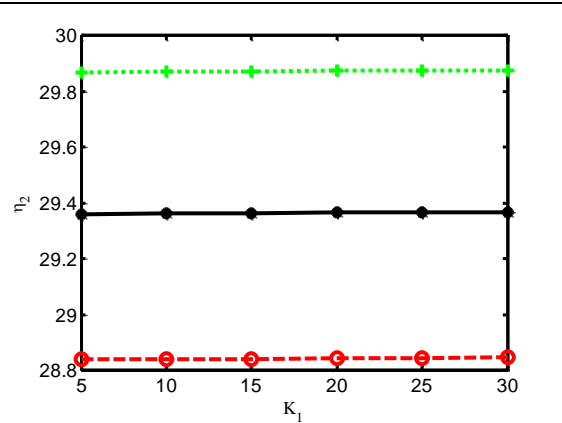


Figure 4.5(b) Effect of Pasternak foundation on second mode frequency of steel-alumina FGSW beam having properties according to exponential as well as power law (foundation shear modulus $K_2=1$): * $n=1.5$, $^{\circ}n=2.5$, +exp law.

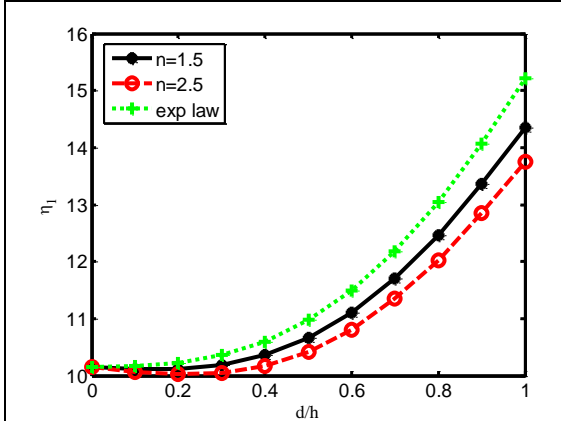


Figure 4.6(a) Effect of FGM content (d/h) on the first mode frequency of a steel-alumina FGSW beam resting on Pasternak foundation ($K_1=5$, $K_2=1$) and having properties as per exponential as well as power law.

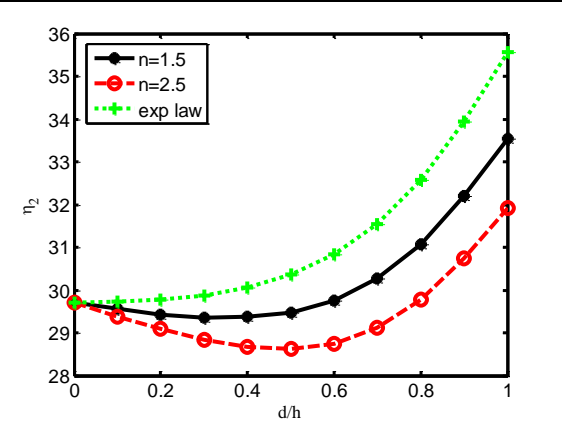


Figure 4.6(b) Effect of FGM content (d/h) on the second mode frequency of a steel-alumina FGSW beam resting on Pasternak foundation ($K_1=5$, $K_2=1$) and having properties as per exponential as well as power law.

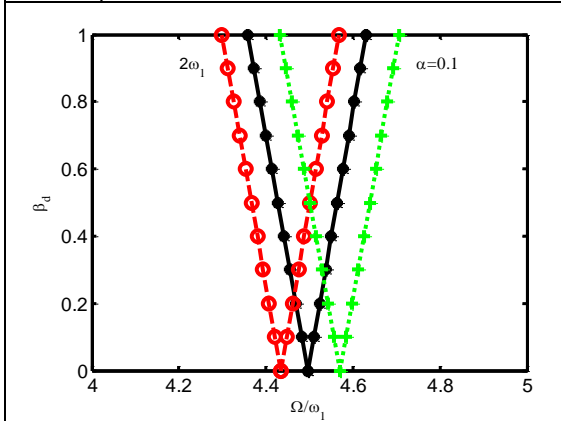


Figure 4.7(a) Regions of instability of steel-alumina FGSW beam on Pasternak foundation ($K_1=5$, $K_2=1$) for first mode: * $n=1.5$, $^{\circ}n=2.5$, +exp. law.

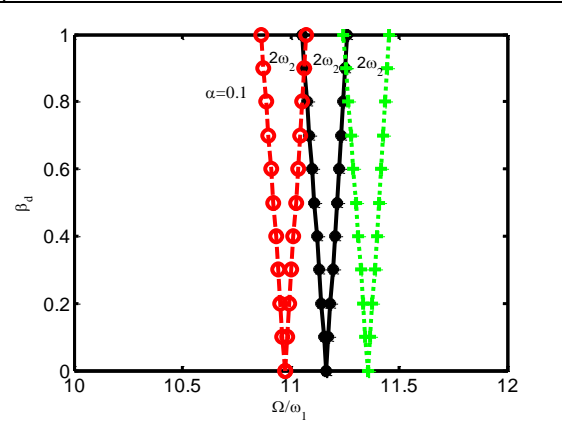


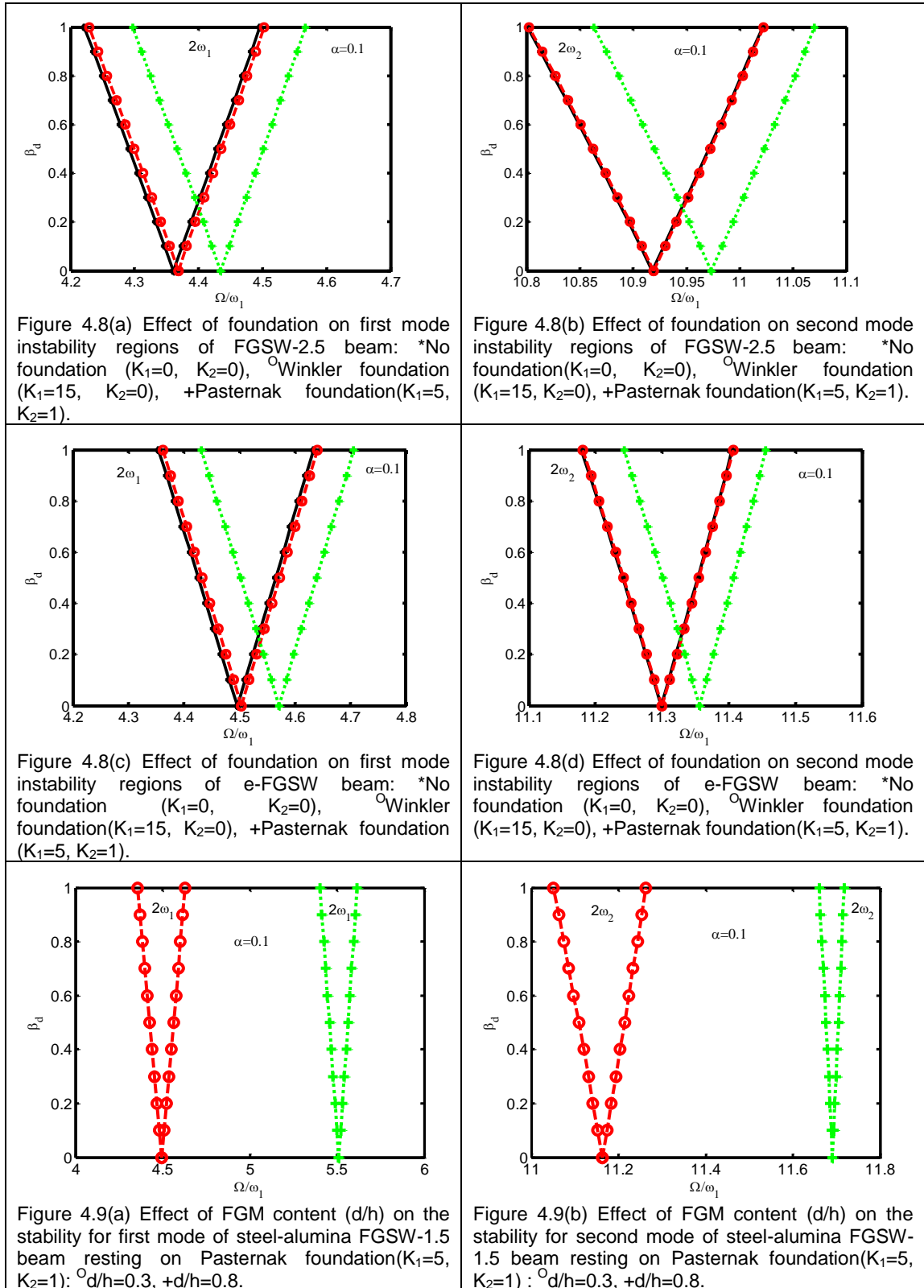
Figure 4.7(b) Regions of instability of steel-alumina FGSW beam on Pasternak foundation ($K_1=5$, $K_2=1$) for second mode: * $n=1.5$, $^{\circ}n=2.5$, +exp. law.

Figures 4.6(a) and 4.6(b) show the effect of FGM content (d/h) on the first mode and second mode non-dimensional frequencies of steel-alumina FGSW beam respectively. It is found that the first two mode frequencies increase nonlinearly with the increase of core thickness for all the type of beams. Moreover, the frequency of the e-FGSW beam is the highest corresponding to any core thickness. Similarly the frequency of FGSW-2.5 beam is the lowest of all. The above effect is found for first two modes.

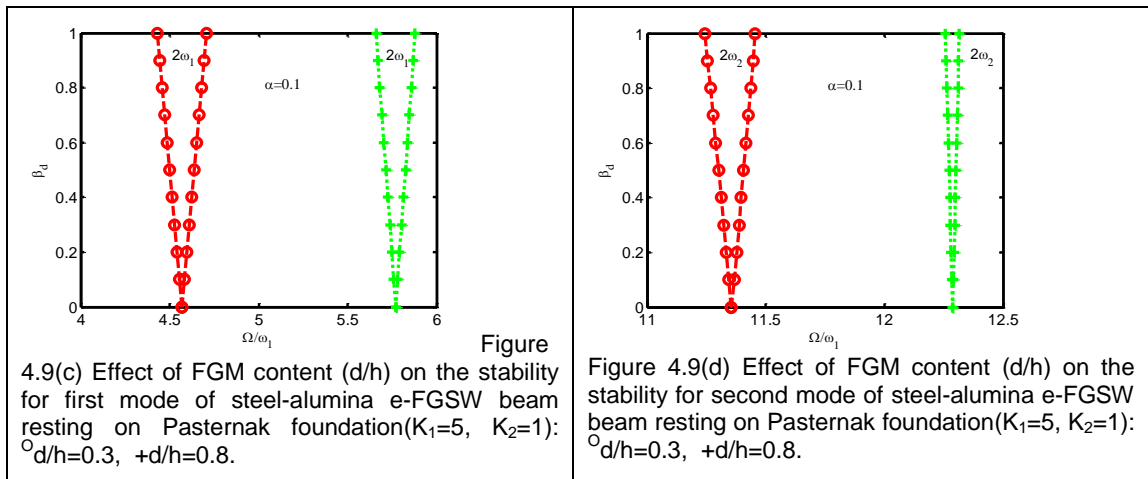
A comparison of principal instability regions of steel-alumina FGSW beam resting on Pasternak foundation and having properties according to power law with $n=1.5$, $n=2.5$ and exponential law are presented in figures 4.7(a) and 4.7 (b) for first mode and second mode respectively. The thickness of the FGM core is taken as 30 percent of the total thickness of the beam. It is observed that the FGSW-2.5 beam is the least stable of all as it's instability region is situated nearest to the dynamic load factor axis. Similarly, the e-FGSW beam is the most stable one and the stability of FGSW-1.5 beam lies in between the above two. The above said results are observed for both the modes. As the property variation along the core thickness as per exponential law renders the core of the beam to be the richest in alumina, so the e-FGSW beam becomes the beam with highest effective stiffness among all. As a result the instability of the beam occurs at the highest excitation frequency. Similarly, the effective stiffness of the FGSW-2.5 beam is the lowest due to the presence of highest amount of steel which leads to the occurrence of instability of the beam at the least excitation frequency.

A comparison of main instability regions of steel-alumina FGSW-2.5 beam resting on Winkler's foundation ($K_1=10$, $K_2=0$), Pasternak foundation ($K_1=5$, $K_2=1$) and no foundation ($K_1=0$, $K_2=0$) are shown in figures 4.8(a) and 4.8(b) for first mode and second mode respectively. The stability of the beam on Winkler's foundation is found to be more than that of the beam on no foundation. This may be due to the fact that the foundation increases the effective stiffness of beam which leads to the occurrence of instability at higher excitation frequencies. The stability of beam on Pasternak foundation is found to be more than that of the beam on Winkler foundation for both first and second modes. The effect of Winkler and Pasternak foundation on the first and second mode principal instability regions of e-FGSW beam is shown in figures 4.8(c) and 4.8(d) respectively. In this case also the enhancing effect on stability due to Pasternak foundation is found to be more than the stability due to Winkler foundation.

The effect of FGM content (d/h) in steel-alumina FGSW-1.5 beam is shown in figures 4.9(a) and 4.9(b) for first mode and second mode respectively. The ratio 'd/h' of values 0.3 and 0.8 are taken for the analysis. It is found that the beam having 80 percent FGM content ($d/h=0.8$) is more stable for both the modes as compared to the



beam with 30 percent FGM content. This result is in contrast to the results obtained in case of FGSW beam shown in figures 3.9(a) and 3.9(b). This may be due to the fact that the effect of foundation supersedes the effect of property distribution laws. Figures 4.9(c) and 4.9(d) show the effect of FGM content in steel-alumina e-FGSW beam for first and second mode respectively. It is clear from figures 4.9(c) and 4.9(d) that the beam having 80 per cent FGM ($d/h=0.8$) is more stable for first and second mode as its instability regions are of less width and are situated farther from the axis of dynamic load factor as compared to the beam having 30 percent FGM.



4.5 Closure

The dynamic stability behaviour of FGO beam and FGSW beam resting on Winkler's as well as Pasternak elastic foundations is investigated. The properties in the functionally graded material are assumed to vary according to power law as well as exponential law.

The first two natural frequencies of FGO beam increase with increase in stiffness of the foundations for both the types of distribution of properties.

The frequencies of first two modes of FGSW beam resting on Pasternak foundation increase with the increase in foundation stiffness for both the types of property distribution laws. The frequencies also increase with increase in core thickness of the beam.

The exponential distribution of properties along the thickness of FGO beam ensures higher stability as compared to power law distribution of properties.

For FGSW beam, the exponential distribution of properties along the thickness of the core ensures higher stability as compared to power law. Also increase in FGM content has a stabilising effect for both the property laws.

Pasternak foundation has got more dominant effect on the dynamic stability of both FGO and FGSW beams as compared to Winkler foundation.

CHAPTER 5

DYNAMIC STABILITY OF FUNCTIONALLY GRADED TIMOSHENKO BEAM IN HIGH TEMPERATURE ENVIRONMENT UNDER PARAMETRIC EXCITATION

5.1 Introduction

Some components of space structures, fusion reactors, space plane structures and turbine engines are used as thermal barriers. There was a need to invent an advanced material which could be used as thermal barriers in order to sustain surface temperature as high as 1800°C and temperature gradient of about 1300°C . The concept of FGMs was first proposed by the Japanese Scientist Koizumi and his co-researchers in 1984, as a solution to prepare such materials. A review of literature on behaviour of materials in thermal environment is presented below.

Paulino and Jin [117] have made an attempt to show that the correspondence principle can be applied to the study of viscoelastic FGM under the assumption that the relaxation moduli for shear dilation are separable functions in space and time. It

has also been predicted that the correspondence principle can be extended to specific instances of thermo-viscoelasticity and fracture of FGMs. Chakraborty et al [30] have developed a beam finite element to study the thermo elastic behaviour of functionally graded beam structures with exponential and power law variation of material properties along thickness. It is found that the presence of FGM in between the layers of metal and ceramic smoothens the stress difference. The effect of FGM on the natural frequency of beam clamped at both the ends has been investigated for both exponential and power law variation of material properties. It is observed that the rate of increase of frequencies with increase in FGM content increases with the exponent and the rate are higher for higher modes. Chaofeng et al. [31] have investigated the stress distribution in thick FGM beam subjected to mechanical and thermal loads with arbitrary end conditions. A semi-analytical method i.e. hybrid of state space method (SSM) and differential quadrature method (DQM) is developed for the analysis. It is observed that the maximum normalized mid-span normal stress occurs in the vicinity of neutral axis whereas the maximum shear stress occurs at the neutral axis. Sladek et al. [144] have developed an efficient numerical method to calculate the fracture parameters such as stress intensity factor and T-stresses of a functionally graded orthotropic beam subjected to thermal and impact mechanical load. The fact that getting fundamental solution for non-homogeneous anisotropic and linear elastic solid is very difficult can be circumvented by using the proposed local integration method. Nirmala et al [113] have derived an analytical expression to determine the thermoelastic stresses in a three layered composite beam system having an FGM as the middle layer. It has been shown that the method can be applicable where the gradation of the FGM is such that it may not be possible to express the volume fraction changes of the FGM constituents as a function of spatial coordinates. Moreover this method can be useful where more than one layer of FGMs are used in a single composite beam structure. Bhangale and Ganeshan [20] have studied the static and dynamic behaviour of FGM sandwich beam in thermal environment having constrained viscoelastic layer by finite element method. It is found that materials with lower thermal coefficient of expansion possess high thermal buckling temperature. The critical buckling temperature for an FGM sandwich beam increases as the power law index increases. Huang et al. [62] investigated the bending problem of a functionally graded anisotropic beam subjected to thermal and uniformly distributed load using a polynomial stress function. Jian and Li [76] have investigated the static and the active vibration control of a piezothermoelastic composite beam using a finite element model. Jurij and Maks [77] have investigated the effect of thermal load on the natural frequencies of simply supported beam and

clamped beam. They have applied the theory of vibration and statistical thermodynamics simultaneously for the purpose. A study of thermal buckling and vibration of sandwich beam with composite facings and viscoelastic core is carried out by Pradeep et al.[120]. Evandro and Joao [48] have used finite element method to evaluate nonlinear response of structures subjected to thermo-mechanical loading. A beam made up of functionally graded material simply supported at both the ends and subjected to lateral thermal shock loads is investigated by Babai et al. [14]. It is found that there is an optimum value of power law index for which the beam's lateral deflection is a minimum. In addition the amplitude of lateral vibration increases considerably as the aspect ratio of the beam decreases. The effect of coupling is to decrease the amplitude of vibration and increase the frequency of the vibration. Guo et al. [56] have investigated the coupled thermoelastic vibration characteristics of axially moving beams using differential quadrature (DQ) method. The effects of the dimensionless coupled thermoelastic factor, the ratio of length to height and the dimensionless moving speed on the stability of the beam are analyzed. The bending response of sandwich plates subjected to thermomechanical loads is studied by Zenkour and Alghamdi [170]. Mahi et al. [101] have studied the free vibration of functionally graded beams with temperature dependent properties. The effects of material constants, transverse shear deformation, temperature-dependent material properties, in-plane loading and boundary conditions on the nonlinear behaviour of FGM beams are investigated by Ma and Lee [99] using a shooting method.

There has been a good account of work on vibration of structures of metals and alloys in high temperature environment. However the amount of work carried out on dynamic stability of beam structures especially of FGM beams is meagre. This chapter explores the dynamic stability behaviour of FGO and FGSW beams in high temperature thermal environment.

5.2 Formulation

The FGSW beam simply supported at both ends as shown in figure 3.1(a) of chapter 3 is considered to be used in steady state high temperature environment. The increase in temperature of the beam causes it to expand freely. If the expansion is restricted at the boundaries stress is induced in the beam which decreases the stiffness of the beam. As the free expansion of beam with increase in temperature is linear the stiffness of beam decreases linearly with increase of temperature. The effect of high temperature is evaluated as a thrust and corresponding thermal

stiffness matrix is given below. A typical two noded beam element with 3-degrees of freedom per node as described in chapter-3 is chosen for the analysis.

5.2.1 Element thermal stiffness matrix

The thrust resulted due to non-uniform thermal expansion in FGM is given by

$$R_{th} = \int_A E(z)\alpha(z)\Delta T dA \quad (5.1)$$

where, $\alpha(z)$ is the co-efficient of thermal expansion of the FGM which varies along thickness and ΔT is the steady temperature change. It is assumed that no temperature gradient exists in any direction.

The work done by the thermal load can be expressed as

$$W_{th} = \frac{1}{2} \int_0^l R_{th} \left(\frac{\partial w}{\partial x} \right)^2 dx \quad (5.2)$$

Substituting the expression of w from eq. (3.20) in eq. (5.2)

$$W_{th} = \frac{1}{2} \{\hat{u}\}^T [k_{th}] \{\hat{u}\} \quad (5.3)$$

$$\text{Where } [k_{th}] = \int_0^l R_{th} [S'_w] [S'_w] dx \quad (5.4)$$

5.3 Governing equations of motion

The total work done on the beam is the sum of work done by axial force as given in eq. (3.35) and work done by thermal load as given in eq. (5.3). The elastic stiffness matrix and mass matrix for the FGSW beam element derived in section 3.2 are also applicable in this case and hence have not been repeated.

The equation of motion for the beam element referring section 3.3 can be modified for the present case and given as

$$[m] \{\ddot{\hat{u}}\} + \left([k_{ef}] - P^{\oplus} (\alpha + \beta_d \cos \Omega t) [k_g] \right) \{\hat{u}\} = 0 \quad (5.5)$$

$$\text{where } [k_{ef}] = [k_e] - [k_{th}] \quad (5.6)$$

$[k_{ef}]$ is the effective stiffness matrix and $[k_e]$, $[k_{th}]$, $[m]$ and $[k_g]$ are element elastic stiffness matrix, thermal stiffness matrix, mass matrix and geometric stiffness matrix respectively.

Assembling the element matrices as used in eq. (5.5), the equation in global matrix form which is the equation of motion for the beam in thermal environment, can be expressed as

$$[M]\{\ddot{\hat{U}}\} + \left([K_{ef}] - P^\oplus (\alpha + \beta_d \cos \Omega t) [K_g] \right) \{\hat{U}\} = 0 \quad (5.9)$$

$$[K_{ef}] = [K_e] - [K_{th}] \quad (5.10)$$

$[M]$, $[K_e]$, $[K_{th}]$, $[K_g]$ are global mass, elastic stiffness, thermal stiffness and geometric stiffness matrices respectively and $\{\hat{U}\}$ is global displacement vector. The condition for existence of the boundary solutions with period $2T$ is given by

$$\left([K_{ef}] - (\alpha \pm \beta_d / 2) P^\oplus [K_g] - \frac{\Omega^2}{4} [M] \right) \{\hat{U}\} = 0 \quad (5.11)$$

The instability boundaries can be determined from the solution of the equation

$$\left| [K_{ef}] - (\alpha \pm \beta_d / 2) P^\oplus [K_g] - \frac{\Omega^2}{4} [M] \right| = 0 \quad (5.12)$$

Following the procedure described in section 3.3.1-3.3.3, the natural frequencies, critical buckling load and instability regions of the beam in high temperature environment are determined.

5.4 Results and discussion

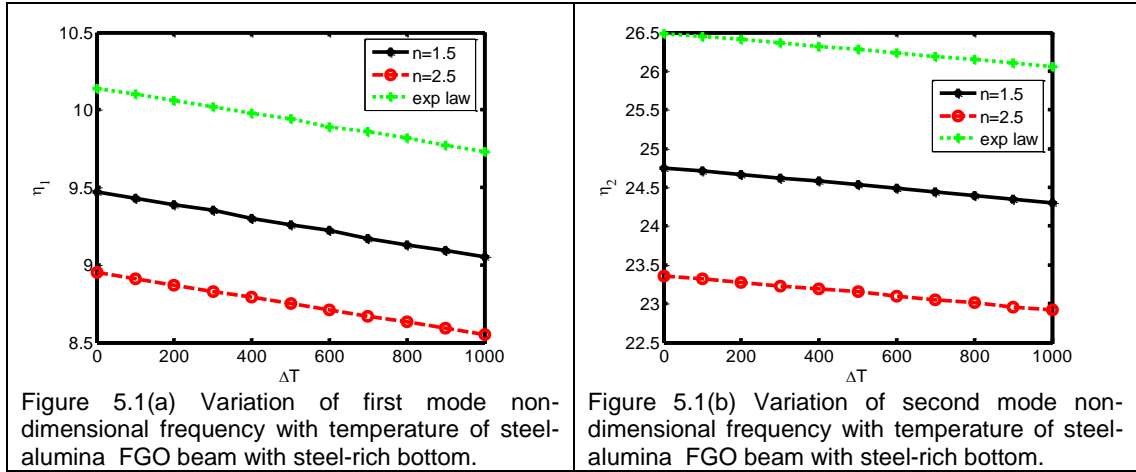
The beam is discretized into 100 elements for the numerical study of vibration and stability. The boundary conditions used are as given below.

At $x = 0$, $w = 0$ and $u = 0$, at $x = L$, $w = 0$.

5.4.1 Functionally graded ordinary beam

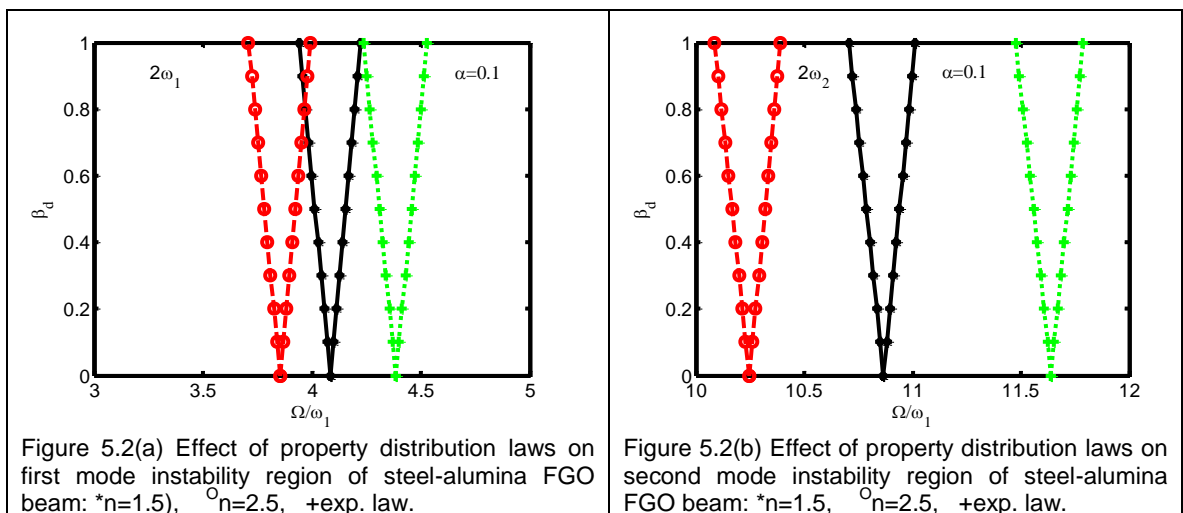
A functionally graded sandwich beam of length 0.5m breadth 0.1m and thickness 0.25m, simply supported at both the ends is considered for vibration and dynamic stability analysis.

Figure 5.1(a) and 5.1(b) show the variation of non-dimensional frequency of steel-alumina FGO beam with steel-rich bottom for first mode and second mode respectively. The properties along the thickness of the beam are assumed to vary as per exponential law as well as power law with index $n=1.5$, and $n=2.5$. It is observed from the plots that increase in temperature decreases the frequency in all the cases. It is also observed that the first as well as the second mode frequency of e-FGO beam is the highest and that of FGO-2.5 beam is the lowest corresponding to any temperature.



For dynamic stability study of the FGO beam the following data are considered. The fundamental natural frequency $\omega_1 = 6724.9$ rad/s and the critical buckling load $P^{\oplus} = 11.37 \times 10^8$ N of an isotropic steel beam ($L=0.5$ m, $b=0.1$ m, $h=0.125$ m) with similar end conditions are calculated from eq. (5.16) and eq. (5.17) respectively without considering the effect of thermal load.

The principal instability regions of FGO beams having properties along the thickness as per exponential law as well as power law are plotted in Figures 5.2(a) and 5.2(b) for first mode and second mode respectively. The beam is used in an environment of temperature 500° K more than the ambient temperature. The instability regions of e-FGO beam are located farthest from the dynamic load factor axis. Hence, it is the most stable beam. Similarly the FGSW-2.5 beam and FGSW-1.5 beam are respectively the least and intermediate stable beams.



The effect of temperature on the main instability regions of steel-alumina FGO beam with steel-rich bottom is shown in figures 5.3(a) through 5.3(d). The main instability

regions of beam at ambient temperature, 500⁰K more and 1000⁰K more than ambient temperature are compared using static load factor (α) as 0.1. The beam material is assumed to be elastic under the high temperature environment. The instability regions of FGO-2.5 beam are shifted towards the axis of dynamic load factor as the temperature of environment increases thereby reducing the stability of the beam which can be noticed from figures 5.3(a) and 5.3(b) for first mode and second mode respectively.

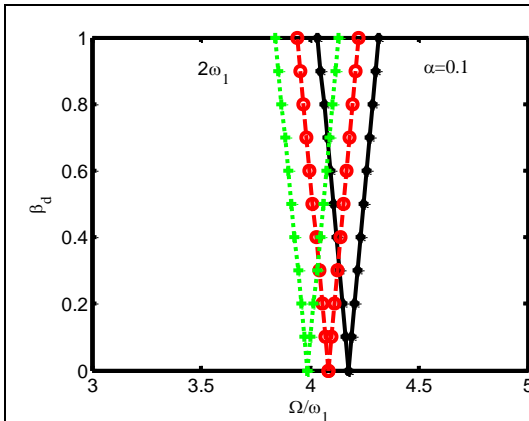


Figure 5.3(a) Effect of temperature on first mode instability region of steel-alumina FGO-2.5 beam: *0⁰, ⁰500⁰, +1000⁰.

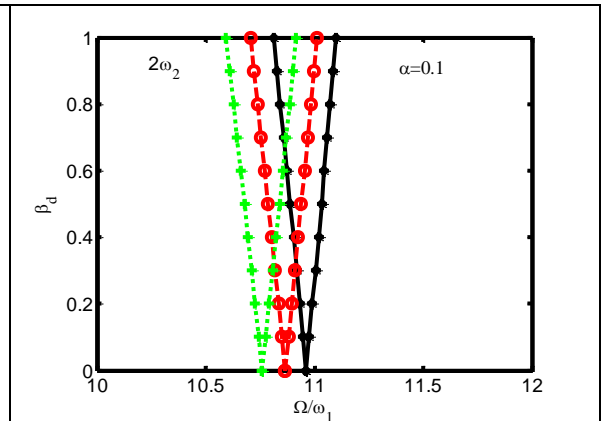


Figure 5.3(b) Effect of temperature on second mode instability region of steel-alumina FGO-2.5 beam: *0⁰, ⁰500⁰, +1000⁰.

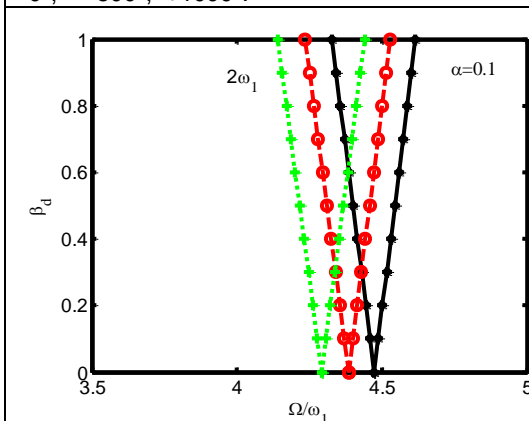


Figure 5.3(c) Effect of temperature on first mode instability region of steel-alumina e-FGO beam: *0⁰, ⁰500⁰, +1000⁰.

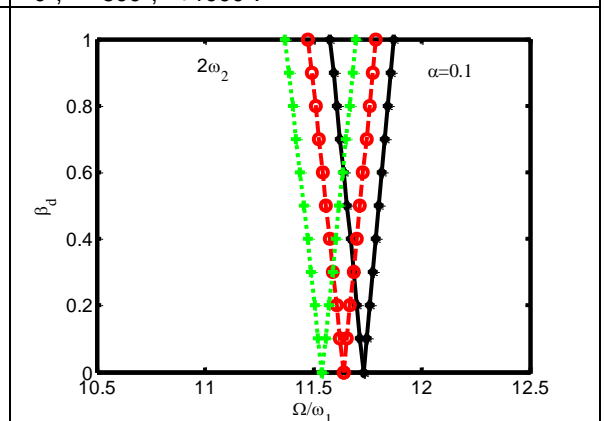


Figure 5.3(d) Effect of temperature on second mode instability region of steel-alumina e-FGO beam: *0⁰, ⁰500⁰, +1000⁰.

Figure 5.3(c) and 5.3(d) show respectively the first and second mode main instability regions of e-FGO beam. Similar trend of results as that of FGO-2.5 beam are observed. Since the instability regions occur at lesser value of excitation frequency, the chance of occurrence of instability is more. Moreover, there is an increase in area of instability region. Hence at higher environmental temperature there is enhanced instability of the beam. This may be due to the fact that the high temperature of the beam reduces its effective stiffness and hence frequencies. The decrease in frequency causes the dynamic instability to occur at lower excitation frequencies.

5.4.2 Functionally graded sandwich beam

A functionally graded sandwich beam of length 0.5m breadth 0.1m and thickness 0.25m is considered for vibration and dynamic stability analysis. The top skin and bottom skin are alumina and steel respectively. The thickness of the core is taken as 0.3 times the thickness of the beam. The properties along the thickness of the core are assumed to follow exponential law and power law with index $n=1.5$ and $n=2.5$. The variation of first mode and second mode non-dimensional frequency with temperature of the beam is plotted in figures 5.4(a) and 5.4(b) respectively. It is observed that the frequency for both the modes decrease with increase of temperature. The e-FGSW beam has the highest frequencies and FGSW-2.5 beam has the lowest frequencies corresponding to any temperature similar to the results obtained in case of FGO beam.

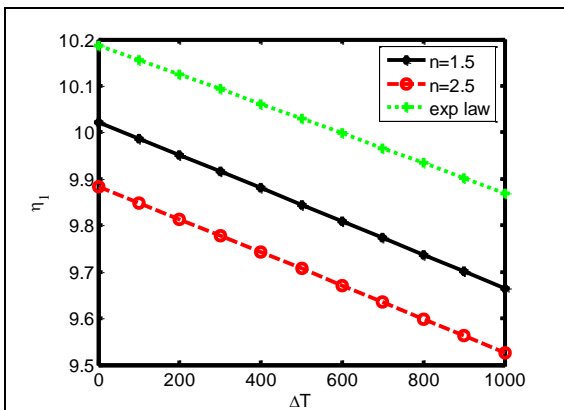


Figure 5.4(a) Variation of first mode non-dimensional frequency of FGSW beam($d/h=0.3$) with temperature.

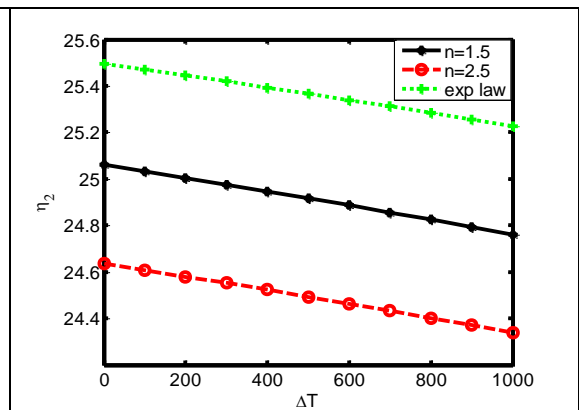


Figure 5.4(b) Variation of second mode non-dimensional frequency of FGSW beam($d/h=0.3$) with temperature.

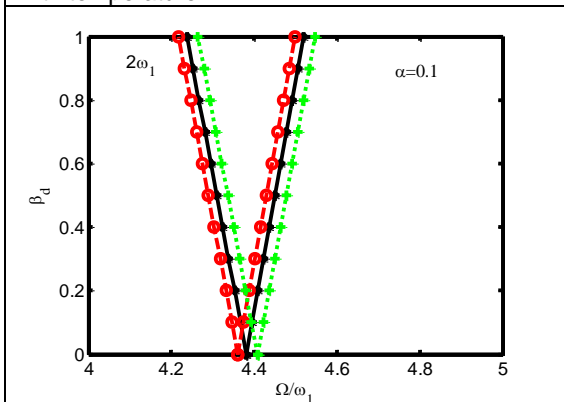


Figure 5.5(a) Effect of property distribution laws on first mode instability region of steel-alumina FGSW beam: * $n=1.5$, $\circ n=2.5$, +exp. law.

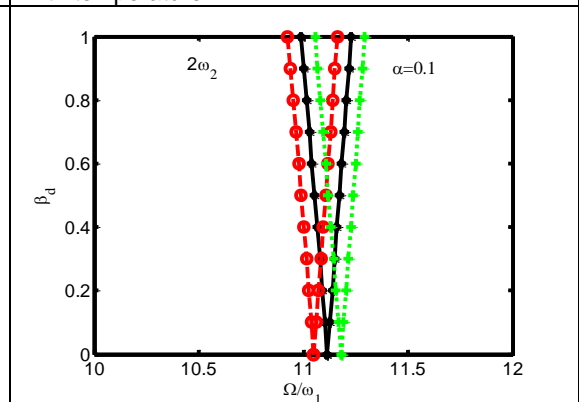


Figure 5.5(b) Effect of property distribution laws on second mode instability region of steel-alumina FGSW beam: * $n=1.5$, $\circ n=2.5$, +exp. law.

The effect of property distributions on the principal instability regions of FGSW beam is plotted in figures 5.5(a) and 5.5(b) for first mode and second mode respectively. The beam is used in an environment of temperature 500°K more than the ambient temperature. The instability regions of e-FGSW beam are at the farthest

from the axis of dynamic load factor. Therefore, it is the most stable beam. Similarly the FGSW-2.5 beam and FGSW-1.5 beam are respectively the least and intermediate stable beams. However, the effect of property distributions is less prominent as compared to that found in case of FGO beam.

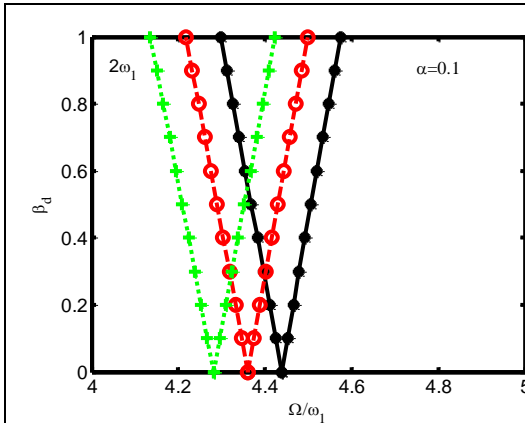


Figure 5.6(a) Effect of temperature on first mode instability region of steel-alumina FGSW-2.5 beam: * 0° , 500° , $+1000^{\circ}$.

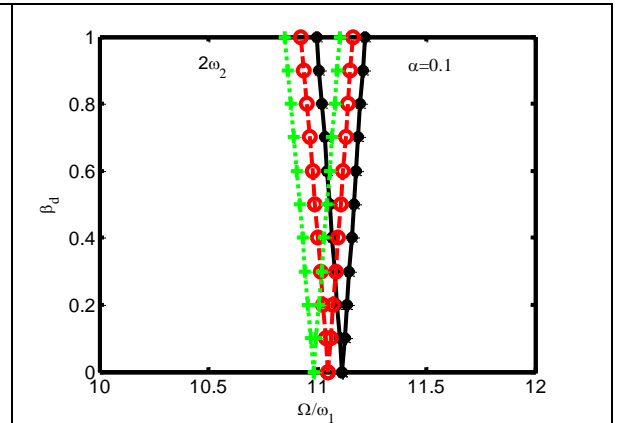


Figure 5.6(b) Effect of temperature on second mode instability region of steel-alumina FGSW-2.5 beam: * 0° , 500° , $+1000^{\circ}$.

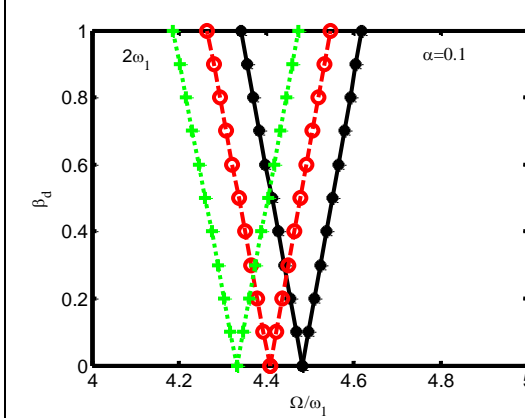


Figure 5.6(c) Effect of temperature on first mode instability region of steel-alumina e-FGSW beam: * 0° , 500° , $+1000^{\circ}$.

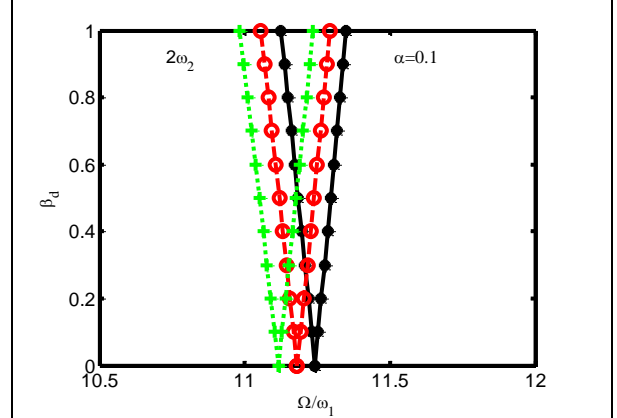


Figure 5.6(d) Effect of temperature on second mode instability region of steel-alumina e-FGSW beam: * 0° , 500° , $+1000^{\circ}$.

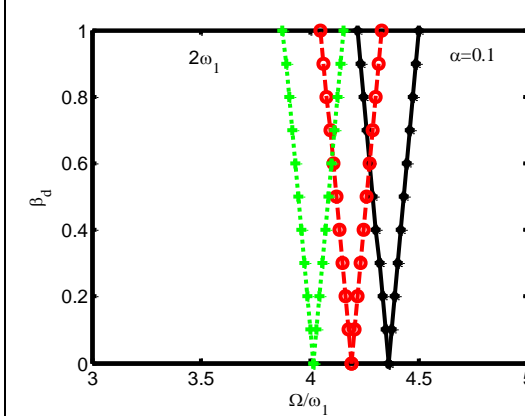


Figure 5.7(a) Effect of ratio (d/h) on the first mode instability regions of FGSW-2.5 beam: * $d/h=0.3$, $0^{\circ}d/h=0.5$, $+d/h=0.8$.

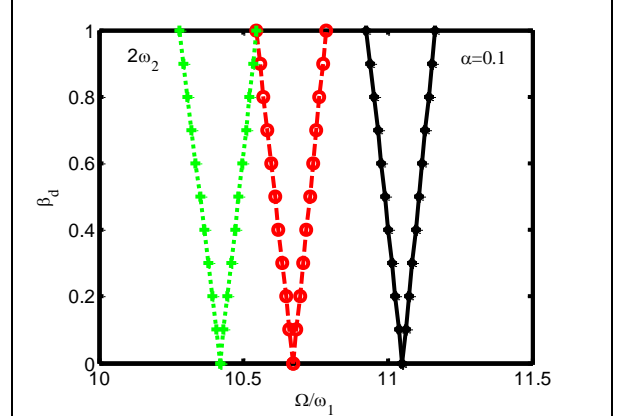
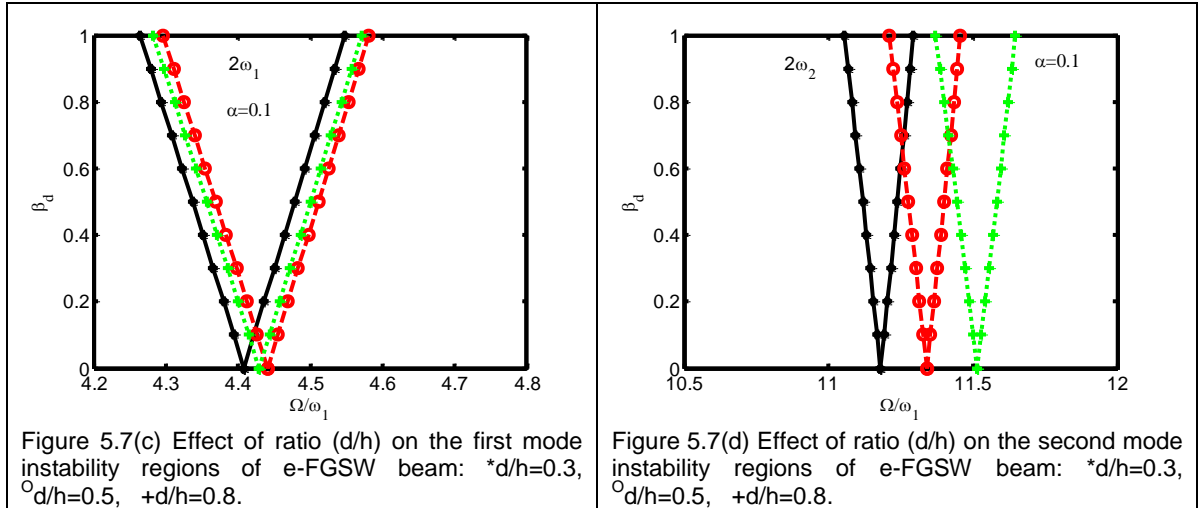


Figure 5.7(b) Effect of ratio (d/h) on the second mode instability regions of FGSW-2.5 beam: * $d/h=0.3$, $0^{\circ}d/h=0.5$, $+d/h=0.8$.



Figures 5.6(a) and 5.6(b) represent respectively the first mode and second mode main instability regions of FGSW-2.5 beam in thermal environment of different temperatures. It is seen that the increase in environment temperature reduces the stability of beam. The higher the environmental temperature lower is the stability of e-FGSW beam which can be clearly noticed from figures 5.6(c) and 5.6(d) for first mode and second mode respectively.

The main instability regions of steel-alumina FGSW beam of different core thickness at a temperature 500°K more than the ambient temperature are compared and shown in figures 5.7(a) through 5.7(d). The core thickness equal to 30, 50 and 80 percent of total thickness are chosen for comparison.

Figures 5.7(a) and 5.7(b) show the principal instability regions of FGSW-2.5 beam for first and second mode respectively. It is observed that increase in FGM content reduces the dynamic stability of the beam. A different result is found for e-FGSW beam. Figure 5.7(c) shows the instability region of e-FGSW beam for first mode. The increase of FGM content from 0.3 to 0.5 enhances the stability of beam whereas the stability decreases as the FGM content increases further from 0.5 to 0.8. The second mode instability region is shifted away from the dynamic load factor axis when the FGM content increases as shown in figure 5.7(d). Therefore it may be noted that the property distribution laws along with the high temperature environment play an important role on the dynamic stability of the FGSW beam.

5.5 Closure

Increase in environmental temperature reduces the frequencies of both FGO and FGSW beam for all the kinds of chosen property variation along their thickness.

Increase in environment temperature enhances the chance of instability of FGO and FGSW beams

Material property distribution as per exponential law ensures better stability of the FGO and FGSW beams compared to material property distribution as per power law.

The property distribution laws along with the high temperature environment play a major role on the dynamic stability of FGO and FGSW beams.

CHAPTER 6

DYNAMIC STABILITY OF ROTATING FUNCTIONALLY GRADED TIMOSHENKO BEAM UNDER PARAMETRIC EXCITATION

6.1 Introduction

Vibration in rotating structures such as wind turbine and helicopter rotors, turbo machinery and rotating space structures is a naturally occurring phenomenon. Therefore, the stability and dynamic behaviour of these rotating structures are of great practical importance. In practice, the aforesaid rotating components are usually pre-twisted and of asymmetric cross-section. However, rotating beams of uniform cross-section can be used as simple model to investigate the stability and dynamic behaviour of the actual rotating structures. A good account of literature surveyed on the research work carried out on rotating structures is reported below.

The effect of rotational speed and slenderness ratio on the error of the upper bound and the influence of root elastic restraints on the fundamental bending frequency of a rotating uniform Timoshenko beam with general elastically restrained root is studied by Lee and Kuo [85] using Rayleigh's principle. The dynamic stiffness matrix of a centrifugally stiffened Timoshenko beam has been developed by Banerjee [16] using Forbenus method of series solution with imposed boundary conditions for

study of free vibration. Wittrick–Williams algorithm has been applied to find the natural frequencies. Rao and Gupta [123] have used finite element method to study vibration of rotating Timoshenko beam. Chung and Yoo [38] investigated the effect of angular speed on the natural frequency of a rotating cantilever beam. They have used finite element method considering stretch deformation of the beam. Kaya [79] has studied the flapwise bending vibration analysis of a rotating cantilever Timoshenko beam using differential transform method. The effect of pre-twist angle of an aerofoil blade simplified as a rotating Timoshenko beam has been investigated by Subuncu and Ervan [127]. Fazelzadeh et al. [50] have studied vibration of rotating thin walled blades made of FGM operating under high temperature supersonic gas flow using differential quadrature method. The effects of Mach number, rotating speed, geometric parameters and material properties on the natural frequencies are examined. Chhabra and Ganguli [40] have developed a two-noded twelve degree of freedom finite element for study of coupled vibration of rotating blades. Saravia et al. [132] have used finite element method to investigate the influence of fiber orientation and rotating speeds on the natural frequencies and the unstable regions of rotating thin walled composite beam. The phenomenon of modal interchange arising in rotating beams is explained by the authors.

The literatures on dynamic stability of rotating beams made of metals, alloys and composites are plenty. But a very less amount of work has been reported on dynamic stability of functionally graded beams. This chapter is devoted to the investigation of the effect of beam geometry, hub radius and rotating speed on dynamic stability of FGO and FGSW beams.

6.2 Formulation

A functionally graded sandwich beam with top skin as alumina, bottom skin as steel and core as FGM is shown in figure 6.1(a). The beam clamped at one end free at the other end is subjected to a pulsating axial force $P(t) = P_s + P_t \cos \Omega t$, acting along its un-deformed axis. The static component of the axial force is P_s . The amplitude and frequency of the dynamic component of the force are P_t and Ω respectively, and t is time. The coordinate system of the typical two noded beam element used to derive the governing equations of motion is shown in figure 3.1(b) of chapter 3. The mid-longitudinal(x-y) plane is chosen as the reference plane for expressing the displacements.

The element matrices for the FGSW beam element are derived in section 3.2 of chapter. Moreover the same element can be used for the analysis of a functionally graded ordinary beam by making the thickness of the skins equal to zero.

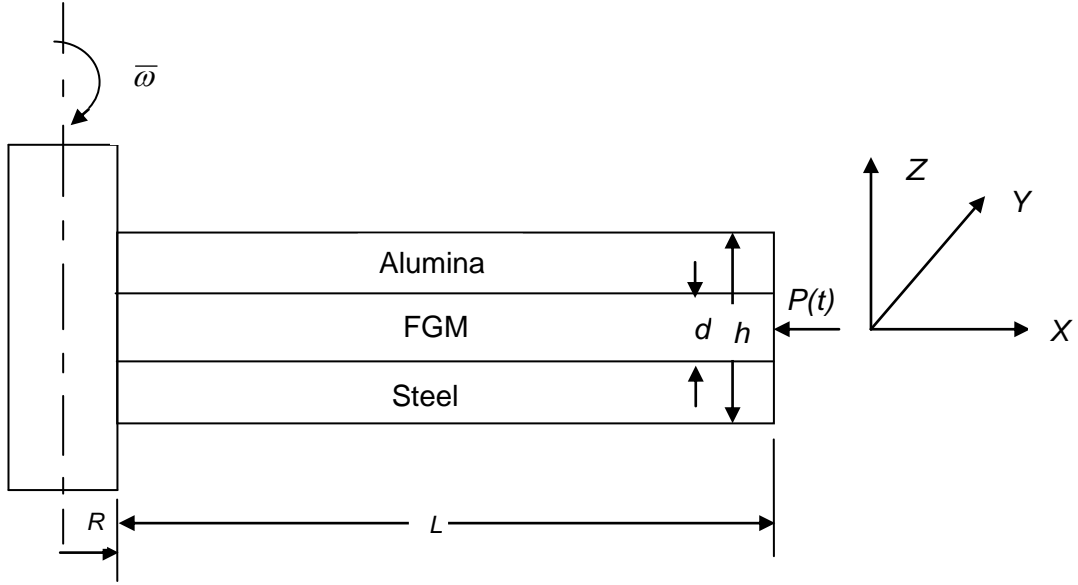


Figure 6.1 Rotating functionally graded sandwich beam fixed at one end free at the other.

The elastic stiffness matrix and mass matrix for the FGSW beam element derived in section 3.2 are also applicable in this case and hence the expressions have not been repeated.

The effect of rotation is introduced as centrifugal stiffness matrix which is derived from the work done by the centrifugal force and presented as follows.

6.2.1 Element centrifugal stiffness matrix

The centrifugal force on i^{th} element of the beam can be expressed as

$$F_c = \int_{x_i}^{x_i+l} \int_{-h/2}^{h/2} b\rho(z)\bar{\omega}^2(R+x)dzdx \quad (6.1)$$

where x_i is the distance of i^{th} node from axis of rotation, $\bar{\omega}$ (rad/s) is angular velocity of beam and R is the radius of hub.

Work done by the centrifugal force is given by

$$W_c = \frac{1}{2} \int_0^l F_c \left(\frac{dw}{dx} \right)^2 dx = \frac{1}{2} \{\hat{u}\} [k_c] \{\hat{u}\} \quad (6.2)$$

Here, the centrifugal element stiffness matrix is

$$[k_c] = \int_0^l F_c [S'_w]^T [S'_w] dx \quad (6.3)$$

6.2.2 Element effective stiffness matrix

The stiffness matrix of the beam element is the addition of element elastic stiffness matrix and element centrifugal stiffness matrix which is expressed as

$$[k_{ef}] = [k_e] + [k_c] \quad (6.4)$$

6.3 Governing equations of motion

The equation of motion for the beam element referring section 3.3 can be modified for the present case and given as

$$[m] \{\ddot{\hat{u}}\} + [[k_{ef}] - P^\oplus (\alpha + \beta_d \cos \Omega t) [k_g]] \{\hat{u}\} = 0 \quad (6.5)$$

$[k_{ef}]$ is the effective stiffness matrix and $[k_e]$, $[k_c]$, $[m]$ and $[k_g]$ are element elastic stiffness matrix, centrifugal stiffness matrix, mass matrix and geometric stiffness matrix respectively.

Assembling the element matrices as used in eq. (6.5), the equation in global matrix form which is the equation of motion for the rotating beam, can be expressed as

$$[M] \{\ddot{\hat{U}}\} + [[K_{ef}] - P^\oplus (\alpha + \beta_d \cos \Omega t) [K_g]] \{\hat{U}\} = 0 \quad (6.6)$$

$$[K_{ef}] = [K_e] + [K_c] \quad (6.7)$$

$[M]$, $[K_e]$, $[K_c]$, $[K_g]$ are global mass, elastic stiffness, centrifugal stiffness and geometric stiffness matrices respectively and $\{\hat{U}\}$ is global displacement vector. The condition for existence of these boundary solutions with period $2T$ is given by

$$\left([K_{ef}] - (\alpha \pm \beta_d / 2) P^\oplus [K_g] - \frac{\Omega^2}{4} [M] \right) \{\hat{U}\} = 0 \quad (6.8)$$

The instability boundaries can be determined from the solution of the equation

$$\left| [K_{ef}] - (\alpha \pm \beta_d / 2) P^\oplus [K_g] - \frac{\Omega^2}{4} [M] \right| = 0 \quad (6.9)$$

Following the procedure described in section 3.3.1-3.3.3, the natural frequencies, critical buckling load and instability regions of the rotating beam are determined.

6.4 Results and discussion

The numerical study is carried out for a cantilever beam using 100 elements. The beam is discretized into 100 elements. The boundary conditions used for the numerical study are as given below.

$$\text{At } x = 0, \quad w = 0, \quad \phi = 0 \text{ and } u = 0.$$

An FGO beam with steel and alumina as its constituent phases is considered for the analysis followed by the study of an FGSW beam made up of steel and alumina.

6.4.1 Validation of the formulation

In order to establish the correctness of calculation, the fundamental non-dimensional natural frequencies of a homogenous rotating steel beam clamped at one end and free at other end are calculated for various rotational speed parameters and compared with [79, 16, and 85]. The present results are found to be in good agreement as shown in table 6.1.

The length of the beam is denoted by L .

$$\text{Hub radius parameter } \delta = \frac{R}{L}, \quad \text{Rotary inertia parameter } r = \frac{1}{L} \sqrt{\frac{I}{A}},$$

$$\text{Frequency parameter } \eta_n = \sqrt{\frac{\rho A L^4 \omega_n^2}{EI}}$$

I is the area moment of inertia of the cross section about the centroidal axis. ω_n is the n^{th} mode frequency of the beam and η_n is the n^{th} mode frequency parameter.

Table 6.1 Variation of fundamental natural frequency of Timoshenko cantilever beam for different rotational speed parameters ($\delta = 0$, $r = 1/30$, $E/kG = 3.059$)

ν	Fundamental natural frequency η_1			
	present	Ref[79]	Ref[16]	Ref[85]
0	3.4798	3.4798	3.4798	3.4798
1	3.6460	3.6445	3.6445	3.6452
2	4.1025	4.0971	4.0971	4.0994
3	4.7617	4.7516	4.7516	4.7558
4	5.5462	5.5314	5.5314	5.5375
5	6.4048	6.3858	6.3858	6.3934
10	11.0971	11.0643	-	-

The following additional non-dimensional parameters are chosen for the analysis of the beam.

Slenderness parameter $s=h/L$

$$\text{Rotational speed parameter } \nu = \sqrt{\frac{\rho AL^4 \bar{\omega}^2}{EI}}$$

E , G and ρ are the Young's modulus, shear modulus and mass density of steel respectively and their values are given in the following section.

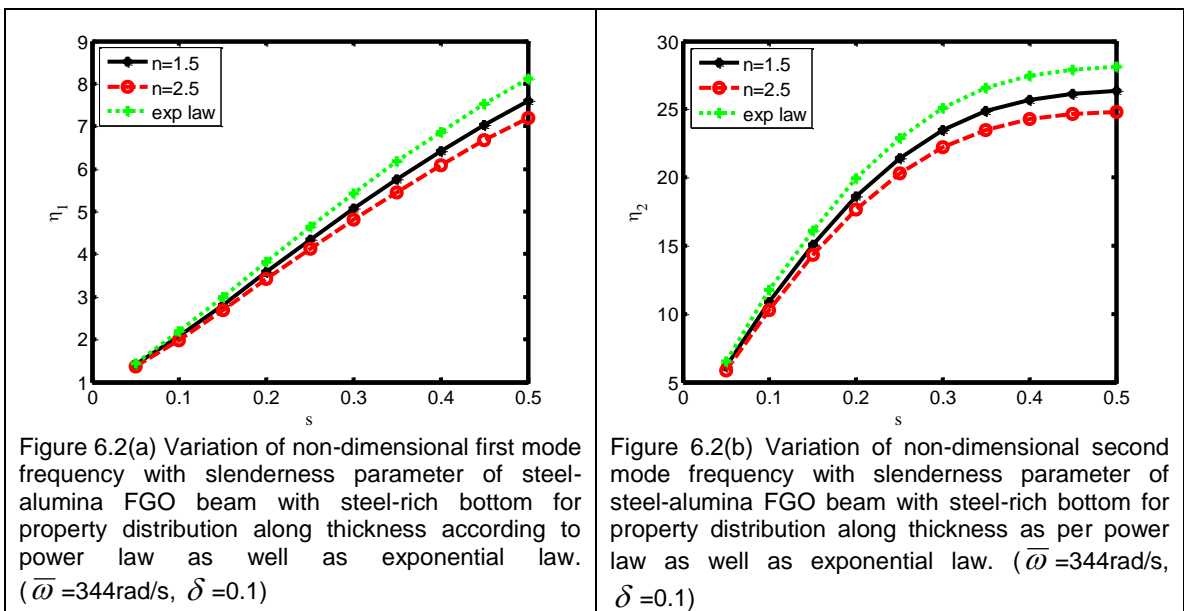
6.4.2 Functionally graded ordinary beam

A steel-alumina FGO rotating cantilever beam of length 1m and width 0.1m is considered for the analysis of free vibration and dynamic stability. The thickness of the beam is h . The beam is rich in steel at bottom. The properties of constituent phases are:

Steel: $E=2.1 \times 10^{11}$ Pa, $G=0.8 \times 10^{11}$ Pa, $\rho=7.85 \times 10^3 \text{kg/m}^3$,

Alumina: $E=3.9 \times 10^{11}$ Pa, $G=1.37 \times 10^{11}$ Pa, $\rho=3.9 \times 10^3 \text{kg/m}^3$, $k=0.8667$ as explained in section 3.4.2.

The variation of non-dimensional frequency with slenderness parameter(s) is shown in figures 6.2(a) and 6.2(b) for first and second mode respectively. The property distribution along the thickness is assumed to follow exponential as well as



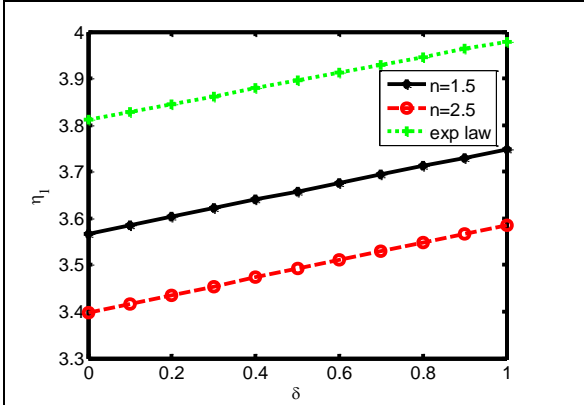


Figure 6.3(a) Variation of non-dimensional first mode frequency with hub radius parameter of steel-alumina FGO beam with steel-rich bottom for property distribution along thickness as per power law as well as exponential law. ($\bar{\omega}=344\text{rad/s}$, $s=0.2$)

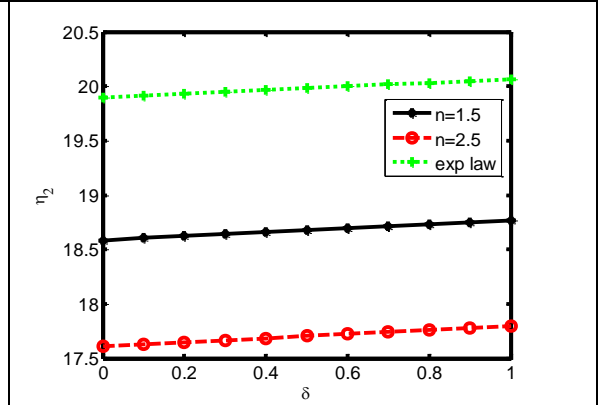


Figure 6.3(b) Variation of non-dimensional second mode frequency with hub radius parameter of steel-alumina FGO beam with steel-rich bottom for property distribution along thickness as per power law as well as exponential law. ($\bar{\omega}=344\text{rad/s}$, $s=0.2$)

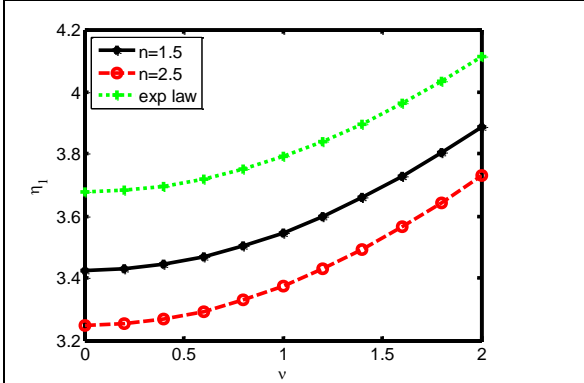


Figure 6.4(a) Variation of non-dimensional first mode frequency with rotational speed parameter of steel-alumina FGO beam with steel-rich bottom for property distribution along thickness as per power law as well as exponential law. ($\delta=0.1$, $s=0.2$)

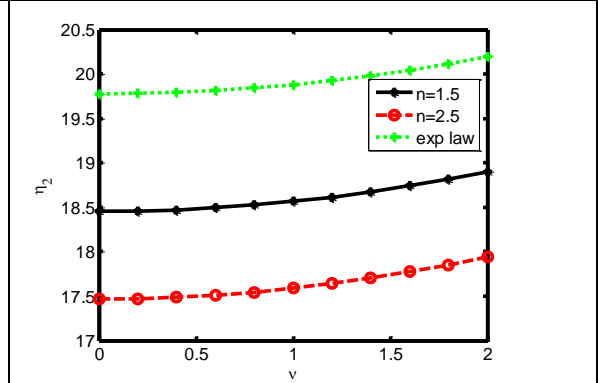


Figure 6.4(b) Variation of non-dimensional second mode frequency with rotational speed parameter of steel-alumina FGO beam with steel-rich bottom for property distribution along thickness as per power law as well as exponential law. ($\delta=0.1$, $s=0.2$)

power law with indices $n=1.5$, and 2.5 . The hub radius parameter and angular velocity are 0.1 and 344 rad/s respectively. The frequencies for both the modes increase with increase in slenderness parameter in all the cases of property distribution. The e-FGO beam has distinctly the highest frequency among all for higher values of s , where as there is no noticeable difference in frequencies for lower values of s . The FGO-2.5 beam has the lowest frequency of all.

The effect of hub radius parameter on first mode frequency of beam is determined and shown in figure 6.3(a). The slenderness parameter and angular velocity are 0.2 and 344 rad/s respectively. The e-FGO beam has the highest first mode frequency for all the values of hub radius parameters. Similarly, the FGO-2.5 beam has the lowest frequency of all. The effect of hub radius on the second mode frequency of beams is similar to that on the first mode frequency which can be noticed from figure 6.3(b). This is due to the fact that increase in hub radius parameter increases the centrifugal force on beam, which in turn increases the

stiffness of beam. Additionally, exponential distribution as compared to power law distribution of properties makes the beam richer in alumina-content thereby making the beam stiffer.

The effect of rotational speed parameter (ν) on the non-dimensional frequency for first and second mode is shown in figures 6.4(a) and 6.4(b) respectively. The hub radius parameter and slenderness parameter are 0.1 and 0.2 respectively. The frequencies for both the modes increase with rotational speed parameter. It is observed that the e-FGO beam and FGO-2.5 beam have respectively the highest and lowest frequencies corresponding to any value of rotational speed parameter. It is also observed that the first two mode frequencies of all the beams increase at increasing rate with rotational speed parameter. This may be due to the fact that the increase in rotational speed parameter increases the centrifugal force at increasing rate that increases the stiffness matrix accordingly.

The additional data for dynamic stability analysis are taken as follows. $P^{\oplus}=6.49 \times 10^7$ N, $\omega_1=1253$ rad/s. P^{\oplus} and ω_1 corresponds to the critical buckling load and fundamental natural frequency of a homogenous steel beam of similar end conditions as of the FGO beam. The thickness of steel beam used to calculate the above two quantities is 0.25m, the length and width remaining the same as that of FGO beam.

Functionally graded ordinary beams having properties along the thickness according to power law with index $n=1.5$ (FGO-1.5), $n=2.5$ (FGO-2.5) and according to exponential law (e-FGO) are considered for dynamic stability analysis. The effect of property distribution on the principal instability region for first mode and second mode are depicted in figure 6.5(a) and figure 6.5(b) respectively. It is observed that the area of the instability region of e-FGO beam is the smallest and situated farthest from the dynamic load factor axis. Therefore e-FGO beam is the most stable beam for both the modes. The area of instability region of FGO-2.5 beam is the largest for both the modes. Hence it is the least stable beam.

The influence of hub radius on first and second mode main instability zones of FGO-2.5 beam is shown in figure 6.6(a) and figure 6.6(b) respectively. It is found that the presence of hub enhances the stability of the beam. The effect of hub radius on dynamic stability of e-FGO beam is similar as that of hub on FGO-2.5 beam which can be seen in figures 6.6(c) and 6.6(d) for first and second mode respectively. The

increase in hub radius causes increase in centrifugal force. As a result the effective stiffness and hence the dynamic stability of the beam is enhanced.

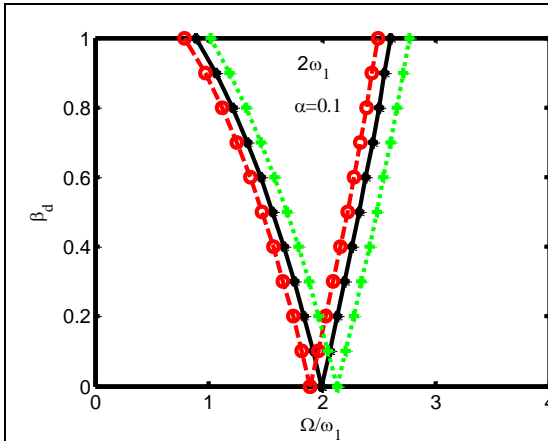


Figure 6.5(a). Effect of property distribution laws on first mode instability region of steel-alumina FGO beam for $\delta=0.1$, $\bar{\omega}=344\text{rad/s}$, $s=0.2$: * $n=1.5$, $^{\circ}n=2.5$, +exp. Law.

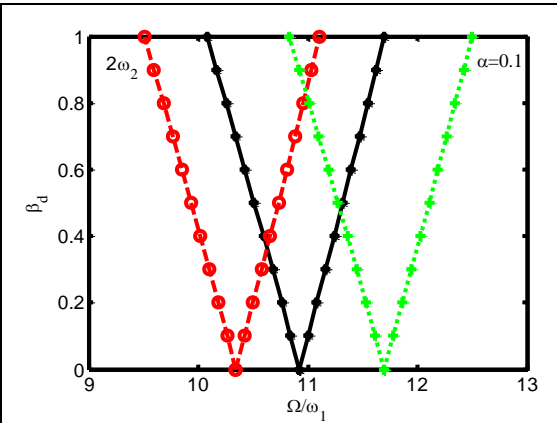


Figure 6.5(b). Effect of property distribution laws on second mode instability region of steel-alumina FGO beam for $\delta=0.1$, $\bar{\omega}=344\text{rad/s}$, $s=0.2$: * $n=1.5$, $^{\circ}n=2.5$, +exp. Law.

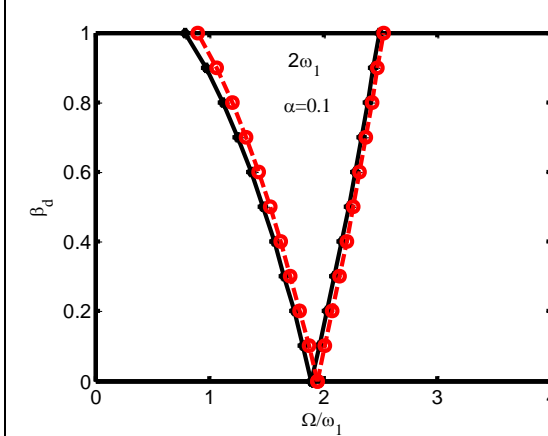


Figure 6.6(a). Effect of hub radius parameter on first mode instability region of steel-alumina FGO beam for $n=2.5$, $s=0.2$, $\bar{\omega}=344\text{ rad/s}$ ($\delta=0.1$, $^{\circ}\delta=0.5$)

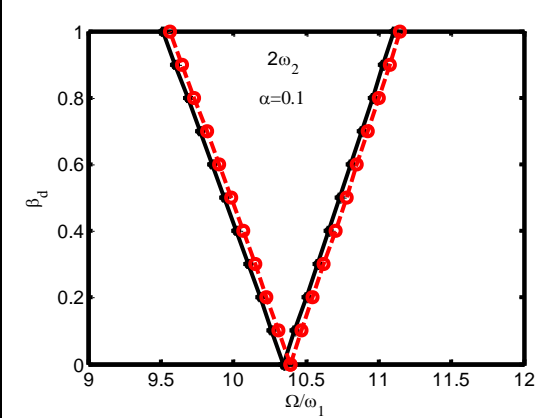


Figure 6.6(b). Effect of hub radius parameter on second mode instability region of steel-alumina FGO beam for $n=2.5$, $s=0.2$, $\bar{\omega}=344\text{ rad/s}$ ($\delta=0.1$, $^{\circ}\delta=0.5$)

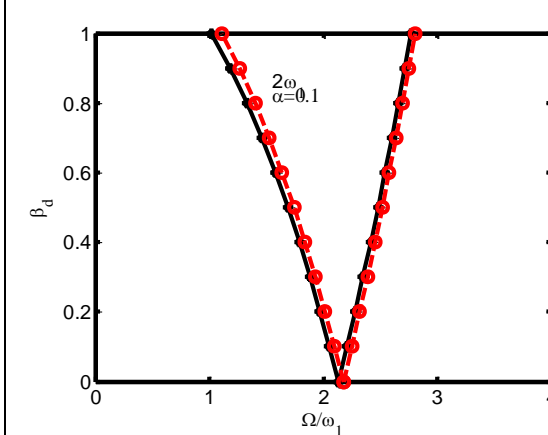


Figure 6.6(c). Effect of hub radius parameter on first mode instability region of steel-alumina FGO beam for exp. law $s=0.2$, $\bar{\omega}=344\text{ rad/s}$ ($\delta=0.1$, $^{\circ}\delta=0.5$)

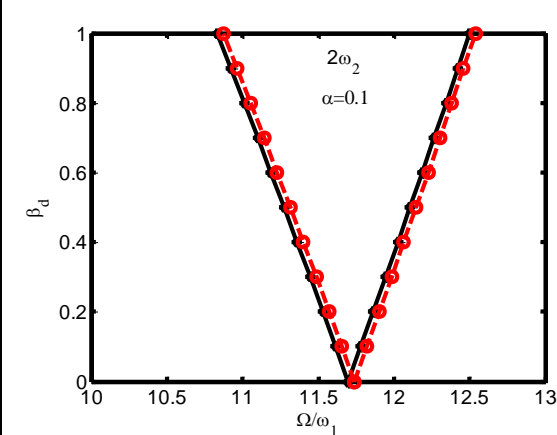


Figure 6.6(d). Effect of hub radius parameter on second mode instability region of steel-alumina FGO beam for exp. Law, $s=0.2$, $\bar{\omega}=344\text{ rad/s}$ ($\delta=0.1$, $^{\circ}\delta=0.5$)

The effect of rotation of FGO-2.5 beam on its dynamic stability is studied and presented in figure 6.7(a) and figure 6.7(b) for first and second mode respectively. The increase in angular speed increases the stability of the beam for both the modes. Figures 6.7(c) and 6.7(d) show the effect of rotation on stability of e-FGO beam for first mode and second mode respectively. The stability, in this case, is also enhanced as the angular speed increases. The increase in rotational speed of the beam increases the centrifugal force acting on it non-linearly which causes the increase of the elements of its effective stiffness matrix accordingly. The increase in effective stiffness of the beam causes the dynamic instability of the beam to occur at higher excitation frequencies. Therefore the dynamic stability of the beam is enhanced.

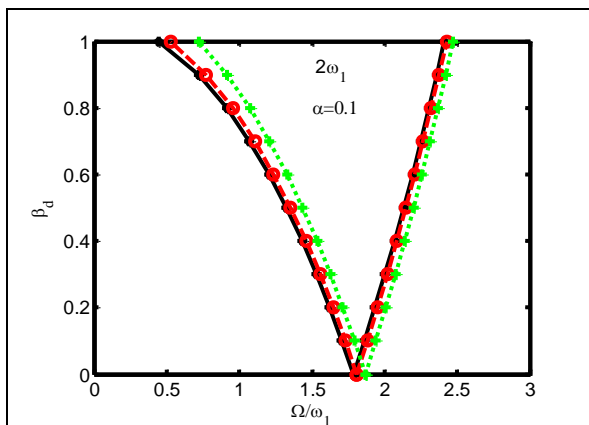


Figure 6.7(a). Effect of rotational speed parameter on first mode instability region of steel-alumina FGO beam for $n=2.5$, $s=0.2$, $\delta=0.1$, (${}^{\circ}v=0.1$, ${}^{\circ}v=0.5$, ${}^{+}v=1.0$)

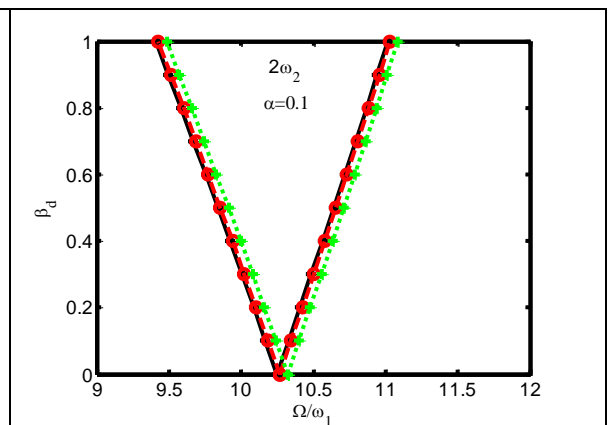


Figure 6.7(b). Effect of rotational speed parameter on second mode instability region of steel-alumina FGO beam for $n=2.5$, $s=0.2$, $\delta=0.1$ (${}^{\circ}v=0.1$, ${}^{\circ}v=0.5$, ${}^{+}v=1.0$)

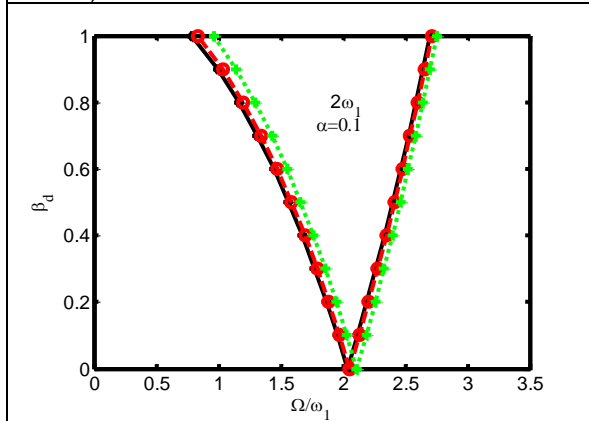


Figure 6.7(c). Effect of rotational speed parameter on first mode instability region of steel-alumina FGO beam for exp. law, $s=0.2$, $\delta=0.1$, (${}^{\circ}v=0.1$, ${}^{\circ}v=0.5$, ${}^{+}v=1.0$)

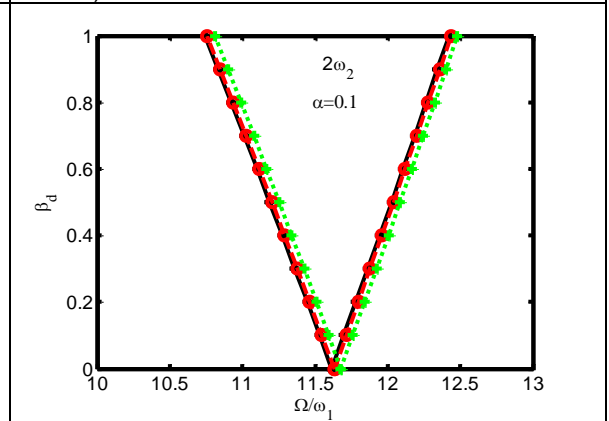


Figure 6.7(d). Effect of rotational speed parameter on second mode instability region of steel-alumina FGO beam for exp. law, $s=0.2$, $\delta=0.1$, (${}^{\circ}v=0.1$, ${}^{\circ}v=0.5$, ${}^{+}v=1.0$)

The role of geometry of the beam on the first and second mode main instability zones of FGO-2.5 beam is presented in figures 6.8(a) and 6.8(b) respectively. The area of instability zone becomes narrower and shifts away from the dynamic load factor axis as the slenderness parameter increases thereby enhancing the stability of the beam. The effect of slenderness parameter on stability of e-FGO beam is similar as on

FGO-2.5 beam which can be noticed from figures 6.8(c) and 6.8(d) respectively for first and second mode.

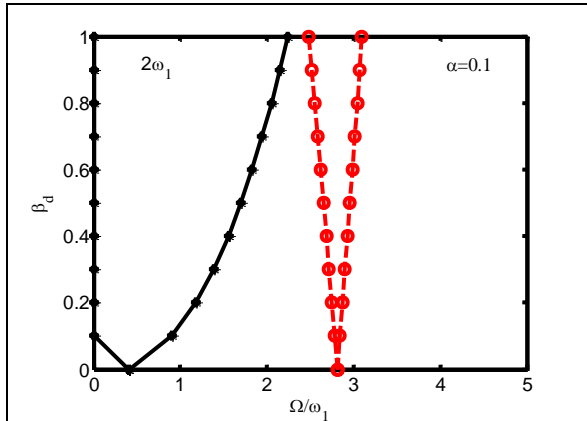


Figure 6.8(a). Effect of slenderness parameter on first mode instability region of steel-alumina FGO beam for $n=2.5$, $\bar{\delta}=0.1$, $\bar{\omega}=344$ rad/s ($^*s=0.1$, $^{\circ}s=0.3$)

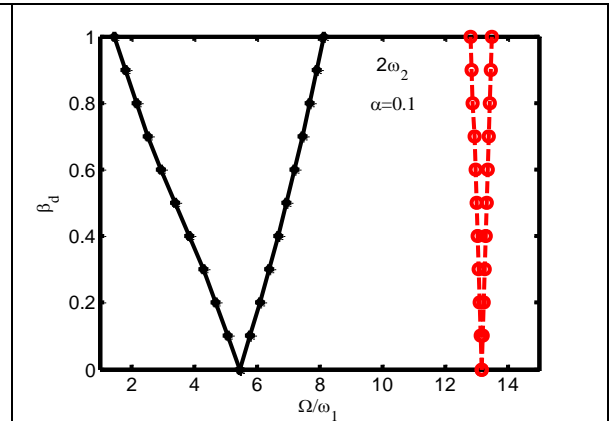


Figure 6.8(b). Effect of slenderness parameter on second mode instability region of steel-alumina FGO beam for $n=2.5$, $\bar{\delta}=0.1$, $\bar{\omega}=344$ rad/s ($^*s=0.1$, $^{\circ}s=0.3$)

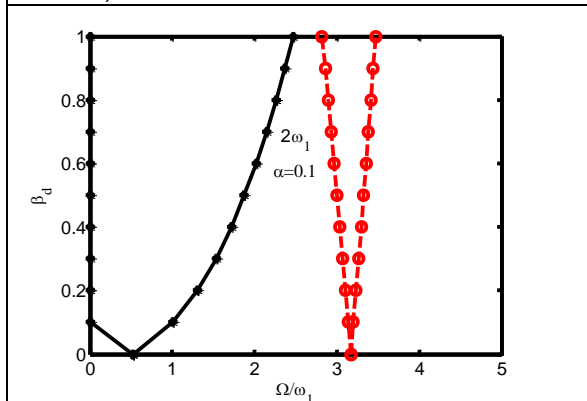


Figure 6.8(c). Effect of slenderness parameter on first mode instability region of steel-alumina FGO beam for exp. law, $\bar{\delta}=0.1$, $\bar{\omega}=344$ rad/s ($^*s=0.1$, $^{\circ}s=0.3$)

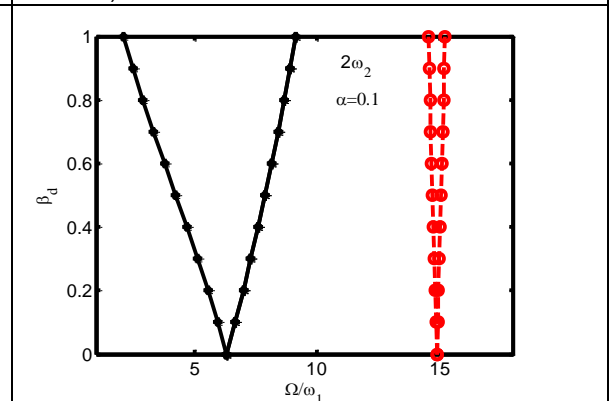


Figure 6.8(d). Effect of slenderness parameter on second mode instability region of steel-alumina FGO beam for exp. law, $\bar{\delta}=0.1$, $\bar{\omega}=344$ rad/s ($^*s=0.1$, $^{\circ}s=0.3$)

6.4.3 Functionally graded sandwich beam

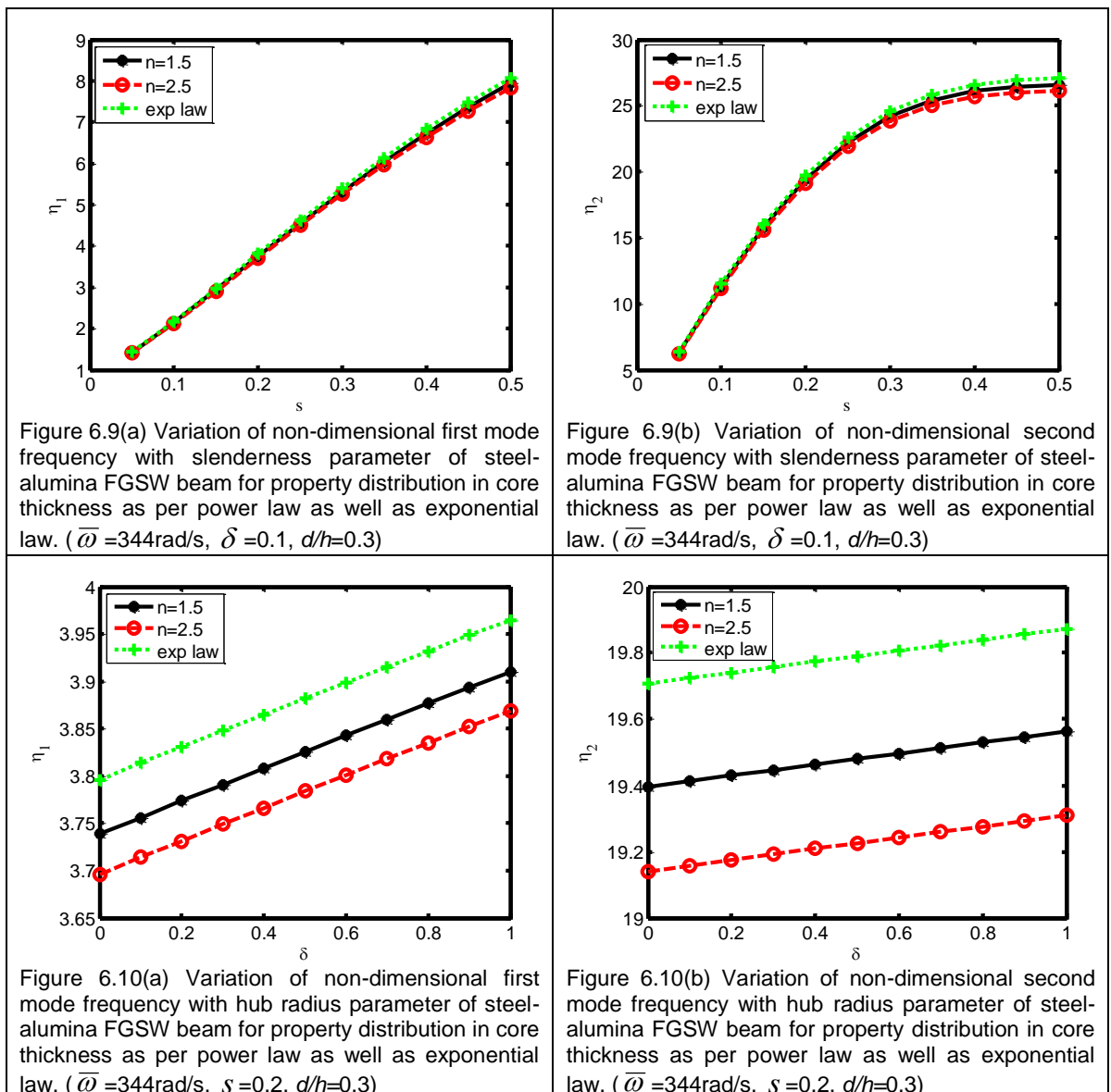
A steel-alumina FGSW rotating cantilever beam of length 1m and width 0.1m is considered for the analysis of free vibration and dynamic stability. The bottom and top skin of the beam are steel and alumina respectively, whereas the core is the mixture of alumina and steel with bottom layer rich in steel. Both the top and bottom skin are of same thickness. The thickness of the core (d) is 0.3 times the total thickness (h).

Figure 6.9(a) and figure 6.9(b) show the effect of slenderness parameter(s) on first and second mode frequency of the FGSW-2.5 beam. The other parameters are as considered for the analysis of the FGO beam in the previous section. Similar trends in the results are observed as in the case of FGO beam. But the effect of

property distribution laws in this case is not that distinct as observed in case of FGO beams.

The effect of hub radius parameter on first and second mode frequency of FGSW beam is shown in figures 6.10(a) and 6.10(b) respectively. The slenderness parameter and angular velocity are 0.2 and 344 rad/s respectively. The first two mode frequencies increase with increase of hub radius parameter. Moreover, the e-FGSW beam and FGSW-2.5 beam have respectively the highest and the lowest frequency corresponding to any hub radius parameter.

The effect of rotational speed parameter on first and second mode frequency of FGSW beam is shown in figures 6.11(a) and 6.11(b) respectively. The first two natural frequencies increase with increase in the rotational speed parameter for both



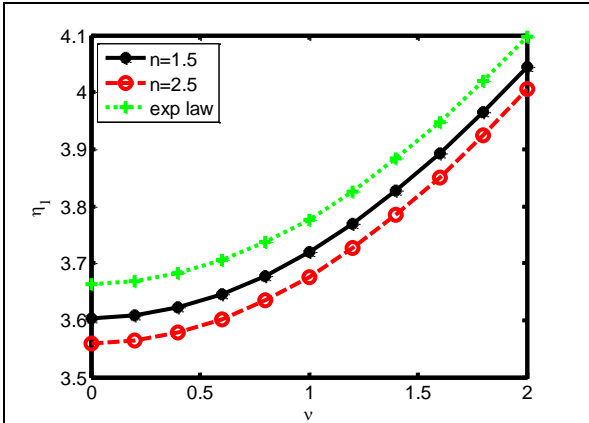


Figure 6.11(a) Variation of non-dimensional first mode frequency with rotational speed parameter of steel-alumina FGSW beam for property distribution in core thickness as per power law as well as exponential law. ($\delta=0.1, s=0.2, d/h=0.3$)

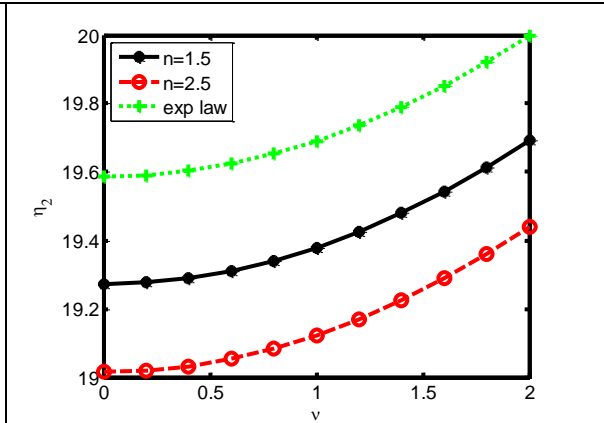


Figure 6.11(b) Variation of non-dimensional second mode frequency with rotational speed parameter of steel-alumina FGSW beam for property distribution in core thickness as per power law as well as exponential law. ($\delta=0.1, s=0.2, d/h=0.3$)

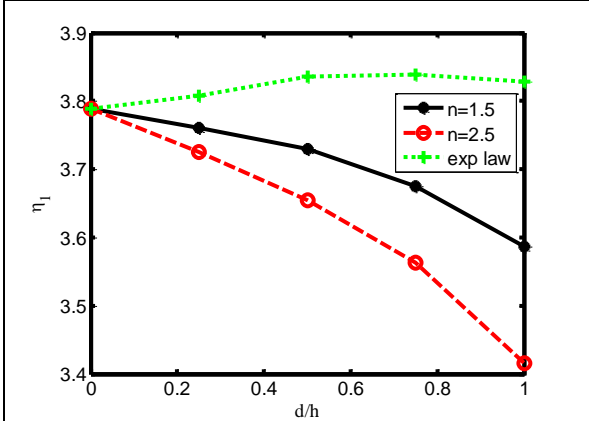


Figure 6.12(a) Variation of non-dimensional first mode frequency with FGM content(d/h) of steel-alumina FGSW beam for property distribution in core thickness as per power law as well as exponential law. ($\bar{\omega}=344\text{rad/s}, \delta=0.1, s=0.2$)

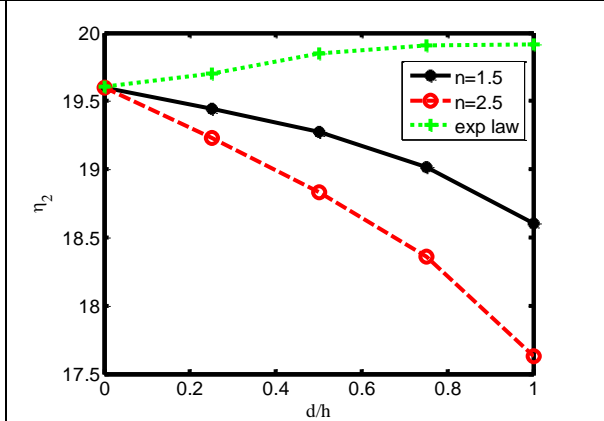


Figure 6.12(b) Variation of non-dimensional second mode frequency with FGM content(d/h) of steel-alumina FGSW beam for property distribution in core thickness as per power law as well as exponential law. ($\bar{\omega}=344\text{rad/s}, \delta=0.1, s=0.2$)

the cases of property distribution in core which is similar to the result obtained in case of FGO beams.

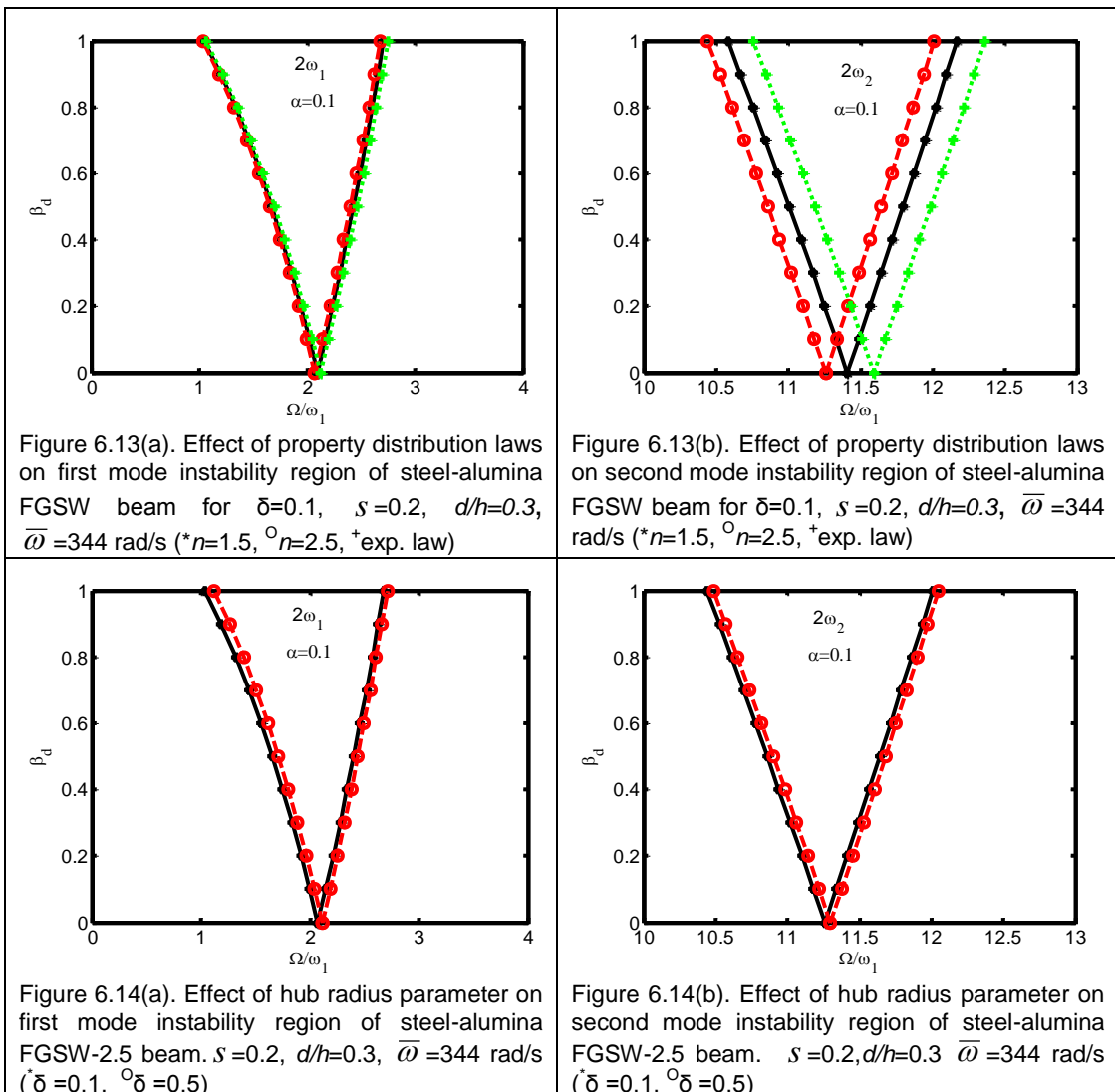
The effect of FGM content (d/h) on first two mode frequencies of the rotating FGSW beam is studied with hub radius parameter and rotational speed 0.1 and 344 rad/s respectively and shown in figure 6.12. The first mode frequencies of FGSW-2.5 and FGSW-1.5 beam decrease with increase of FGM content whereas the corresponding frequencies of e-FGSW beam increases with the increase of FGM content.

Figure 6.13 shows the effect of property distribution in the core on the dynamic stability of the FGSW beam. It is observed that exponential distribution of properties along the thickness of core ensures less sensitiveness to parametric instability for both the principal modes.

The effect of hub radius parameter on the main instability zone of FGSW-2.5 beam is investigated and presented in figures 6.14(a) and 6.14(b) for first mode and second mode respectively. Figures 6.14(c) and 6.14(d) depict the plot of first and second mode instability regions of e-FGSW beam. Similar trends in the results are observed as in the case of FGO beam. Moreover, the effect is more prominent on FGSW beam as compared to that on FGO beams.

The Figures 6.15(a) and 6.15(b) represent the effect of rotational speed on first and second mode principal instability zones of FGSW-2.5 beam and 6.15(c) and 6.15(d) show the corresponding plots of e-FGSW beam. In all the cases it is found that increase in rotational speed enhances the stability of the beams.

Figures 6.16(a) and 6.16(b) show the effect of the geometry of FGSW-2.5 beam on its first and second mode principal instability zones respectively. The stability of the beam is enhanced appreciably with the increase in slenderness



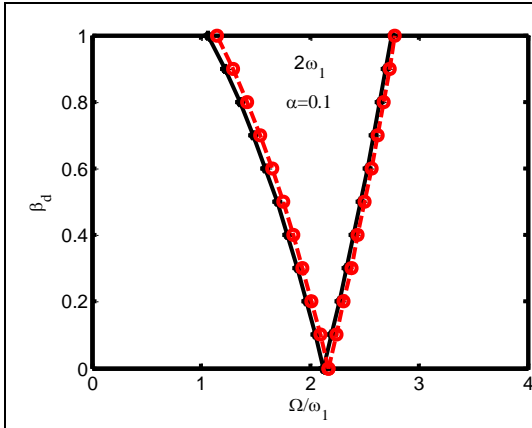


Figure 6.14(c). Effect of hub radius parameter on first mode instability region of steel-alumina e-FGSW beam. $s=0.2, d/h=0.3, \bar{\omega}=344 \text{ rad/s}$ ($\delta=0.1, \delta^0=0.5$)

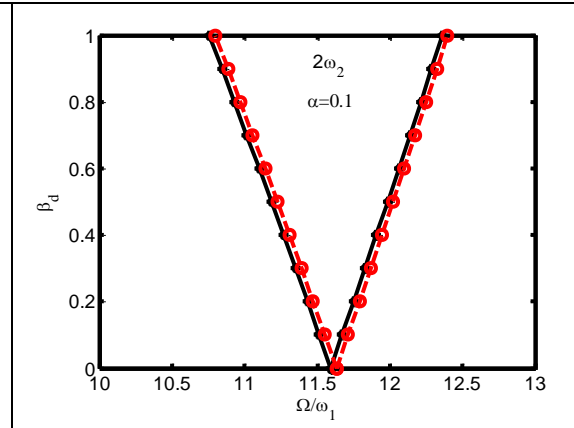


Figure 6.14(d). Effect of hub radius parameter on second mode instability region of steel-alumina e-FGSW beam. $s=0.2, d/h=0.3, \bar{\omega}=344 \text{ rad/s}$ ($\delta=0.1, \delta^0=0.5$)

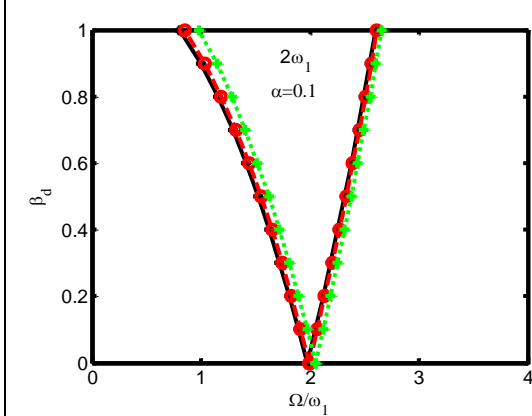


Figure 6.15(a). Effect of rotational speed parameter on first mode instability region of steel-alumina FGSW-2.5 beam. $s=0.2, \delta=0.1, d/h=0.3$ ($v=0.1, v^0=0.5, v^+=1.0$)

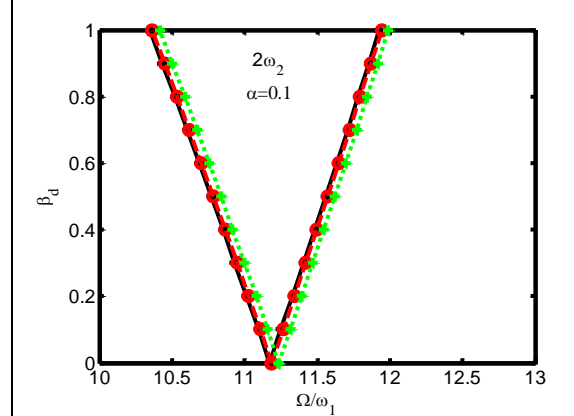


Figure 6.15(b). Effect of rotational speed parameter on second mode instability region of steel-alumina FGSW-2.5 beam. $s=0.2, \delta=0.1, d/h=0.3$ ($v=0.1, v^0=0.5, v^+=1.0$)

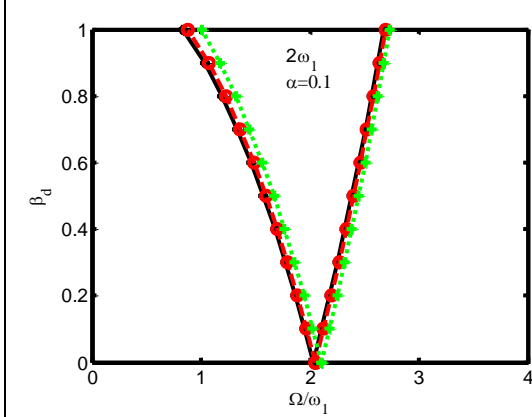


Figure 6.15(c). Effect of rotational speed parameter on first mode instability region of steel-alumina e-FGSW beam. $s=0.2, \delta=0.1, d/h=0.3$ ($v=0.1, v^0=0.5, v^+=1.0$)

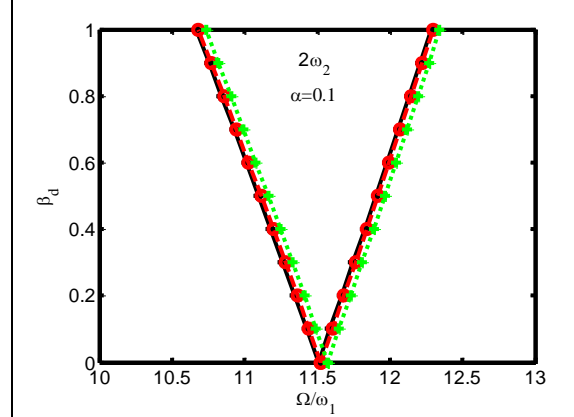
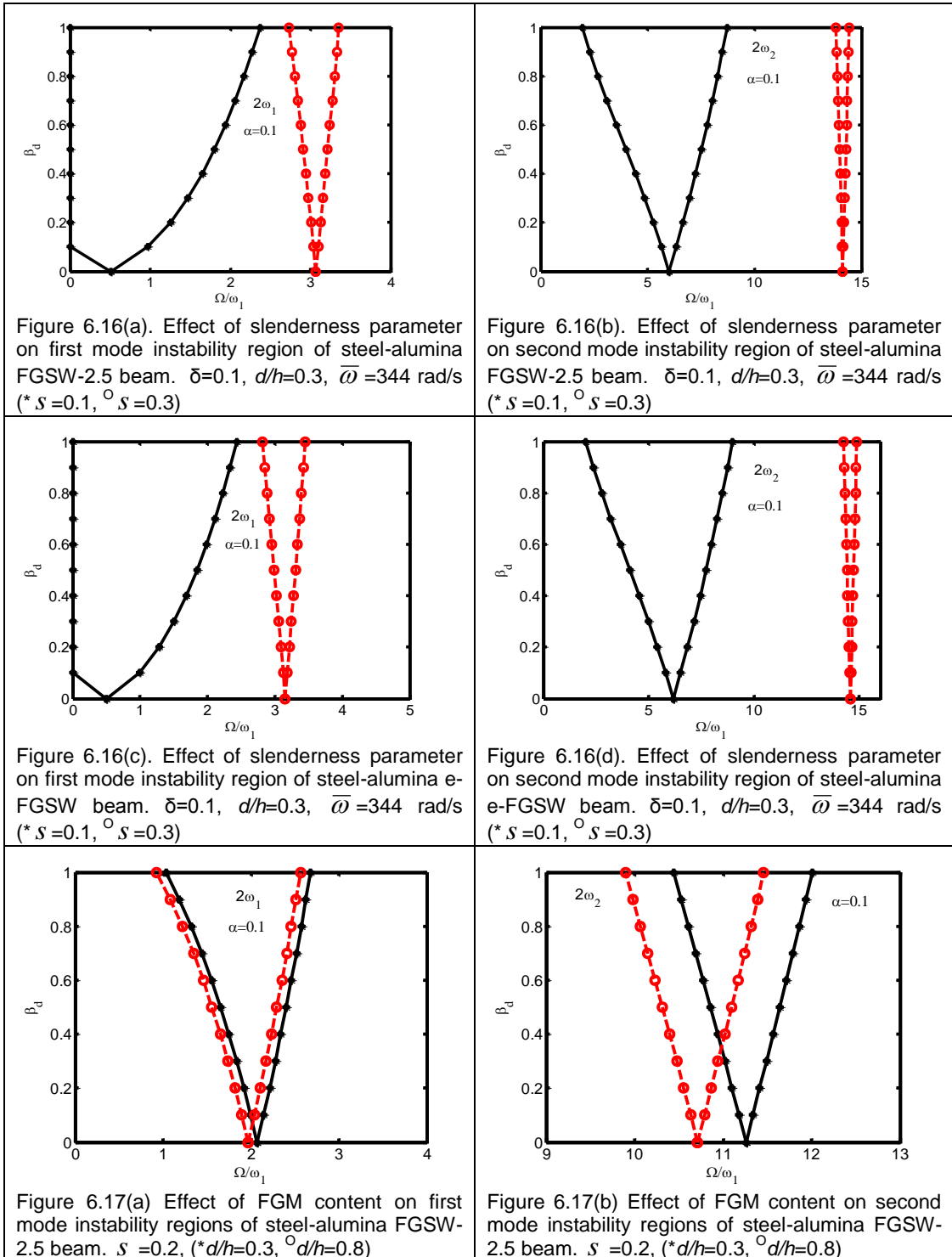
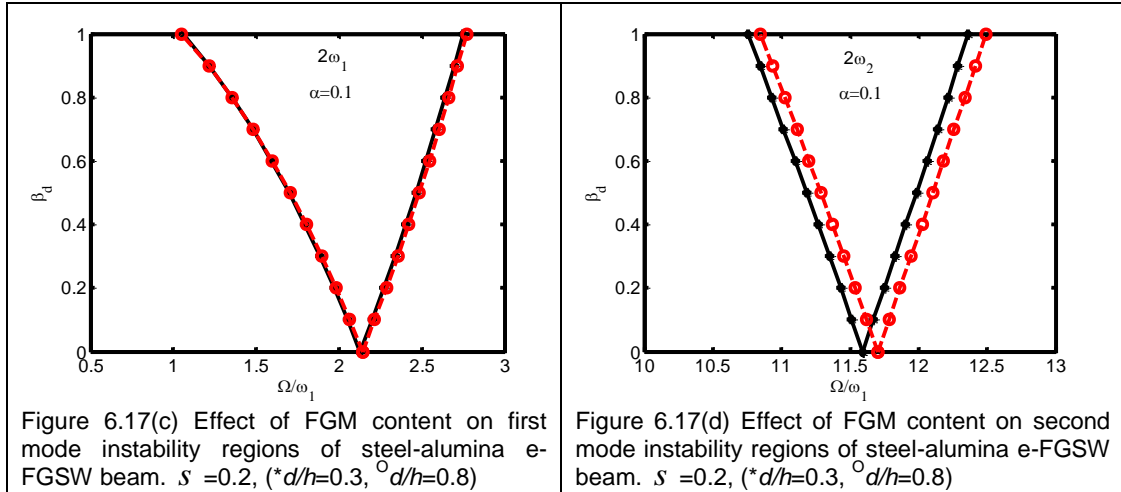


Figure 6.15(d). Effect of rotational speed parameter on second mode instability region of steel-alumina e-FGSW beam. $s=0.2, \delta=0.1, d/h=0.3$ ($v=0.1, v^0=0.5, v^+=1.0$)

parameter. The increase in slenderness parameter has similar effect on the principal instability zones of e-FGSW beam as on FGSW-2.5 beam which is shown in figures 6.16(c) and 6.16(d) for first and second mode respectively.

The effect of FGM content on dynamic stability of FGSW-2.5 beam is shown in figures 6.17(a) and 6.17(b) for first mode and second mode respectively. The corresponding plots for e-FGSW beam are shown in figures 6.17(c) and 6.17(d). It is observed that increase in FGM content makes the FGSW-2.5 beam more prone to dynamic instability whereas it enhances the dynamic stability of e-FGSW beam. This effect is found to be prominent in case of FGSW-2.5 beam than e-FGSW beam.





As the increase in FGM content increases the effective stiffness of e-FGSW beam while decreasing the effective stiffness of FGSW-2.5 beam, so the chance of parametric instability in the former case is reduced and it is enhanced in the later case.

6.5 Closure

Free vibration and dynamic stability analysis of FGO and FGSW rotating cantilever beams is carried out using finite element method. The material properties through the thickness of FGO and along the thickness of core of FGSW beam are assumed to follow exponential and power law. The effect of beam geometry, property distribution, rotation and hub radius on vibration and parametric instability is investigated.

The increase in rotational speed and hub radius of beams increase their frequencies and enhance their stability as well.

Increase in slenderness parameter increases the frequencies of both FGO and FGSW beams and enhances their dynamic stability as well.

Material property distribution along the thickness of beams is found to play an important role with regards to their dynamic stability behaviour.

The exponential distribution of properties ensures less sensitiveness to parametric instability compared to power law distribution of properties for both FGO and FGSW beams.

CHAPTER 7

DYNAMIC STABILITY OF PRETWISTED FUNCTIONALLY GRADED TIMOSHENKO BEAM UNDER PARAMETRIC EXCITATION

7.1 Introduction

Some machine components are twisted for functional point of view. The blades of helicopter rotor, turbine and aircraft propeller are given pre-twist and usually are subjected to vibration. The study of vibration and dynamic stability of pre-twisted components therefore remains an important area of research.

Carnegie [27] studied the dynamic behaviour of a pre-twisted cantilever blade taking into account torsion, bending rotary inertia and shear deformation. Dawson et al. [42] investigated the effect of shear deformation and rotary inertia on the natural frequencies of pre-twisted cantilever beams using numerical technique. They also verified their results conducting experiments. Carnegie and Thomas [28] used finite difference method to study the vibration of uniform and tapered pre-twisted cantilevers. Yardimoglu and Yildirim [165] have developed a finite element model with reduced number of nodal degree of freedom to investigate the vibration of a pre-twisted cantilever beam. The effect of pre-twist angle of an aerofoil blade simplified

as a rotating Euler as well as Timoshenko beam has been investigated by Subuncu and Ervan [127, 128] using finite element method. Mohanty [105] has studied parametric instability of pre twisted cantilever with localized damage. The effects of various parameters such as shroud dimensions, pre-twist angle, stagger angle, rotational speed and distance of shear centre from the centroid on the stability of the rotating pre-twisted blade packets of aerofoil cross-section are investigated by Sakar and Sabunku [130] using finite element method.

Though the literatures on dynamic stability of pre-twisted beams are appreciable, the literatures on dynamic stability of functionally graded pre-twisted beams are very less. FGM made of the mixture of turbine material and ceramics can be applied as a coating on the surface of the blade such that the surface of the coated blade is rich in ceramics to improve the performance of the blade in high temperature environment. This chapter presents a study of vibration and dynamic stability of a functionally graded pre-twisted Timoshenko beam of cantilever type.

7.2 Formulation

A functionally graded pre-twisted beam is considered for analysis as shown in figure 7.1(a). The beam, fixed at one end and free at the other, is subjected to a dynamic axial load $P(t) = P_s + P_t \cos \Omega t$, acting at the free end along its un-deformed axis. The static component of the axial force is P_s . The amplitude and frequency of the dynamic component of the force are P_t and Ω respectively, and t is time. The coordinate system of the typical two noded beam element used to derive the governing equations of motion is shown in figure 7.1(b). The mid-longitudinal (x-y) and (x-z) planes are chosen as the reference planes for expressing the displacements as shown in figure 7.1(b).

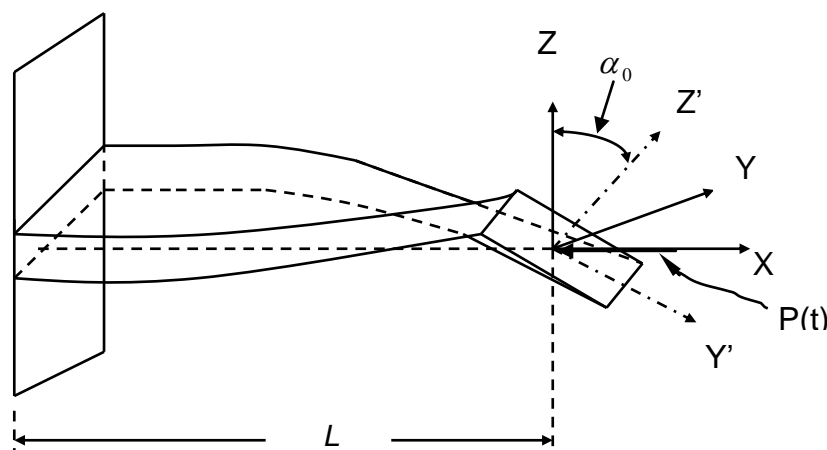


Figure 7.1(a) Pre-twisted cantilever beam subjected to dynamic axial force.

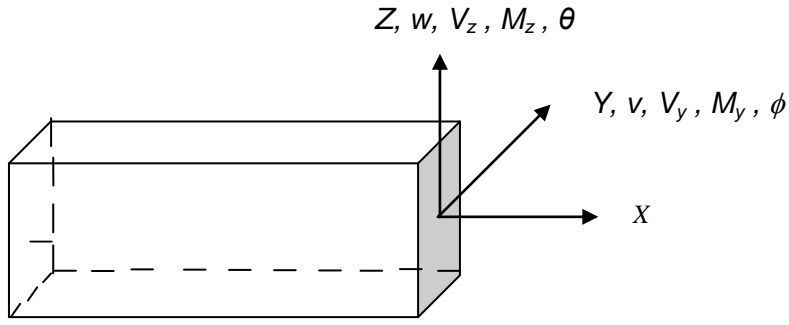


Figure 7.1(b) The coordinate system with generalized forces and displacements for the beam element.

The breadth and thickness coordinates are measured as y and z respectively from the reference plane. Figure 7.1(c) shows the beam element with four degrees of freedom per node. The transverse displacement along y direction and the rotation of the cross-section about y -axis are v and ϕ respectively. Similarly, the transverse displacement along z direction and the rotation of the cross-section about z -axis are w and θ respectively. The element matrices [165] for the functionally graded beam element are derived.

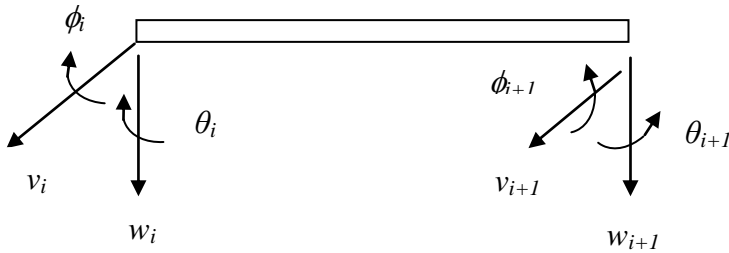


Figure 7.1 (c) Beam element showing generalized degrees of freedom for i^{th} element.

7.2.1 Shape functions

The differential equation of motion [27, 42, 28] for the FGSW beam element is given as

$$\frac{\partial M_y}{\partial x} + V_z = -(I_2 \cos^2 \alpha(x) + I_{22} \sin^2 \alpha(x)) \frac{\partial^2 \phi}{\partial t^2} + \frac{1}{2} (I_{22} - I_2) \sin 2\alpha(x) \frac{\partial^2 \theta}{\partial t^2} \quad (7.1)$$

$$\frac{\partial M_z}{\partial x} + V_y = (I_{22} \cos^2 \alpha(x) + I_2 \sin^2 \alpha(x)) \frac{\partial^2 \theta}{\partial t^2} - \frac{1}{2} (I_{22} - I_2) \sin 2\alpha(x) \frac{\partial^2 \phi}{\partial t^2} \quad (7.2)$$

$$\frac{\partial V_y}{\partial x} = I_0 \frac{\partial^2 v}{\partial t^2} \quad (7.3)$$

$$\frac{\partial V_z}{\partial x} = I_0 \frac{\partial^2 w}{\partial t^2} \quad (7.4)$$

where

$$M_y = -(D_{11} \cos^2 \alpha(x) + D_{22} \sin^2 \alpha(x)) \frac{\partial \phi}{\partial x} - \frac{1}{2} (D_{22} - D_{11}) \sin 2\alpha(x) \frac{\partial \theta}{\partial x} \quad (7.5)$$

$$M_z = (D_{22} \cos^2 \alpha(x) + D_{11} \sin^2 \alpha(x)) \frac{\partial \theta}{\partial x} + \frac{1}{2} (D_{22} - D_{11}) \sin 2\alpha(x) \frac{\partial \phi}{\partial x} \quad (7.6)$$

$$V_z = -A_{55} \left(\frac{\partial w}{\partial x} - \phi \right) \quad (7.7)$$

$$V_y = A_{55} \left(\frac{\partial v}{\partial x} - \theta \right) \quad (7.8)$$

Where,

$$\left. \begin{aligned} D_{11} &= \int E(z') z'^2 dA, \quad D_{22} = \frac{A_{11} b^2}{12}, \quad A_{11} = \int E(z') dA, \\ I_{22} &= \frac{I_0 b^2}{12}, \quad I_2 = \int \rho(z') z'^2 dA \\ I_0 &= \int \rho(z') dA, \quad A_{55} = k \int G(z') dA. \end{aligned} \right\} \quad (7.9)$$

And,

$$\alpha(x) = \alpha_0 + \varphi x \quad (7.10)$$

α_0 is the twist angle at the starting end and φ is the change in twist angle per unit length of the beam.

The material properties along thickness (z-direction) are assumed to vary according to power law and exponential law given respectively as

$$R(z') = (R_t - R_b) \left(\frac{z'}{h} + \frac{1}{2} \right)^n + R_b,$$

$$R(z') = R_t \exp(-e(1 - 2z'/h)), \quad e = \frac{1}{2} \log \left(\frac{R_t}{R_b} \right) \quad (7.11)$$

where, $R(z')$ denotes a material property such as, E , G , ρ etc., R_t and R_b denote the values of the properties at topmost and bottommost layer of the beam respectively, and n is an index.

The homogeneous form of Eq.(7.1, 7.2, 7.3, 7.4) corresponding to static equilibrium condition is given as

$$\frac{\partial M_y}{\partial x} + V_z = 0 \quad (7.12)$$

$$\frac{\partial M_z}{\partial x} + V_y = 0 \quad (7.13)$$

$$\frac{\partial V_y}{\partial x} = 0 \quad (7.14)$$

$$\frac{\partial V_z}{\partial x} = 0 \quad (7.15)$$

The following polynomials may be assumed for the displacement field.

$$\left. \begin{aligned} v &= p_1 + p_2x + p_3x^2 + p_4x^3, \\ w &= p_5 + p_6x + p_7x^2 + p_8x^3, \\ \phi &= q_1 + q_2x + q_3x^2, \\ \theta &= q_4 + q_5x + q_6x^2. \end{aligned} \right\} \quad (7.16)$$

Eq. (7.16) can be expressed in matrix form as

$$\{\bar{u}_d\} = \begin{bmatrix} [N_v] \\ [N_w] \end{bmatrix} \{p\} \quad (7.17)$$

$$\{\bar{u}_r\} = \begin{bmatrix} [N_\phi] \\ [N_\theta] \end{bmatrix} \{q\} \quad (7.18)$$

here, $\bar{u}_d = [v \ w]^T$ and $\bar{u}_r = [\phi \ \theta]^T$ are deflection and rotation vector respectively.

N_v , N_w , N_ϕ and N_θ are the corresponding shape functions.

The coefficient vector q can be expressed in terms of the coefficient vector p by substituting eq. (7.16) in eq. (7.12) and eq. (7.13) and by equating the coefficients of same powers of x . The mentioned procedure yields the following.

$$\begin{aligned} q_1 &= \beta_1 p_3 + \beta_2 p_4 + p_6 + \beta_3 p_7 + \beta_4 p_8, \quad q_2 = \beta_5 p_4 + 2p_7 + \beta_6 p_8, \quad q_3 = 3p_8, \\ q_4 &= p_2 + \beta_7 p_3 + \beta_8 p_4 + \beta_1 p_7 + \beta_2 p_8, \quad q_5 = 2p_3 + \beta_9 p_4 + \beta_5 p_8, \quad q_6 = 3p_4. \end{aligned} \quad (7.19)$$

Where, $\beta_1 = 2\varphi D_c \cos 2\alpha(x)$,

$$\begin{aligned} \beta_2 &= 6\varphi D_c \cos 2\alpha(x) (\varphi D_c (\sin 2\alpha(x) - \sin 2\alpha(x))) + 3D_c \sin 2\alpha(x), \\ \beta_3 &= 2\varphi D_c \sin 2\alpha(x), \quad \beta_4 = 6\varphi^2 D_c^2 (\sin^2 2\alpha(x) + \cos^2 2\alpha(x)), \quad \beta_5 = 6\varphi D_c \cos 2\alpha(x), \\ \beta_6 &= 6\varphi D_c \sin 2\alpha(x), \quad \beta_7 = -\beta_3, \quad \beta_8 = \beta_4, \quad \beta_9 = -\beta_6 \end{aligned} \quad (7.20)$$

$$D_c = (D_{22} - D_{11}) / A_{55} \quad (7.21)$$

The coefficient vector q can be expressed in terms of the coefficient vector p in matrix form as $\{q\} = [B]\{p\}$ (7.22)

where,

$$[B] = \begin{bmatrix} 0 & 0 & \beta_1 & \beta_2 & 0 & 1 & \beta_3 & \beta_4 \\ 0 & 0 & 0 & \beta_5 & 0 & 0 & 2 & \beta_6 \\ 0 & 0 & 0 & 0 & 0 & 0 & 0 & 3 \\ 0 & 1 & \beta_7 & \beta_8 & 0 & 0 & \beta_1 & \beta_2 \\ 0 & 0 & 2 & \beta_9 & 0 & 0 & 0 & \beta_5 \\ 0 & 0 & 0 & 3 & 0 & 0 & 0 & 0 \end{bmatrix} \quad (7.23)$$

A two noded Timoshenko beam element with 4-degree of freedom per node as shown in figure 7.1(c) is considered for analysis. The nodal degree of freedom vector of the i^{th} element is given as

$$\{\hat{u}\} = [v_i \ w_i \ \phi_i \ \theta_i \ v_{i+1} \ w_{i+1} \ \phi_{i+1} \ \theta_{i+1}]^T \quad (7.24)$$

Using eq. (7.16) and eq. (7.19) the nodal degree of freedom vector can be expressed as

$$\{\hat{u}\} = [C]\{p\} \quad (7.25)$$

$$[C] = \begin{bmatrix} 1 & 0 & 0 & 0 & 0 & 0 & 0 & 0 \\ 0 & 0 & 0 & 1 & 0 & 0 & 0 & 0 \\ 0 & 0 & \beta_1 & \beta_2 & 0 & 1 & \beta_3 & \beta_4 \\ 0 & 1 & \beta_7 & \beta_8 & 0 & 0 & \beta_1 & \beta_2 \\ 1 & L & L^2 & L^3 & 0 & 0 & 0 & 0 \\ 0 & 0 & 0 & 0 & 1 & L & L^2 & L^3 \\ 0 & 0 & \beta_1 & \beta_2 + \beta_5 L & 0 & 1 & \beta_3 + 2L & \beta_4 + \beta_6 L + 3L^2 \\ 0 & 1 & \beta_7 + 2L & \beta_8 + \beta_9 L + 3L^2 & 0 & 0 & \beta_1 & \beta_2 + \beta_5 L \end{bmatrix} \quad (7.26)$$

Substituting eq. (7.22) in eq. (7.18) we get

$$\phi = [N_\phi][B]\{p\}$$

$$\theta = [N_\theta][B]\{p\} \quad (7.27)$$

7.2.2 Element elastic stiffness matrix

The strain energy of the element [28] is given as

$$S = \frac{1}{2} \int_0^L \left[\begin{aligned} & (D_{11} \cos^2 \alpha(x) + D_{22} \sin^2 \alpha(x)) \left(\frac{\partial \phi}{\partial x} \right)^2 + (D_{22} - D_{11}) \left(\frac{\partial \phi}{\partial x} \right) \left(\frac{\partial \theta}{\partial x} \right) \sin 2\alpha(x) \\ & + (D_{22} \cos^2 \alpha(x) + D_{11} \sin^2 \alpha(x)) \left(\frac{\partial \theta}{\partial x} \right)^2 + A_{55} \left\{ \left(\frac{\partial v}{\partial x} - \theta \right)^2 + \left(\frac{\partial w}{\partial x} - \phi \right)^2 \right\} \end{aligned} \right] dx \quad (7.28)$$

Substituting eq. (7.9, 7.10, 7.17 and 7.27) into eq. (7.28) the expression of strain energy is given as

$$S = 0.5\{\hat{u}\}^T [k_e] \{\hat{u}\} \quad (7.29)$$

Where $[k_e]$ is the element elastic stiffness matrix and is given as follows

$$[k_e] = \int_0^L [C]^T [k] [C]^{-1} dx \quad (7.30)$$

$$[k] = [B]^T \begin{bmatrix} (D_{11} \cos^2 \alpha(x) + D_{22} \sin^2 \alpha(x)) [N'_\phi]^T [N'_\phi] \\ (D_{22} \cos^2 \alpha(x) + D_{11} \sin^2 \alpha(x)) [N'_\theta]^T [N'_\theta] \\ (D_{22} - D_{11}) \sin 2\alpha(x) ([N'_\phi]^T [N'_\theta] + [N'_\theta]^T [N'_\phi]) \end{bmatrix} [B] \\ + A_{55} \begin{bmatrix} [N'_v]^T [N'_v] + [N'_w]^T [N'_w] + [B]^T ([N_\phi]^T [N_\phi] + [N_\theta]^T [N_\theta]) \end{bmatrix} [B] \\ - A_{55} \begin{bmatrix} [B]^T ([N_\phi]^T [N'_w] + [N_\theta]^T [N'_v]) + [N'_w]^T [N_\phi] + [N'_v]^T [N_\theta] \end{bmatrix} [B] \quad (7.31)$$

7.2.3 Element mass matrix

The kinetic energy of the beam element [27] is expressed as follows

$$T = \frac{1}{2} \int_0^L \left[I_0 \left(\left(\frac{\partial v}{\partial t} \right)^2 + \left(\frac{\partial w}{\partial t} \right)^2 \right) + (I_2 \cos^2 \alpha(x) + I_{22} \sin^2 \alpha(x)) \left(\frac{\partial \phi}{\partial t} \right)^2 \right. \\ \left. + 2(I_{22} - I_2) \left(\frac{\partial \phi}{\partial t} \right) \left(\frac{\partial \theta}{\partial t} \right) + (I_{22} \cos^2 \alpha(x) + I_2 \sin^2 \alpha(x)) \left(\frac{\partial \theta}{\partial t} \right)^2 \right] dx \quad (7.32)$$

Substituting eq. (7.9, 7.10, 7.17 and 7.27) in eq. (7.32) the kinetic energy is expressed as follows.

$$T = 0.5\{\hat{u}\}^T [m] \{\hat{u}\} \quad (7.33)$$

where $[m]$ is the element mass matrix which is presented below.

$$[m] = \int_0^L [C]^T [D] [C]^{-1} dx \quad (7.34)$$

$$[D] = I_0 \begin{bmatrix} [N_v]^T [N_v] + [N_w]^T [N_w] \end{bmatrix} \quad (7.35)$$

$$+ [B]^T \begin{bmatrix} (I_2 \cos^2 \alpha(x) + I_{22} \sin^2 \alpha(x)) [N_\phi]^T [N_\phi] \\ (I_{22} - I_2) ([N_\phi]^T [N_\theta] + [N_\theta]^T [N_\phi]) \\ (I_{22} \cos^2 \alpha(x) + I_2 \sin^2 \alpha(x)) [N_\theta]^T [N_\theta] \end{bmatrix} [B]$$

7.2.4 Element geometric stiffness matrix

The work done by the axial force $P(t)$ can be expressed as

$$W_p = \frac{1}{2} \int_0^L P(t) \left(\left(\frac{\partial v}{\partial x} \right)^2 + \left(\frac{\partial w}{\partial x} \right)^2 \right) dx \quad (7.36)$$

Substituting for v and w from eq. (7.17) and using eq. (7.27) the work done can be expressed as

$$W_p = \frac{P(t)}{2} \{\hat{u}\}^T [k_g] \{\hat{u}\} \quad (7.37)$$

where, k_g is the element geometric stiffness matrix which is given below.

$$[k_g] = \int_0^L [C]^{-T} \left[[N_v]^T [N_v] + [N_w]^T [N_w] \right] [C]^{-1} dx \quad (7.38)$$

7.3 Governing equations of motion

The equation of motion for the element subjected to axial force $P(t)$ can be expressed in terms of nodal degrees of freedom as

$$[m] \{\ddot{\hat{u}}\} + \left[[k_e] - P^\oplus (\alpha + \beta_d \cos \Omega t) [k_g] \right] \{\hat{u}\} = 0 \quad (7.39)$$

where, $[k_e]$, $[m]$ and $[k_g]$ are element elastic stiffness matrix, mass matrix and geometric stiffness matrix respectively. Assembling the element matrices as used in eq. (7.39), the equation in global matrix form which is the equation of motion for the pre-twisted beam, can be expressed as

$$[M] \{\ddot{\hat{U}}\} + \left[[K_e] - P^\oplus (\alpha + \beta_d \cos \Omega t) [K_g] \right] \{\hat{U}\} = 0 \quad (7.40)$$

$[M]$, $[K_e]$, $[K_g]$ are global mass, elastic stiffness, and geometric stiffness matrices respectively and $\{\hat{U}\}$ is global displacement vector. The condition for existence of these boundary solutions with period $2T$ is given by

$$\left([K_e] - (\alpha \pm \beta_d / 2) P^\oplus [K_g] - \frac{\Omega^2}{4} [M] \right) \{\hat{U}\} = 0 \quad (7.41)$$

The instability boundaries can be determined from the solution of the equation

$$\left| [K_e] - (\alpha \pm \beta_d / 2) P^\oplus [K_g] - \frac{\Omega^2}{4} [M] \right| = 0 \quad (7.42)$$

Following the procedure described in section 3.3.1-3.3.3, the natural frequencies, critical buckling load and instability regions of the pre-twisted beam are determined.

7.4 Results and discussion

The numerical study is carried out for a pre-twisted cantilever beam. The beam is discretized into 10 elements. The boundary conditions used for the numerical study are as given below.

$$\text{At, } x = 0, \quad v = 0, w = 0, \quad \phi = 0 \text{ and } \theta = 0.$$

7.4.1 Validation of the formulation

The numerical study is carried out for a steel-alumina pre-twisted FGO beam of cantilever type. The properties along the thickness of the beam are assumed to follow exponential law as well as power law. If the index of power law is made zero the beam becomes a homogeneous steel beam for the case of alumina-rich bottom. In order to verify the correctness of calculation, simulation is carried out for a FGO beam with alumina-rich bottom considering the index of power law as zero and the first four mode frequencies are provided along with the previously reported results in table 7.1. A good agreement of the present result with reported results is observed.

Table 7.1 Comparison of first four mode frequencies.

Frequency(Hz)	Present	[165]	[94]	[151]	[151]	[26]
ω_1	62.1	61.8	61.7	62.0	61.9	59.0
ω_2	305.2	304.8	300.9	305.1	304.7	290.0
ω_3	945.0	944.5	917.0	955.1	937.0	920.0
ω_4	1157.7	1193.0	1175.1	1214.7	1205.1	1110.0

$L=15.24$ cm, $b=2.54$ cm, $h=0.17272$ cm, $k=0.847458$, $E=206.86$ GPa, $G=82.74$ GPa, $\rho=7857.6$ kg/m³, $\alpha_0=45^\circ$.

7.4.2 Functionally graded ordinary (FGO) beam

A steel-alumina FGO beam with steel-rich bottom, clamped at one and free at other is considered for vibration and dynamic analysis. The length, breadth and thickness of the beam are 50.8 cm, 2.54 cm and 0.3175 cm respectively. The material properties of the constituent phases are given below.

Properties of steel: $E = 2.1 \times 10^{11}$ Pa, $G = 3E/8k$, $\rho = 7.8 \times 10^3$ kg/m³,

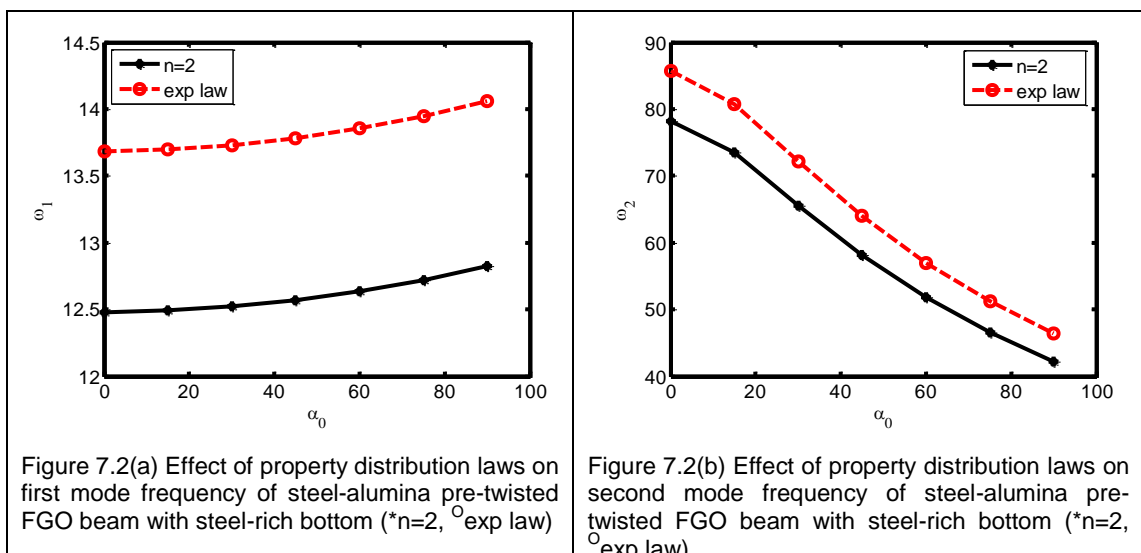
Properties of alumina: $E = 3.9 \times 10^{11}$ Pa, $G = 3E/8k$, $\rho = 3.9 \times 10^3$ kg/m³,

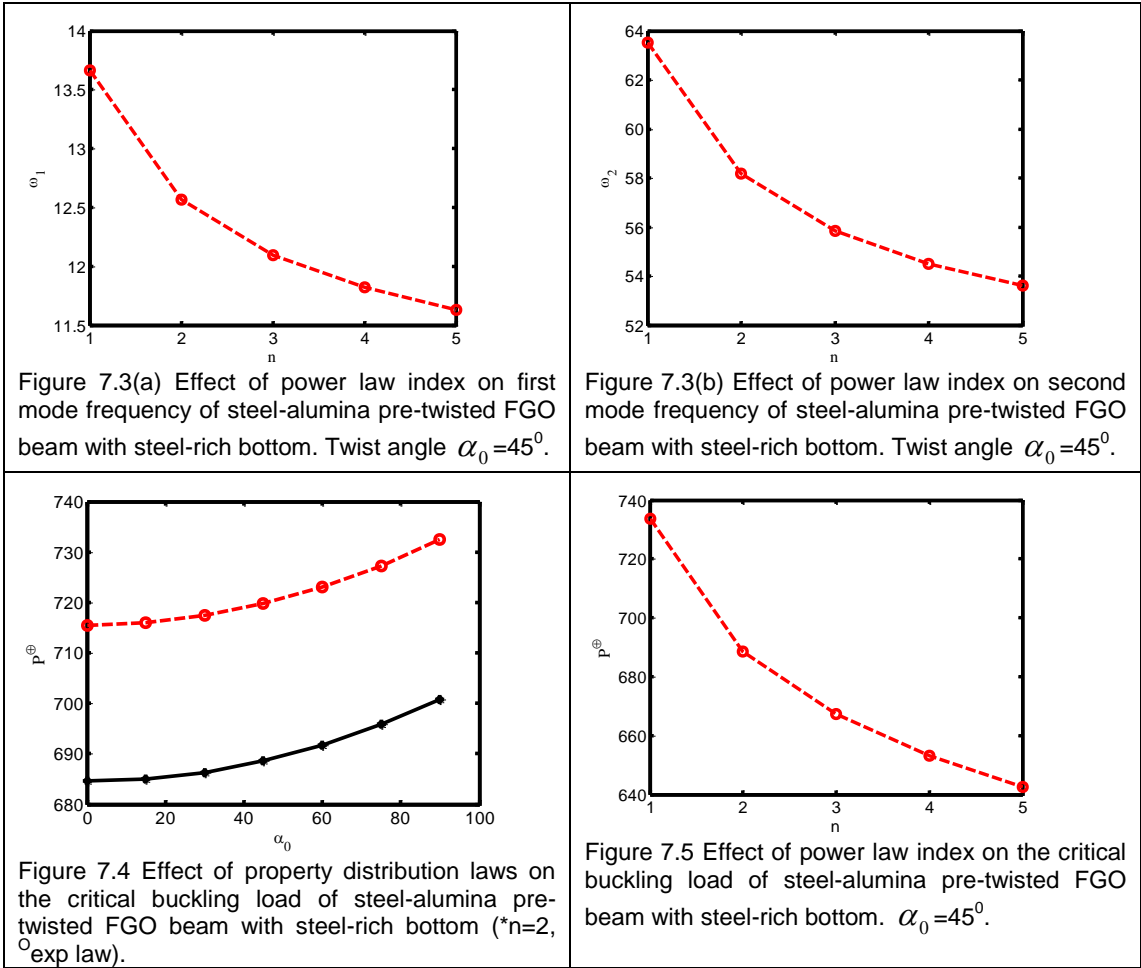
The shear correction factor [165] is chosen as $k=5/6=0.833$.

The effect of property distribution laws on the first and second mode natural frequencies is presented in figures 7.2(a) and 7.2(b) respectively. It is found that increase in pre-twist angle increases the first mode natural frequency whereas the second mode frequency decreases with increase in pre-twist angle. A similar trend of results was obtained by Yardimoglu and Yildirim [165] for homogeneous steel beam. As regards the variation of frequencies with pre-twist angle, a little variation of first mode frequency and a visible variation of second mode frequency with increase of pre-twist angle are observed. The above observations occur in both the cases of property distribution laws. Moreover, the first as well as second mode frequency of e-FGO beam is more than FGO-2 beam corresponding to any pre-twist angle. Because exponential distribution of properties renders the beam higher relative amount of alumina compared to power law distribution of properties which makes the effective stiffness and hence the frequency of e-FGO beam to be higher than the frequency of FGO-2 beam.

The effect of power law index on the natural frequencies of the FGO beam is investigated and is presented in figures 7.3(a) and 7.3(b) for first and second mode respectively. It is observed from the figure that the increase in power law index decreases the first and second mode frequencies. This may be due to the fact that increase in the value of index causes increase in the relative amount of steel which in turn decreases the effective elastic stiffness of the beam.

The figure 7.4 shows the variation of the critical buckling load with the pre-twist angle. The increase in pre-twist angle increases the buckling load of the beam.





The buckling load of e-FGO beam has higher value compared to FGO-2 beam corresponding to any pre-twist angle, a similar trend of result as obtained in case of natural frequencies.

The effect of power law index on critical buckling load of the beam is shown in figure 7.5. The increase in power law index is found to have a detrimental effect on the buckling load.

The additional data for dynamic stability analysis are taken as follows. $P^\oplus = 136$ N, $\omega_1 = 64.79$ rad/s. P^\oplus and ω_1 corresponds to the critical buckling load and fundamental natural frequency of a homogenous steel beam of same dimensions and end conditions as of the FGO beam.

The effect of property distribution law on the parametric instability of the beam is studied and presented in figures 7.6(a) and 7.6(b) for first and second mode principal instability regions respectively. It is found that the increase in the value of index decreases the dynamic stability of the beam for both the modes, as the instability regions are shifted nearer to the dynamic load factor axis. This is due to the

fact that with increase in power law index value both the first and second mode natural frequencies decrease as well as the critical buckling load decrease. Hence increase in the value of power law index renders more dynamic instability of the FGO beams. Moreover the e-FGO beam ensures better dynamic stability compared to FGO-2 and FGO-3 beam for both the modes.

The figures 7.7(a) and 7.7(b) represent respectively the plot of main instability regions for first and second mode of FGO-2 beam for different pre-twist angles. It is observed that the first mode instability region is shifted away from the axis of dynamic load factor when the pre-twist angle of the beam is increased from 30° to 45° . In contrary, the second mode instability region is shifted nearer to the axis of dynamic load factor as the pre-twist angle increases. The reason is, with increase in pre-twist angle there is an increase in first mode frequency and decrease in second mode frequency. Hence increase of pre-twist angle enhances the dynamic stability of the beam with respect to first principal region of instability whereas its increase has a detrimental effect on the second principal region of instability. Increase in pre-twist angle increases the frequency of first mode which causes the occurrence of dynamic instability at a higher excitation frequency. Similarly, the occurrence of instability corresponding to second main mode occurs at a lesser excitation frequency due to decrease in frequency of second mode with increase of pre-twist angle.

Figure 7.8(a) and 7.8(b) show the first and second principal region of instability of e-FGO beam respectively. A similar trend of results as obtained in case of FGO-2 beam is observed.

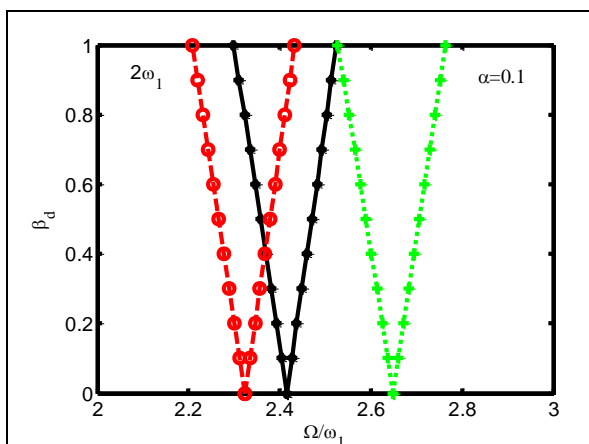


Figure 7.6(a) Effect of property distribution laws on first mode instability zone of steel-alumina pre-twisted FGO beam with steel-rich bottom. (* $n=2$, $\circ n=3$, +exp. law)

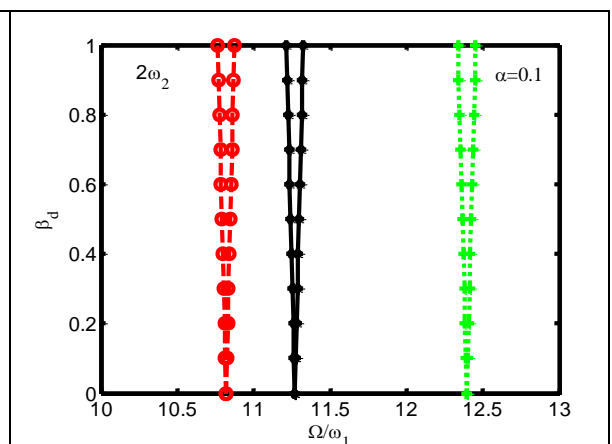
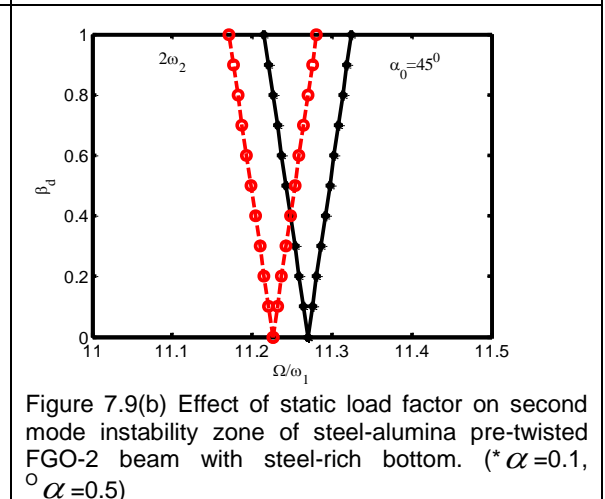
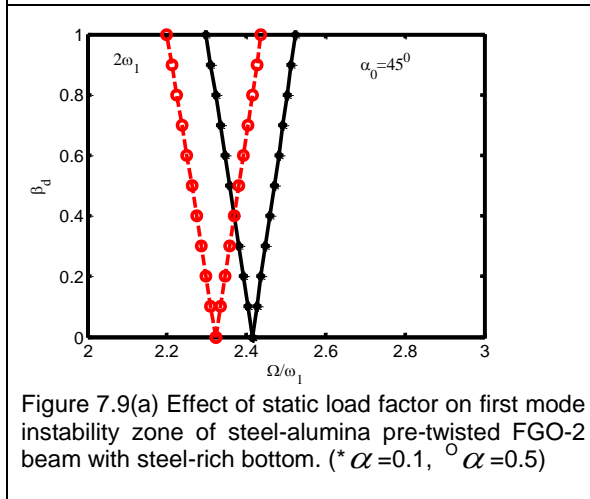
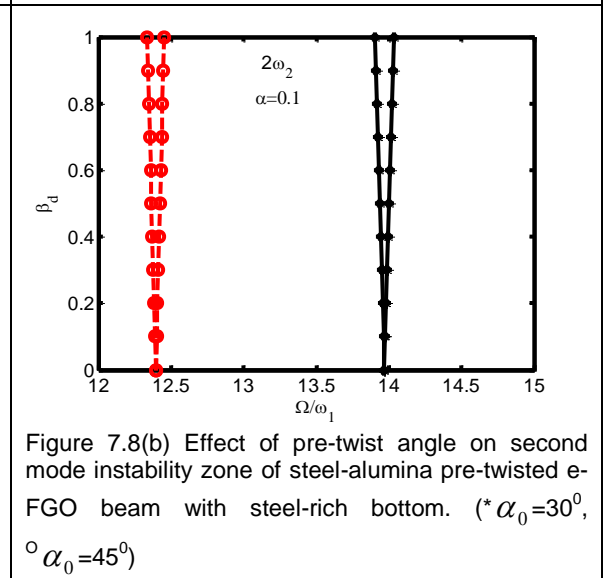
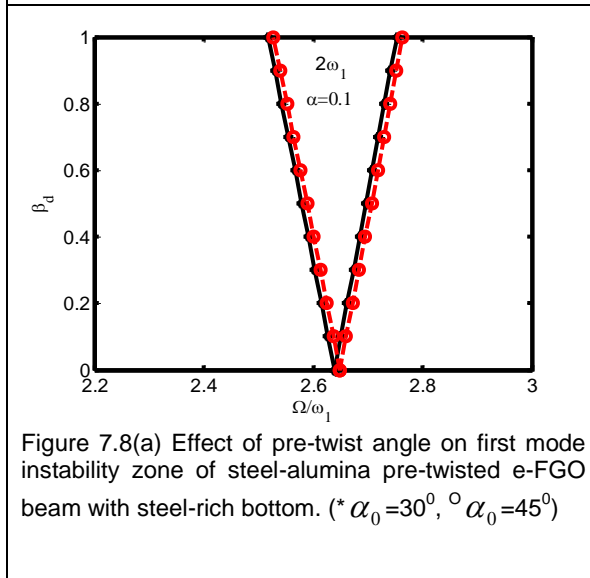
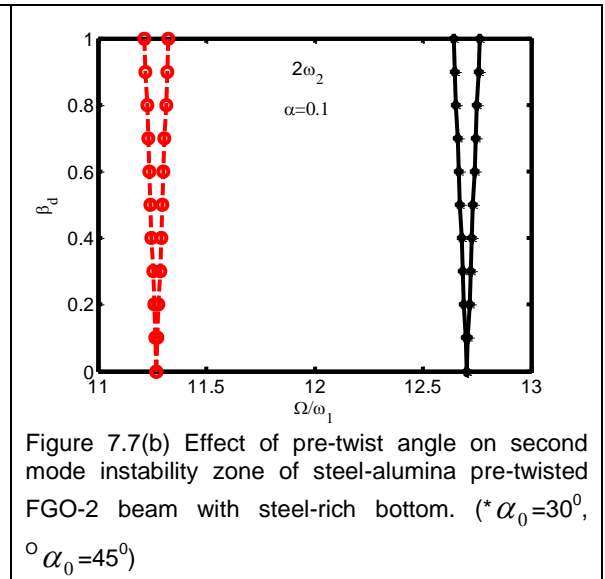
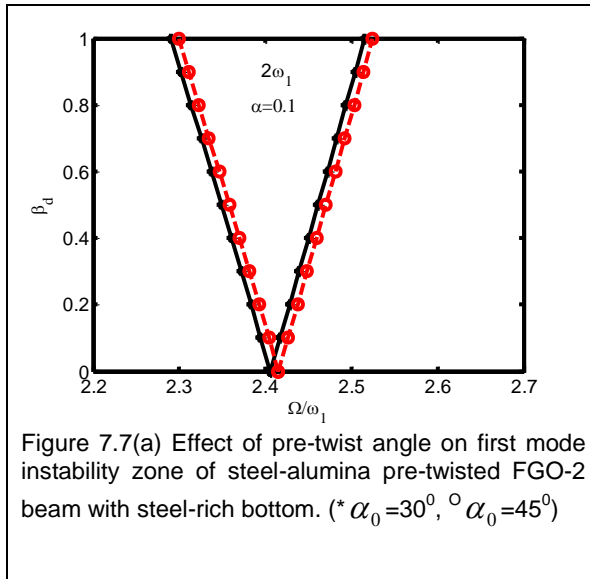


Figure 7.6(b) Effect of property distribution laws on second mode instability zone of steel-alumina pre-twisted FGO beam with steel-rich bottom. (* $n=2$, $\circ n=3$, +exp. law)

The increase in static load factor from 0.1 to 0.5 as expected has a detrimental effect on the dynamic stability of FGO-2 beam which can be seen from figures 7.9(a) and 7.9(b) for first and second mode respectively.



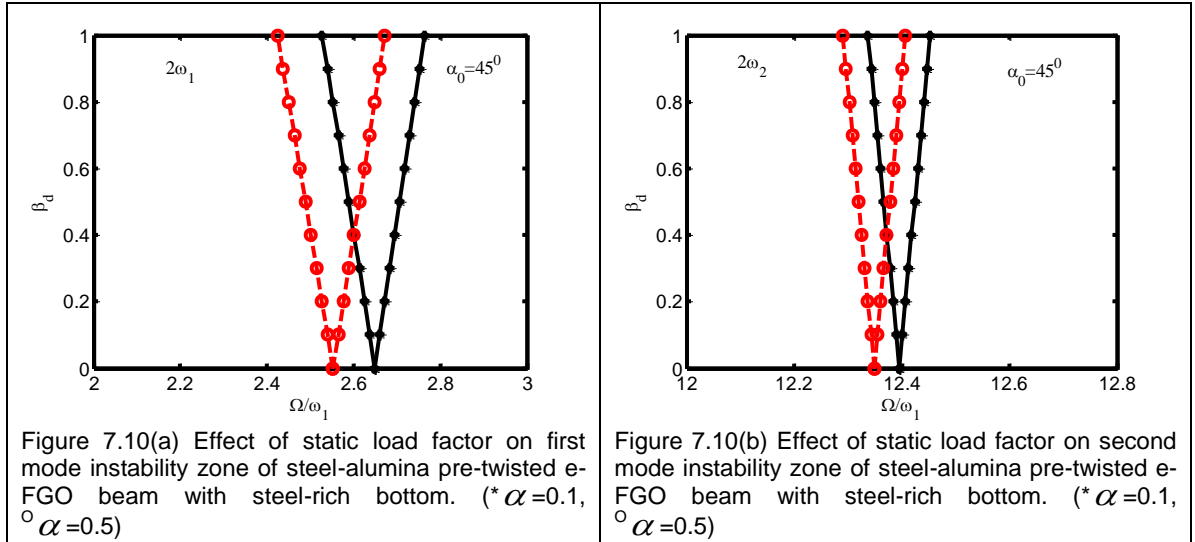


Figure 7.10(a) and 7.10(b) representing respectively the first and second principal region of instability of e-FGO beam reveals the similar effect of static load factor as obtained in case of FGO-2 beam.

7.5 Closure

The dynamic stability behaviour of a steel-alumina functionally graded pretwisted cantilever beam with steel-rich bottom is studied. The material properties along the thickness of the beam are assumed to vary according to power law and exponential law. Some of the important conclusions are outlined below.

Increase in the value of power law index decreases the critical buckling load as well as the first two mode frequencies of the beam.

Increase in the value of power law index has a detrimental effect on dynamic stability of the beam.

The dynamic stability of the beam is enhanced with increase of pre-twist angle with respect to the first principal region of instability, whereas increase in pre-twist angle has a detrimental effect on the second principal region of instability of the beam. This result is observed for both exponential and power law distribution of properties along the thickness of beam.

The exponential distribution of properties ensures better dynamic stability compared to power law distribution of properties.

Increase in static load component reduces the stability of the beam.

CHAPTER 8

CONCLUSION AND SCOPE FOR FUTURE WORK

8.1 Introduction

The conventional composite materials replace alloys in modern engineering applications due to their higher specific stiffness and strength. Those materials are not suitable for high temperature applications and applications where materials with large differences in their properties are used. The de-lamination at interface of those materials occurs either due to heavy load or due to high temperature. Functionally graded materials can be used at the interface to prevent the de-lamination. Moreover, these materials with ceramic rich surface can be used to retain the required strength in high temperature applications.

The FGMs [155] have got wide applications in various sectors like aerospace, automobile and biomedical due to a number of advantages over conventional composites. The behaviour of the FGM in various circumstances as regards to main and parametric resonance need to be explored to cement its place as an advanced modern engineering material. In the present study an attempt is made to study the dynamic stability of FGM beams for different cases such as FGM beams on foundation, in thermal environment, under rotation and with pre-twist.

8.2 Summary of findings

The effect of various system parameters on dynamic stability behaviour of both FGO and FGSW Timoshenko beams have been studied using finite element method. Floquet's theory is used to establish the dynamic instability boundaries. A steel-alumina FGO beam with steel-rich bottom is considered for analysis. In case of

study of FGSW beam, the top and bottom skin are alumina and steel respectively and the core is FGM with steel and alumina as its constituent phases. The important findings are outlined below.

8.2.1 FGO and FGSW beams

- The critical buckling load of the FGO beam decreases with the increase of power law index.
- The critical buckling load of FGSW beam decreases with increase of FGM content in it. This result is obtained in case of property distributions along thickness of core as per power law and exponential law as well.
- Increase in power law index decreases the first two natural frequencies of both FGO and FGSW beams.
- The frequencies of first two modes of FGSW beam increase with increase of FGM content.
- Exponential distribution of properties along thickness direction ensures better dynamic stability compared to power law distribution of properties for both FGO and FGSW beams.
- Increase in power law index enhances the chances of parametric instability in both FGO and FGSW beams.
- Increase in FGM content enhances the dynamic stability of e-FGSW beam it reduces the dynamic stability of FGSW beam with power law property distribution, both beams being used in ambient temperature.

8.2.2 FGO and FGSW beams resting on elastic foundations

- The first two natural frequencies of both FGO and FGSW beams increase with increase of the stiffness of the foundations.
- The frequencies of first two modes of FGSW beam increase with increase of FGM content.
- Exponential distribution of properties ensures better dynamic stability while compared to power law distribution properties for both FGO and FGSW beams resting on elastic foundations.

- Pasternak foundation has got more dominant effect on the dynamic stability of both FGO and FGSW beams as compared to Winkler foundation.

8.2.3 FGO and FGSW beams in high temperature thermal environment

- The first two natural frequencies of both FGO and FGSW beams decrease with increase in temperature of environment.
- In high temperature environment, increase of FGM content reduces the dynamic stability of FGSW beam with power law property distribution. In contrast, increase of FGM content from 30 percent to 50 percent in e-FGSW beam enhances its dynamic stability while further increase to 80 percent reduces its stability.
- Increase in environment temperature enhances the chance of dynamic instability of FGO and FGSW beams.

8.2.4 Rotating FGO and FGSW cantilever beams

- The increase in rotational speed and hub radius of FGO as well as FGSW beams increase their frequencies of first two modes.
- The increase in rotational speed and hub radius of FGO as well as FGSW beams enhance their dynamic stability.
- Increase in slenderness parameter of FGO and FGSW beams increases their stability.
- The exponential distribution of properties ensures less sensitiveness to parametric instability compared to power law distribution of properties for both FGO and FGSW beams.

8.2.5 Pre-twisted FGO cantilever beam

- Increase in the value of power law index decreases the critical buckling load of the beam.
- The frequencies of first two modes of the beam decrease with increase of power law index.

- Increase in pre-twist angle of the beam causes marginal increase in its fundamental frequency.
- The frequency of second mode of the beam decreases significantly with increase in pre-twist angle of the beam.
- Exponential distribution of properties along thickness direction ensures better dynamic stability compared to power law distribution. Increase in power law index enhances the chances of parametric instability.
- The dynamic stability of the beam is enhanced with increase of pre-twist angle with respect to the first principal region of instability, whereas increase in pre-twist angle has a detrimental effect on the second principal region of instability of the beam. This result is observed for both exponential and power law distribution of properties along the thickness of beam.

8.2.6 Important conclusions with respect to dynamic stability of FGM beams

Some of the important conclusions with respect to dynamic stability of FGM beams are given as follows.

- Exponential distribution of properties along the thickness direction ensures better dynamic stability compared to power law distribution of properties for both FGO and FGSW beams.
- Increase in the value of power law index enhances the chances of parametric instability in both FGO and FGSW beams.
- Increase in FGM content of e-FGSW beam enhances its dynamic stability whereas it reduces the dynamic stability of FGSW beam with power law property distribution, both beams being used at ambient temperature.
- Exponential distribution of properties ensures better dynamic stability for both FGO and FGSW beams resting on elastic foundations.
- Pasternak foundation has got more dominant effect on the dynamic stability of both FGO and FGSW beams as compared to Winkler foundation.

- In high temperature environment, increase of FGM content reduces the dynamic stability of the FGSW beam with power law property distribution. dynamic stability of FGSW beam with power law property distribution In contrast, increase of FGM content from 30% to 50 % in e-FGSW beam enhances its dynamic stability while further increase to 80% reduces its stability.
- Increase in environment temperature enhances the chance of dynamic instability of FGO and FGSW beams.
- The increase in rotational speed and hub radius of FGO as well as FGSW beams enhance their dynamic stability.
- Increase in slenderness parameter of FGO and FGSW beams increases their stability.
- The exponential distribution of properties ensures less sensitiveness to parametric instability compared to power law distribution of properties for rotating FGO and FGSW beams.
- The dynamic stability of pre-twisted FGO beam is enhanced with increase of pre-twist angle with respect to the first principal region of instability, whereas increase in pre-twist angle has a detrimental effect on the second principal region of instability of the beam. This result is observed for both exponential and power law distribution of properties along the thickness of beam. Exponential distribution of properties along thickness direction ensures better dynamic stability compared to power law distribution. Increase in power law index enhances the chances of parametric instability.

8.2.7 Some design guidelines for FGM beams under parametric excitation.

- For FGO and FGSW beams, with and without elastic foundation support, subjected to thermal environment, under rotation and FGO beams with pretwisting, exponential property distribution law along the thickness should be adopted to ensure better dynamic stability.
- If other design and manufacturing constraints force the designer to adopt power law distribution of properties along the thickness, lower value of the power law index should be adopted to ensure better dynamic stability.

- For FGM beams supported on elastic foundation, Pasternak foundation type should be preferred to Winkler's foundation type. More over with Pasternak foundation care should be taken to increase the foundation stiffness to further enhance the dynamic stability.
- Centrifugal stiffening enhances the dynamic stability of both the FGO and FGSW beams; hence rotating beams should be designed for minimum speed, which will ensure dynamic stability at higher speed.
- If there is a choice for selection of hub radius, rotating FGO and FGSW beams should be designed for minimum hub radius, which will ensure dynamic stability for larger hub radius.
- For FGSW beams used at ambient temperature, the FGM content should have the maximum permissible value with exponential law of property distribution along the core thickness, in contrast, with power law distribution the FGM content should have the minimum permissible value. For FGSW beams with exponential property distribution and used at higher temperature the optimum value of FGM content should be decided based on the operating temperature.
- Pre-twisting decreases the dynamic stability of the FGO beam, especially at higher frequencies of excitation. So smaller pretwist angle are preferred to ensure better dynamic stability.

8.3 Scope for future work

Present investigation explores some important aspects of the dynamic stability of functionally graded material beams. There are some other aspects of the beams which remain as open problems. The works that can be undertaken in future are presented as follows.

In the present analysis the beams are modeled on the basis of first order shear deformation theory. Higher order shear deformation theory may be used to get precise results in case of thick beams.

The specific resistances of elastic foundations in present analysis are assumed to be constants. But in practice these resistances may be variable along the length of the beams. The effect of variable foundation on dynamic stability of functionally graded beams may be taken up as a future work of research.

The high temperature thermal environment considered in the present analysis is of constant temperature environment. The analysis of beams subjected to temperature gradient may be undertaken.

In the present investigation the dynamic stability analysis of rotating functionally graded un-twisted beam and pre-twisted non rotating beams are carried out. But in practice, turbo-machinery blades are pre-twisted rotating blades. Hence the dynamic stability analysis of rotating pre-twisted blades can be done next. Moreover, the tapered beams can be considered for their parametric instability analysis.

Sometimes the loading may be such that the structural components are stressed beyond elastic limit. Then the material behaves nonlinearly. In present study the beam materials are considered to be stressed within elastic limit. The study of dynamic stability of FGM beams considering material nonlinearity may be undertaken as a future work of research. Moreover, higher order stretching strain may be considered to include geometric nonlinearity.

The results obtained need to be verified with experimental results. Therefore experimental analysis of dynamic stability of functionally graded material beams may be taken as a future work in order to validate the used computational method and obtained theoretical results.

Bibliography

- [1] Abbas, B. A. H. and Thomas, J., Dynamic stability of Timoshenko beams resting on an elastic foundation. *Journal of sound and vibration*, 60, 33 – 44, 1978.
- [2] Ahmad, M. and Naeem, M. N., Vibration characteristics of rotating FGM circular cylindrical shells using wave propagation method. *European Journal of Scientific Research*, 36 (2), 184-235, 2009.
- [3] Ahuja, R. and Duffield, R. C., Parametric instability of variable cross-section beams resting on an elastic foundation. *Journal of Sound and Vibration*, 39(2), 159-174, 1975.
- [4] Akhtar, K. and Kadoli, R., Stress analysis of SUS 304-ceramics functionally graded beams using third order shear deformation theory. *IE(I) Journal-MC*, 89, 31-37, 2008.
- [5] Alexanderson, Ernst F. W., A magnetic amplifier for audio telephony, *Proceedings of the Institute of Radio Engineers*, 4, 101-149, 1916.
- [6] Alshorbagy, A. E, Eltahir, M. A. and Mahmoud, F. F., Free vibration characteristics of a functionally graded beam by finite element method. *Applied Mathematical Modelling*, 35, 412-425, 2011.
- [7] Aminbaghai, M., Murin, J. and Kutis, V., Free Vibration of the multilayer FGM beams under longitudinal variable elastic foundation with effect of large axial force. *New Trends in Statics and Dynamics of Buildings*, 8th International Conference, Bratislava, Slovak Republic, October 21 – 22, 1-8, 2010.
- [8] Aminbaghai, M., Murin, J. and Kutis, V., Modal analysis of the FGM-beams with continuous symmetric and longitudinal variation of material properties with effect of large axial force. *Engineering Structures*, 34, 314-329, 2012.
- [9] Ariarathnam, S. T., Parametric resonance, *proceedings of the tenth U.S. National Congress of applied Mechanics*.1986.
- [10] Aristizabal-Ochoa, J. D., Statics stability and vibration of non-prismatic beams and columns. *Journal of Sound and Vibration*, 162(3), 441-455, 1993.

- [11] Arnaldo, J. M. Jr. and Rechard, A. S., Effect of functionally graded materials on resonances of bending shafts under time-dependent axial loading. *Journal of Vibration and Acoustics*, 133, 061005-1-11, 2011.
- [12] Attarnejad, R. and Shahba, A., Application of differential transform method in free vibration analysis of rotating non-prismatic beams. *World Applied Sciences Journal*, 5 (4), 441-448, 2008.
- [13] Aydogdu, M. and Taskin, V., Free vibration analysis of functionally graded beams with simply supported edges. *Materials & Design*, 28(5), 1651-1656, 2007.
- [14] Babai, M. H., Abhasi, M. and Eslami, M. R., Coupled thermoelasticity of functionally graded beam. *Journal of Thermal Stresses*, 31 (8), 680-697, 2008.
- [15] Baghani M., Jafari-Talookolaei, R. A. and Salarieh, H., Large amplitudes free vibrations and post-buckling analysis of unsymmetrically laminated composite beams on nonlinear elastic foundation. *Applied Mathematical Modelling*, 35, 130-138, 2011.
- [16] Banerjee, J. R., Dynamic stiffness formulation and free vibration analysis of centrifugally stiffened Timoshenko beams. *Journal of Sound and Vibration*, 247 (1), 97-115, 2001.
- [17] Bazoune, A., Effect of tapering on natural frequencies of rotating beams. *Shock and Vibration*, 14, 169–179, 2007.
- [18] Beliaev, N. M., Stability of prismatic rods subjected to variable longitudinal forces. *Collection of papers: Eng. Construct, Struct. Mech., Put', Leningrad*, 149 – 167, 1924.
- [19] Benatta, M. A., Mechab, I., Tounsi, A. and Adda Bedia, E. A., Static analysis of functionally graded short beams including warping and shear deformation effect. *Computational Materials Science*, 44, 765-773, 2008.
- [20] Bhangale, R. K. and Ganeshan, N., Thermoelastic buckling and vibration behavior of a functionally graded sandwich beam with constrained viscoelastic core. *Journal of Sound and Vibration*, 295, 294-316, 2006.
- [21] Bolotin, V. V., *The dynamic stability of elastic Systems*. Holden – Day, Inc., san Frasnisco, 1964.

- [22] Briseghella, L., Majorana, C. E. and Pellegrino, C., Dynamic stability of elastic structures: a finite element approach. *Computers and Structures*, 69, 11-25, 1998.
- [23] Brown, J. E., Hutt, J. M. and Salama, A. E., Finite element solution to dynamic stability of bars. *AIAA J.*, 6, 1423-1425, 1968.
- [24] Burney, S. Z. H. and Jaeger, L. G., A method of determining the regions of instability of a column by a numerical method approach. *Journal of Sound and Vibration*, 15(1), 75-91, 1971.
- [25] Calim, F. F. and Akkurt, F. G., Static and free vibration analysis of straight and circular beams on elastic foundation. *Mechanics Research Communication*, 38, 89-94, 2011.
- [26] Carnegie, W., Vibration of pre-twisted cantilever blading. *Proceedings of the institution of Mechanical Engineers*, 173, 343-374, 1959.
- [27] Carnegie, W., Vibration of pre-twisted cantilever blading allowing for rotary inertia and shear deflection. *Journal of Mechanical Engineering Science* 6, 105–109, 1964.
- [28] Carnegie, W. and Thomas, J., The effects of shear deformation and rotary inertia on the lateral frequencies of cantilever beams in bending. *Journal of Engineering for Industry Transactions of the American Society of Mechanical Engineers*, 94, 267–278, 1972.
- [29] Celep, Z., Dynamic stability of pre-twisted columns under periodic axial loads. *Journal of sound and vibration*, 103, 35–48, 1985.
- [30] Chakraborty, A., Gopalakrishnan, S. and Reddy, J. N., A new beam finite element for the analysis of functionally graded materials. *International Journal of Mechanical Science*, 45, 519-539, 2003.
- [31] Chaofeng, L. U., Chen, W. and Zhong, Z., Two dimensional thermoelasticity solution for functionally graded thick beams. *Science in China Series G: Physics, Mechanics and Astronomy*, 49(4), 451-460, 2006.
- [32] Chattopadhyay, A., Gu, H. and Liu, Q., Modeling of smart composite box beam with non-linear induced strain. *Composites, Part B*, 30, 603-612, 1999.
- [33] Chen, Q. and Chan, Y. W., Integral finite element method for dynamical analysis of elastic-viscoelastic composite structures. *Computers and Structures*, 74, 51-64, 2000.

- [34] Chen, Q. and Levy, C., Vibration analysis and control of flexible beams by using smart damping structure. *Composites, Part B*, 30, 395-406, 1999.
- [35] Chen, L. W. and Ku, M. K., Dynamic stability of a cantilever shaft-disk system. *Journal of Vibration and Acoustics, Trans of ASME*, 114,326-329, 1992.
- [36] Chen, W. -R., On the vibration and stability of spinning, axially loaded pre-twisted Timoshenko beams. *Finite Elements in Analysis and Design*, 46, 1037-1047, 2010.
- [37] Chen, W. R., Parametric instability of spinning twisted Timoshenko beams under compressive axial pulsating loads. *International Journal of Mechanical Science*, 52, 1167-1175, 2010.
- [38] Chung, J. and Yoo, H. H., Vibration analysis of rotating cantilever beams. *Journal of Sound and Vibration*, 249 (1), 147-164, 2002.
- [39] Chung, Y. L., Chen, L. W., Dynamic stability of spinning pre-twisted sandwich beams with a constrained damping layer subjected to periodic axial loads. *Composite Structures*, 70, 275-286, 2005.
- [40] Chhabra, P. P. S. and Ganguli, R., Superconvergent finite element for coupled torsional-flexural-axial vibration analysis of rotating blades. *International Journal for computational Methods in Engineering Science and Mechanics*, 11, 48-69, 2010.
- [41] Das, D., Sahoo, P. and Saha, K. N., Large displacement free vibration analysis of rotating beam. *Proceedings of the International Conference on Mechanical Engineering*, Dhaka, Bangladesh, December, 2007.
- [42] Dawson, B., Ghosh, N. G. and Carnegie, W., Effect of slenderness ratio on the natural frequencies of pre-twisted cantilever beams of uniform rectangular cross-section. *Journal of Mechanical Engineering Science*, 13, 51–59, 1971.
- [43] Dutta, P. K. and Nagraj, C. S., Dynamic instability behaviour of tapered bars with flaws supported on an elastic foundation. *Journal of Sound and Vibration*, 131(2), 229-237, 1989.
- [44] Eisenberger, M. and Clastronik, J., Vibration and buckling of a beam on a variable Winkler elastic foundation. *Journal of Sound and Vibration*, 115(2), 233-241, 1987.
- [45] Emam, S. A., A static and dynamic analysis of the postbuckling of geometrically imperfect composite beams. *Composite Structures*, 90(2), 247-253, 2009.

- [46] Engel, R. S., Dynamic stability of an axially loaded beam on an elastic foundation with damping. *Journal of Sound and Vibration*, 146(3), 463-477, 1991.
- [47] Evan – Iwanowski, R. M. On the parametric response of structures. *Applied Mechanics review*, 18, 699 – 702, 1965.
- [48] Evandro, P. Jr. and Joao, B. M. de S. Jr. Design sensitivity analysis of nonlinear structures subjected thermal load. *Computers and Structures*, 86, 1369-1384, 2008.
- [49] Faraday, M., On a peculiar class of acoustical figures and on certain forms assumed by a group of particles upon vibrating elastic surfaces. *Phil. Trans., Roy. Soc., London*, 299 – 318, 1831.
- [50] Fazelzadeh, S. A., Malekzadeh, P., Zahedinezad, and Hosseini, M., Vibration analysis of functionally graded thin-walled rotating blades under high temperature supersonic flow using differential quadrature method, *Journal of Sound and Vibration*. 306, 333-348, 2007.
- [51] Ganapathi, M., Patel, B. P., Boisse, P. and Polit, O., Flexural loss factors of sandwich and laminated composite beams using linear and non-linear dynamics. *Composites, Part B*, 30, 245-256, 1999.
- [52] Gharib, A., Salehi, M. and Fazeli, S., Deflection control of functionally graded material beams with bounded piezoelectric sensors and actuators. *Material Science and Engineering A*, 498, 110-114, 2008.
- [53] Giunta, G., Crisafulli, D., Belouettar, S. and Carrera, E., Hierarchical theories for the analysis of free vibration of functionally graded beams. *Composite Structure*, 94, 68-74, 2011.
- [54] Gunda, J. B. and Ganguli, R., Stiff-string basis functions for vibration analysis of high speed rotating beams. *Journal of Applied Mechanics*, 75, 1-5, 2008.
- [55] Gunda, J. B., Singh, A. P., Chhabra, P. S., and Ganguli, R., Free vibration analysis of rotating tapered blades using Fourier- p super element. *Structural Engineering and Mechanics*, 27 (2), 000-000, 2007.
- [56] Guo, X. -X., Wang, Z. M., Wang, Y. Y. and Zhou, Y. F., Analysis of the coupled thermoelastic vibration for axially moving beam. *Journal of Sound and Vibration*, 325, 597-608, 2009.

- [57] Hosseini, S. A. A. and Khadem, S. E., Free vibrations analysis of a rotating shaft with nonlinearities in curvature and inertia. *Mechanism and Machine Theory*, 44, 272–288, 2009.
- [58] Hsu, C. S., On the parametric excitation of a dynamic system having multiple degrees of freedom. *J. Appl. Mech., Trans. ASME*, 30, 367 – 372, 1963.
- [59] Hsu, C. S., Further results on parametric excitation of a dynamic system. *J. Appl. Mech., Trans. ASME*, 32, 373 – 377, 1965.
- [60] Hsu, M. H., Vibration analysis of pre-twisted beams using the spline collocation method. *Journal of Marine Science and Technology*, 17(2), 106-115, 2009.
- [61] Huang, C. L., Lin, W. Y. and Hsiao, K. M., Free flapping vibration of rotating inclined Euler beams. *World Academy of Science, Engineering and Technology*, 56, 604-610, 2009.
- [62] Huang, D. J., Ding, H. J. and Chen, W. Q., Analytical solution for functionally graded anisotropic cantilever beam under thermal and uniformly distributed load. *J Zhejiang Univ. Sci. A*, 8 (9), 1351-1355, 2007.
- [63] Hutchinson, J. R., Discussion “shear coefficients for Timoshenko beam theory”. *ASME Journal of Applied Mechanics*, 68, 87-92, 2001.
- [64] Ibrahim, R. A., Parametric vibration, Part III: Current problems (1). *Shock vib. Dig.*, 10 (3), 41 –57, 1978.
- [65] Ibrahim, R. A., Parametric vibration, Part IV: Current problems (2). *Shock Vib Dig.*, 10 (4), 19 – 47, 1978.
- [66] Ibrahim, R. A., and Roberts, J. W., parametric vibration, Part V: Stochastic problems. *Shock Vib. Dig.*, 10 (5), 17 – 38, 1978.
- [67] Ibrahim, R. A., Parametric vibration, Part Vi: Stochastic problems (2). *Shock Vib. Dig.*, 13 (9), 23 – 35, 1981.
- [68] Ibrahim, R. A., *Parametric Random Vibration*, Research Studies Press Ltd., England, 1985.
- [69] Ibrahim, R. A. and Barr, A. D. S., Parametric vibration, Part I: Mechanics of linear problems. *Shock Vib. Dig.*, 10(1), 15 – 29, 1978.
- [70] Ibrahim, R. A. and Barr, A. D. S., Parametric vibration, part II: Mechanics of nonlinear problems. *Shock Vib. Dig.*, 10(20), 9 – 24, 1978.

- [71] Ishida, Y., Ikeda, T., Yamamoto, T. and Esaka, T., Parametrically excited oscillations of a rotating Shaft under a periodic axial force. *JSME Int. J., Series III*, 31, 698 – 704, 1988.
- [72] Iwatsubo, T., Saigo, M. and Sugiyama, Y., Parametric instability of clamped – clamped and clamped – simply supported columns under periodic axial load. *Journal of sound and vibration*, 30, 65 – 77, 1973.
- [73] Iwatsubo, T., Sugiyama, Y. and Ogino, S., Simple and combination resonances of columns under periodic axial loads. *Journal of sound and vibration*, 33, 211 – 221, 1974.
- [74] Jensen, J. J., Harmonic vibrations of pretwisted plates. *International Journal of Solids and Structures*, 9, 1117-1131, 1973.
- [75] Jhung, M. J. and Jo, J. C., Dynamic characteristics of rectangular twisted beam with fins surrounded with liquid. *Nuclear Engineering and Design*, 237, 64-73, 2007.
- [76] Jian, J. P. and Li, D. X., A new finite element model for piezothermoelastic composite beam. *Journal of Sound and Vibration*, 306, 849-864, 2007.
- [77] Jurij, A. and Maks, O., Thermal vibrational analysis of simply supported beam and clamped beam. *Journal of Sound and Vibration*, 308, 514-525, 2007.
- [78] Kapuria, S., Bhattacharyya, M. and Kumar, A. N., Bending and free vibration response of layered functionally graded beams: A theoretical model and its experimental validation. *Composite Structures*, 82, 390-402, 2008.
- [79] Kaya, M. O., Free vibration analysis of a rotating Timoshenko beam by differential transform method. *Aircraft Engineering and Aerospace Technology: An International Journal*, 78 (3), 194–203, 2006.
- [80] Ke, L. -L., Yang, J. and Kitipornchai, S., Postbuckling analysis of edge cracked functionally graded Timoshenko beams under end shortening. *Composite Structures*, 90(2), 152-160, 2009.
- [81] Khalili, S. M. R., Jafari, A. A. and Eftekhari, S. A., A mixed Ritz-DQ method for forced vibration of functionally graded beams carrying moving loads. *Composite Structures*, 92(10), 2497-2511, 2010.
- [82] Kim, J. and Paulino, G. H., Finite element evaluation of mixed mode stress intensity factors in functionally graded materials. *International Journal for Numerical Methods in Engineering*, 53, 1903–1935, 2002.

- [83] Kocaturk, T. and Simsek, M., Dynamic analysis of eccentrically prestressed viscoelastic Timoshenko beam under a moving harmonic load. *Computers and Structures*, 84, 2113-2127, 2006.
- [84] Lau, S. L., Cheung, Y. K. and Wu, S. Y., A variable parameter incrementation method for dynamic instability of linear and nonlinear elastic systems. *J. Appl. Mech., Trans. ASME*, 49, 849 – 853, 1982.
- [85] Lee, S.Y. and Kuo, Y.H., Bending frequency of a rotating Timoshenko beam with general elastically restrained root. *Journal of Sound and Vibration*, 162, 243-250, 1993.
- [86] Lee, S. -Y., Lin, S. -M. and Lin, Y. -S., Instability and vibration of a rotating Timoshenko beam with precone. *International Journal of Mechanical Sciences*, 51, 114–121, 2009.
- [87] Lee, S. Y. and Sheu, J. J., Free vibration of an extensible rotating inclined Timoshenko beam. *Journal of Sound and Vibration*, 304, 606–624, 2007.
- [88] Lee, S. Y. and Yang, C. C., Non-conservative instability of a Timoshenko beam resting on Winkler elastic foundation. *Journal of Sound and Vibration*, 162(1), 177-184, 1993.
- [89] Lee, U., Kim, J. and Oh, H., Spectral analysis for the transverse vibration of an axially moving Timoshenko beam. *Journal of Sound and Vibration*, 271, 685-703, 2004.
- [90] Lesaffre, N., Sinou, J.J. and Thouverez, F., Stability analysis of rotating beams rubbing on an elastic circular structure. *Journal of Sound and Vibration*, 299 (4-5), 1005-1032, 2007.
- [91] Leung, A. Y. T. and Fan, J., Natural vibration of pre-twisted shear deformable beam systems subject to multiple kinds of initial stresses. *Journal of Sound and Vibration*, 329, 1901-1923, 2010.
- [92] Li, X. F., A unified approach for analyzing static and dynamic behaviours of functionally graded Timoshenko and Euler-Bernoulli beams, 318 (4-5), 1210-1229, 2008.
- [93] Liao, C. -L. and Huang, B. -W., Parametric instability of a spinning pretwisted beam under periodic axial force. *International Journal of Mechanical Science*, 37 (4), 423-439, 1995.

- [94] Lin, S. M., Wu, C. T. and Lee, S. Y., The dynamic analysis of nonuniformly pre-twisted Timoshenko beams with elastic boundary conditions. *International Journal of Mechanical Science*, 43, 2385-2405, 2001.
- [95] Lim, T. S., Lee, C. S. and Lee, D. G., Failure modes of foam core sandwich beams under static and impact loads. *Journal of Composite Materials*, 38, 1639-1662, 2004.
- [96] Lin, S. -M., Lee, S. -Y. and Lin, Y. -S., Modeling and bending vibration of the blade of a horizontal-axis wind power turbine. *CMES*, 23 (3), 175-186, 2008.
- [97] Lin, S. M., Wu, C. T. and Lee, S. Y., Analysis of rotating nonuniform pretwisted beams with an elastically restrained root and a tip mass. *International Journal of Mechanical Science*, 45, 741-755, 2003.
- [98] Liu, K.-C., Friend, J. and Yeo, L., The axial-torsional vibration of pre-twisted beams. *Journal of Sound and Vibration*, 321, 115-136, 2009.
- [99] Maa, L. S. and Lee, D. W., A further discussion of nonlinear mechanical behavior for FGM beams under in-plane thermal loading. *Composite Structures*, 93, 831–842, 2011.
- [100] Machado, S. P., Filipich, C. P. and Cortinez, V. H., Parametric vibration of thin-walled composite beams with shear deformation. *Journal of Sound and Vibration*, 305, 563-581, 2007.
- [101] Mahi, A., Adda Bedia, E. A., Tounsi, A. and Mechab, I., An analytical method for temperature-dependent free vibration analysis of functionally graded beams with general boundary conditions. *Composite Structures*, 92, 1877–1887, 2010.
- [102] Matsunaga, H., Vibration and buckling of deep beam-coulmns on two parameter elastic foundations. *Journal of Sound and Vibration*, 228(2), 359-376, 1999.
- [103] Melde, F., über erregung stehender wellen eines fadenformigen korpers. *ANN. PHys. Chem.*, 109, 193 – 215, 1859.
- [104] Mettler, E., Allgemeine theorie der stabilitat erzwungener schwingungen elastischer koper. *Ing. Arch*, 17, 418-449, 1949.
- [105] Mohanty, S. C., Parametric instability of a pretwisted cantilever beam with localised damage. *International Journal of Acoustics and Vibration*, 12(4), 153-161, 2007.

- [106] Mohanty, S. C., Dash, R. R. and Rout, T., Parametric instability of a functionally graded Timoshenko beam on Winkler's elastic foundation. *Nuclear Engineering and Design*, 241, 2698-2715, 2011.
- [107] Mohanty, S. C., Dash, R. R. and Rout, T., Static dynamic stability analysis of a functionally graded Timoshenko beam. *International Journal of Structural Stability and Dynamics*, 12(4), 2012.
- [108] Morfidis, K., Exact matrices for beams on three parameter elastic foundation. *Computers & Structures*, 85, 1243-1256, 2007.
- [109] Nakra, B. C., Vibration control with viscoelastic materials. *The Shock and Vibration Digest*, 8, 3-12, 1976.
- [110] Nakra, B. C., Vibration control with viscoelastic materials-II. *The Shock and Vibration Digest*, 13, 17-20, 1981.
- [111] Nakra, B. C., Vibration control with viscoelastic materials-III. *The Shock and Vibration Digest*, 16, 17-22, 1984.
- [112] Nayfeh, A. H. and Mook, D.T., *Nonlinear Oscillations*. John Willey & Sons, Inc., New York, 1979.
- [113] Nirmala, K., Upadhyay, P. C., Prucz, J. and Loyns, D., Thermoelastic stresses in composite beams with functionally graded layer. *Journal of Reinforced Plastics and Composites*, 25 (12), 1241-1254, 2006.
- [114] Onipede Jr., O. and Dong, S.B., Propagating waves and end modes in pretwisted beams. *Journal of Sound and Vibration*, 195 (2), 313-330, 1996.
- [115] Ouyang, H. and Wang, M., A dynamic model for a rotating beam subjected to axially moving forces. *Journal of Sound and Vibration*, 308, 674–682, 2007.
- [116] Ozturk, H. and Sabuncu, M., Stability analysis of a cantilever composite beam on elastic support. *Composite Science and Technology*, 65, 1982-1995, 2005.
- [117] Paulino, G. H. and Jin, Z. H., Correspondence principle in viscoelastic functionally graded materials. *Journal of Applied Mechanics*, 68, 129-132, 2001.
- [118] Piovan, M. T. and Machado, S. P., Thermoelastic dynamic stability of thin-walled beams with graded material properties. *Thin-Walled Structures*, 49, 437-447, 2011.

- [119] Piovan, M. T. and Sampaio, R., A study on the dynamics of rotating beams with functionally graded properties. *Journal of Sound and Vibration*, 327, 134-143, 2009.
- [120] Pradeep, V., Ganesan, N. and Bhaskar, K., Vibration and thermal buckling of composite sandwich beams with viscoelastic core. *Composite Structures*, 81, 60-69, 2007.
- [121] Pradhan, S. C. and Murmu, T., Thermomechanical vibration of FGM sandwich beams under variable elastic foundations using differential quadrature method. *Journal of Sound and Vibration*, 321(1-2), 342-362, 2009.
- [122] Raju, K. K. and Rao, G. V., Vibration, stability and frequency-axial load relation of short beam. *Journal of Sound and Vibration*, 95(3), 426-429, 1984.
- [123] Rao, S. S. and Gupta, R. S., Finite element vibration analysis of rotating Timoshenko beams. *Journal of Sound and Vibration*, 242 (1), 103-124, 2001.
- [124] Ray, K. and Kar, R. C., Parametric instability of a symmetric sandwich beam with higher order effects. *Computers and Structures*, 60 (5), 817-824, 1996.
- [125] Sabuncu, M. and Evran, K., Dynamic stability of a rotating asymmetric cross-section Timoshenko beam subjected to an axial periodic force. *Finite Elements in Analysis and Design*, 41, 1011–1026, 2005.
- [126] Sabuncu, M. and Evran, K., The dynamic stability of rotating asymmetric cross-section Timoshenko beam subjected to lateral parametric excitation. *Finite Elements in Analysis and Design*, 42, 454-469, 2006.
- [127] Sabuncu, M. and Evran, K., Dynamic stability of a rotating pre-twisted asymmetric cross-section Timoshenko beam subjected to an axial periodic force. *International Journal of Mechanical Sciences*, 48, 579–590, 2006.
- [128] Sabuncu, M. and Evran, K., Dynamic stability of a rotating pre-twisted asymmetric cross-section blade subjected to a lateral parametric excitation. *Finite Elements in Analysis and Design*, 42, 1113–1122, 2006.
- [129] Saito, H. and Otomi, K., Parametric response of viscoelastically supported beams. *Journal of Sound and Vibration*, 63, 169 – 178 1979.
- [130] Sakar, G. and Sabuncu, M., Dynamic stability analysis of pre-twisted aero-foil cross-section blade packets under rotating conditions. *International Journal of Mechanical Science*, 50, 1-13, 2008.

- [131] Sallai, B. O., Tounsi, A., Mechab, I., Bachir B. M., Meradjah, M. and Adda, B. E. A., A theoretical analysis of flexional bending of Al/Al₂O₃ S-FGM thick beams. *Computational Materials Science*, 44(4), 1344-1350, 2009.
- [132] Saravia, C. M., Machado, S. P. and Cortinez, V. P., Free vibration and dynamic stability of rotating thin-walled composite beams. *European Journal of Mechanics A/Solids*, 30, 432-441, 2011.
- [133] Santare M. H. and Lambros, J., Use of graded finite elements to model the behavior of non-homogeneous materials. *Journal of Applied Mechanics*, 67, 819-822, 2000.
- [134] Schmidt, G., *Parametererregte Schwingungen*. VEB Deutscher verlag der Wissenschaften, Berlin, 1975.
- [135] Shastry, B. P. and Rao, G. V., Dynamic stability of a cantilever column with an intermediate concentrated periodic load. *Journal of Sound and Vibration*, 113, 194 – 197, 1987.
- [136] Shastry, B. P. and Rao, G. V., Stability boundaries of a cantilever column subjected to an intermediate periodic concentrated axial load. *Journal of Sound and Vibration*, 116, 195 – 198, 1987.
- [137] Shastry, B. P. and Rao, G. V., Dynamic stability of columns with two symmetrically placed intermediate supports. *Journal of Sound and Vibration*, 104(3), 524-527, 1986.
- [138] Shooshtari, A. and Rafiee, M., Nonlinear forced vibration analysis of clamped functionally graded beams. *Acta Mech*, 221, 23-38, 2011.
- [139] Simitises, G. J., Instability of dynamically – loaded structures. *Appl. Mech, Rev.*, 40, 1403 – 1408, 1987.
- [140] Simsek, M., Vibration analysis of a functionally graded beam under a moving mass by using different beam theories. *Composite Structures*, 92(4), 904-917, 2010.
- [141] Simsek, M., Fundamental frequency analysis of functionally graded beams by using different higher-order beam theories. *Nuclear Engineering and Design*, 240, 697-705, 2010.
- [142] Simsek, M., Non-linear vibration analysis of a functionally graded Timoshenko beam under action of a moving harmonic load. *Composite Structures*, 92(10), 2532-2546, 2010.

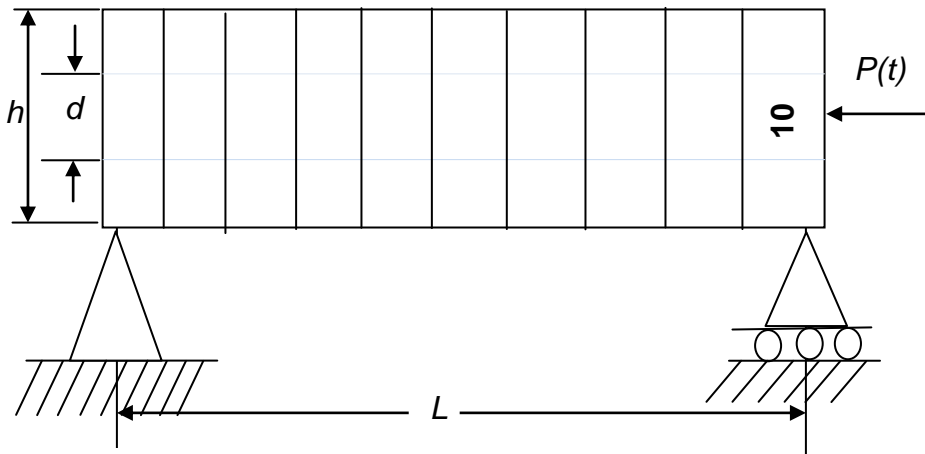
- [143] Simsek, M. and Kocatürk, T., Free and forced vibration of a functionally graded beam subjected to a concentrated moving harmonic load. *Composite Structures*, 90(4), 465-473, 2009.
- [144] Sladek, J., Sladek, V., Zhang, C. Z. and Tan, C. L., Evaluation of fracture parameters for crack problems in FGM by a mesh less method, *Journal of Theoretical and Applied Mechanics*, 44 (3), 603-636, 2006.
- [145] Song, O., Jeong, N.-H. and Librescu, L., Vibration and stability of pretwisted spinning thin-walled composite beams featuring bending-bending elastic coupling. *Journal of Sound and Vibration*, 237 (3), 513-533, 2000.
- [146] Stafford, R. O. and Giurdiuti, V., Semi-analytic methods for rotating Timoshenko beam. *International Journal of Mechanical Science*, 17, 719-727, 1975.
- [147] Stevens, K. K., On the parametric excitation of a viscoelastic column. *AIAA journal*, 4, 2111-2115, 1966.
- [148] Strutt, J. W. (Lord Rayleigh), On maintained vibrations, *Philosophical Magazine*, 15, 229-235, 1883.
- [149] Strutt, J. W. (Lord Rayleigh), On the maintenance of vibrations by forces of double frequency, and on the propagation of waves through a medium endowed with periodic structure, *Philosophical Magazine*, 24, 145-159, 1887.
- [150] Strutt, J. W. (Lord Rayleigh), *The Theory of Sound*, 2nd. ed. (N.Y., N.Y.: Dover), 1, 81-85, 1945.
- [151] Subrahmanyam, K. B., Kulkarni, S. V. And Rao, J. S., Coupled bending-bending vibration of pre-twisted cantilever blading allowing for shear deflection and rotary inertia by the Reisner method. *Internationa Journal of Mechanical Science*, 23, 517-530, 1981.
- [152] Subrahmanyam, K. B. and Rao, J. S., Coupled bending-bending vibrations of pretwisted tapered cantilever beams treated by the Reissner method. *Journal of Sound and Vibration*, 82 (4), 577-592, 1982.
- [153] Svensson, I., Dynamic instability regions in a damped system. *Journal of Sound and Vibration*, 244,779-793, 2001.
- [154] Takahashi, K., An approach to investigate the instability of the multiple-degree-of-freedom parametric dynamic systems. *Journal of Sound and Vibration*, 78, 519 – 529, 1981.

- [155] Tan, T. H., Lee, H. P. and Leng, G. S. B., Parametric instability of spinning pretwisted beam subjected to spin speed perturbation. *Computer Methods in Applied Mechanics and Engineering*, 148, 139-163, 1997.
- [156] Tan, T. H., Lee, H. P. and Leng, G. S. B., Parametric instability of spinning pretwisted beam subjected to sinusoidal compressive axial loads. *Computers and Structures*, 66 (6), 745-764, 1998.
- [157] Telli, S. and Kopmaz, O., On the mathematical modelling of beams rotating about a fixed axis. *Mathetical and Computational Application*, 9 (3), 333-347, 2004.
- [158] Tylikowski, A., Stabilization of beam parametric vibrations with shear deformation and rotary inertia effects. *International Journal of Solids and Structures*, 42, 5920-5930, 2005.
- [159] Victor, B. and Larry, W. B., Modeling and analysis of functionally graded materials and structures. *Appl. Mech. Rev.*, 60, 195-216, 2007.
- [160] Vielsack, P., Lateral bending vibration of a beam with small pretwist. *Engineering Structures*, 22, 691-698, 2000.
- [161] Vinod, K. G., Gopalakrishnan, S. and Ganguli, R., Free vibration and wave propagation analysis of uniform and tapered rotating beams using spectrally formulated finite elements. *International Journal of Solids and Structures*, 44, 5875–5893, 2007.
- [162] Wakashima, K., Hirano, T. and Niino, M., Space applications of advanced structural materials. ESA, SP-303:97, 1990.
- [163] Wattanasakulpong, N., Prusty, B. G. and Kelly, D. W., Thermal buckling and elastic vibration of third order shear deformable functionally graded beams. *International Journal of Mechanical Science*, 53, 734-743, 2011.
- [164] Yardimoglu, B., A novel finite element model for vibration analysis of rotating tapered Timoshenko beam of equal strength. *Finite Elements in Analysis and Design*, 46, 838–842, 2010.
- [165] Yardimoglu, B. and Yildirim, T., Finite element model for vibration analysis of pre-twisted Timoshenko beam. *Journal of Sound and vibration*, 273, 741-754, 2004.
- [166] Yoo, H. H., Lee, S. H. and Shin, S. H., Flapwise bending vibration analysis of rotating multi-layered composite beams. *Journal of Sound and Vibration*, 286, 745–761, 2005.

- [167] Yoo, H. H. and Shin, S. H., Vibration analysis of cantilever beams. *Journal of Sound and Vibration*, 212 (5), 807-828, 1998.
- [168] Young, T. H. and Gau, C. Y., Dynamic stability of spinning pretwisted beams subjected to axial random forces. *Journal of sound and Vibration*, 268, 149-165, 2003.
- [169] Yuksel, S. and Aksoy, T. M., Flexural vibrations of a rotating beam subjected to different base excitations. *G.U. Journal of Science*, 22 (1), 33-40, 2009.
- [170] Zenkour, A. M. and Alghamdi, N. A., Bending Analysis of Functionally Graded Sandwich Plates Under the Effect of Mechanical and Thermal Loads. *Mechanics of Advanced Materials and Structures*, 17, 419–432, 2010.
- [171] Zhu, H. and Sankar, B. V., A combined Fourier Series-Galerkin method for the analysis of functionally graded beams. *Journal of Applied Mechanics*, 71, 421-424, 2004.

APPENDIX

$$[N] = \begin{bmatrix} 1 - \frac{x}{l} & \frac{6\eta x(x-l)}{l(\beta l^2 + 12)} & \frac{3\eta x(x-l)}{\beta l^2 + 12} & \frac{x}{l} & -\frac{6\eta x(x-l)}{l(\beta l^2 + 12)} & \frac{3\eta x(x-l)}{\beta l^2 + 12} \\ 0 & 1 - \frac{12x - \beta x^2(2x-3l)}{l(\beta l^2 + 12)} & \frac{\beta x l(x-l)^2 - 6x(x-l)}{l(\beta l^2 + 12)} & 0 & \frac{12x - \beta x^2(2x-3l)}{l(\beta l^2 + 12)} & \frac{\beta x l(x-l)^2 - 6x(x-l)}{l(\beta l^2 + 12)} \\ 0 & \frac{6\beta x(x-l)}{l(\beta l^2 + 12)} & 1 - \frac{\beta x l(3x+4l) + 12x}{l(\beta l^2 + 12)} & 0 & -\frac{6\beta x(x-l)}{l(\beta l^2 + 12)} & \frac{\beta x l(3x-2l) + 12x}{l(\beta l^2 + 12)} \end{bmatrix}$$



A Typical Ten Element Discretization of the Beam

RESUME

Name: Mr. Trilochan Rout.
Date of birth: 26-06-1973.
Permanent address: Village: Gopinath pur, P.O: Hatasahi Kutchery
Dist.: Kendrapara, Odisha, India
Pin-755016.

Educational qualifications:

Degree	University	Year of Passing	Division
B.E. (Mechanical)	Sambalpur University	1995	First
M.M.E. (Machine Design)	Jadavpur University	2004	First

Teaching experience: Faculty in Department of Mechanical Engineering I.G.I.T. Sarang, Odisha, India from 24-11-2004 to 26-04-2012 (Lecturer-24-11-2004 to 23-11-2009, Lecturer (Sr. Scale-24.04-2009 to 26-04-2012).

Faculty in Department of Mechanical Engineering, P.M.E.C., Berhampur, Odisha, India from 27-04-2012 (Assistant professor-27-04-2012 till date.

Research publications: 09 International Journal papers
03 International conference papers
04 National conference papers

Publications related to the Ph.D. thesis work.

International Journal:

Published/To be published:

1. S.C. Mohanty, R.R.Dash, **T.Rout**, Static and Dynamic Analysis of a Functionally Graded Timoshenko Beam on Winkler's Elastic Foundation, Journal of Engineering Research and Studies, 1(2) , 149-165, 2010.
2. S. Mohaptra, S.C. Mohanty, R.R.Dash, **T.Rout**, Free vibration of a Functionally Graded Timoshenko beam by Finite Element Method, International Journal of Advanced Engineering and Technology, 2(3), 338-346, 2011.
3. S.C. Mohanty, R.R. Dash and **T.Rout**, Parametric Instability of a Functionally Graded Timoshenko beam on Winkler's Elastic Foundation, Nuclear Engineering and Design 241, 2698-2715, 2011.
4. S.C.Mohanty, R.R.Dash, **T.Rout**, Static and Dynamic Stability analysis of a Functionally Graded Timoshenko Beam, International Journal of Structural Stability and Dynamics, Vol.12,(4), 2012. DOI: 10.1142/S0219455412500253.
5. S. C. Mohanty, R.R.Das, **T.Rout**, Vibration and Dynamic Stability Analysis of a Functionally Graded Timoshenko beam on Pasternak Elastic Foundation, International Journal of Aerospace Lightweight Structures (IJALS), Vol. 2, No. 3, 1–21, 2012.
6. S.C.Mohanty, R.R.Dash, **T.Rout**, "Free Vibration of a Functionally Graded Rotating Timoshenko Beam" Advances in Structural Engineering, Vol. 16, No. 2, 405-418, 2013.
7. S.C.Mohanty, R.R.Dash, **T.Rout**, Parametric Instability of Functionally Graded Timoshenko Beam in High Temperature Environment, Advances in Vibration Engineering, (Accepted).
8. S.C.Mohanty, R.R.Dash, **T.Rout**, Parametric Instability of Functionally Graded Rotating Timoshenko Beam, Applied Mathematical Modelling, (Accepted).
9. S.C.Mohanty, R.R.Dash, **T.Rout**, Vibration and Dynamic Stability of Pre-twisted Thick Cantilever Beam Made of Functionally Graded Material, International Journal of Structural Stability and Dynamics. (1st Review completed).

International Conference:

1. S.C.Mohanty, R.R.Dash, **T.Rout**, D. Dhupal, Free Vibration of Rotating Timoshenko Beam with Functionally Graded Properties Using FEM, Proceedings of International conference on design and advances in mechanical engineering (**ICDAAME-2011, December 16-17**) SKP engineering college, Tiruvannamalai, India.

National Conference:

1. **T.Rout**, R.R.Dash, D.K.Behera, Stability of Functionally Graded Timoshenko Beam, Proceedings of **RAMP-10, March 2010**, MITS, Rayagada, Orissa.
2. S.C.Mohanty, R.R.Dash, **T.Rout**, Static and Dynamic analysis of Functionally Graded Timoshenko beam on Pasternak Elastic Foundation, **ETME-2011**, January 21-22, 2011, CVRCE, Bhubaneswar, Odisha.